Quantum Corrections to the Lepton Flavour Structure and Applications

Jörn Kersten

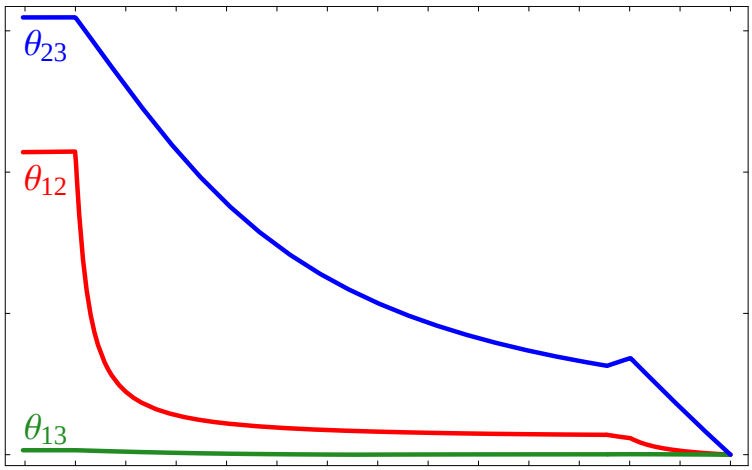

Dissertation
July 2004

Technische Universität München
Physik-Department
Institut für Theoretische Physik T30d

Prof. Dr. Manfred Lindner

Technische Universität München
Physik-Department
Institut für Theoretische Physik T30d
Univ.-Prof. Dr. M. Lindner

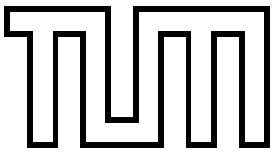

Quantum Corrections to the Lepton Flavour Structure and Applications

Dipl.-Phys. Univ. Jörn Kersten

Vollständiger Abdruck der von der Fakultät für Physik der Technischen Universität München zur Erlangung des akademischen Grades eines

Doktors der Naturwissenschaften (Dr. rer. nat.)

genehmigten Dissertation.

Vorsitzender: Univ.-Prof. Dr. Reiner Krücken

Prüfer der Dissertation:

1. Univ.-Prof. Dr. Manfred Lindner
2. Univ.-Prof. Dr. Andrzej J. Buras

Die Dissertation wurde am 22.7.2004 bei der Technischen Universität München eingereicht und durch die Fakultät für Physik am 14.9.2004 angenommen.

Contents

Chapter 1

Introduction

Among the areas of particle physics, neutrino physics certainly belongs to those which have exhibited the most rapid experimental progress in recent years. After the discovery of the solar neutrino deficit by experiments like Homestake, GALLEX and SAGE, which was the first hint for interesting new effects in the neutrino sector, a breakthrough was achieved in 1998 by the Super-Kamiokande detector that found evidence for oscillations or, more precisely, flavour transitions of atmospheric neutrinos [1]. In the few years since then, further experiments managed to establish a standard picture of the neutrino parameters, narrowing down the allowed ranges for the mixing angles and mass squared differences relevant for oscillations. The detectors SNO and KamLAND proved that the solar neutrino deficit is caused by oscillations and that the parameters lie in the range of the so-called LMA solution [2–4]. Finally, recent data from Super-Kamiokande and K2K confirm that the flavour transitions of atmospheric neutrinos are indeed due to oscillations [5, 6]. While all these experiments have significantly improved the knowledge about the neutrino mass differences, the absolute mass scale remains unknown. Nevertheless, measurements of nuclear beta and double beta decay as well as cosmological observables have made important progress, pushing the upper limit well below 1 eV [7–10]. A challenge to the standard picture with three very light active neutrinos is still posed by the result of the LSND experiment [11, 12] which found evidence for oscillations that can only be reconciled with the other data, if light sterile neutrinos exist or if there are other rather dramatic effects like CPT violation.

Regardless of this problem, the existence of neutrino oscillations has been firmly established. This is very exciting, because it requires the neutrinos to have non-zero masses, which is not possible in the Standard Model. Thus, neutrino experiments provide the first solid evidence for new physics beyond this theory.

This poses interesting challenges for theoretical physics. While an extension of the Standard Model by right-handed neutrinos in order to accommodate neutrino masses is straightforward, this already leads to the question if neutrinos are Dirac or Majorana particles, which is related to the issue of lepton number violation. For Majorana neutrinos, the smallness of their masses can be elegantly explained by the see-saw mechanism [13–16]. This model has the additional advantage of providing a mechanism for the generation of the asymmetry between matter and antimatter in the universe, called

leptogenesis. In contrast, explaining the observed values of the oscillation parameters turned out to be a much more difficult task. Inspired by the idea of Grand Unified Theories (GUTs), where quarks and leptons belong to common multiplets, one would naively expect their mass hierarchies and mixing patterns to be comparable. However, it turned out that only one of the lepton mixing angles is small, while the other two are very large, which is completely different from the quark sector. The hierarchy of the neutrino masses is also considerably weaker than that of the quarks and charged leptons, and even nearly degenerate masses are possible.

A large number of models have been proposed in order to solve this problem and to explain the observed flavour structure of quarks and leptons. The ideas employed are very diverse and include, for example, Grand Unification, Abelian or non-Abelian flavour symmetries, textures, radiative effects, extra dimensions, or combinations thereof. A common feature of many models is that they operate at very high energies such as the GUT scale. In this context, fermion masses and mixings can be regarded as a probe of otherwise inaccessible high-energy physics. Neutrinos appear especially promising for this purpose, as the smallness of their masses is a direct consequence of new physics at a high scale, if it is indeed explained by the see-saw mechanism. As argued above, neutrino experiments have already provided significant restrictions on fermion mass models by establishing the existence of large mixing in the lepton sector. The situation will be further improved by future experiments, which will reach a much higher precision. It may even surpass that of measurements in the quark sector, as it is not limited by hadronic uncertainties. Consequently, the determination of neutrino properties has the potential to play a role for GUT-scale physics that is similar to the one of electroweak precision tests for low-energy physics beyond the Standard Model.

In order to use experimental data for testing fermion mass models, one has to take into account that all parameters of a quantum field theory, including particle masses and mixing angles, depend on energy because of quantum corrections. Thus, the data, which are obtained at energies between about 1 MeV and 100 GeV, and the predictions of high-energy models are not directly comparable. The necessary link is provided by the renormalization group running, which can be calculated by solving a set of differential equations, the renormalization group equations. While the running of gauge couplings and fermion masses is always significant, the change of the quark mixing angles is very small due to the strong hierarchy between their masses. This is not true in the lepton sector, if neutrino masses are nearly degenerate. In this case the running of the mixing parameters can be drastic, so that the flavour structure at high energies may be completely different from the one measured at low energies. Even if this does not happen, the maximal hierarchy between the neutrino masses is still weaker than that between the other fermion masses, so that quantum corrections can be large enough to be relevant for precision measurements of neutrino mixing angles.

This work is concerned with the effects of renormalization on the flavour structure in the lepton sector, in particular the running of neutrino masses as well as leptonic mixing angles and CP phases. In the first chapter of the main part, the theoretical and

experimental framework for neutrino masses is introduced. Among other things, the possible neutrino mass terms and some options for their generation in extensions of the Standard Model are described. Besides, the definition of the neutrino mass parameters and the current experimental knowledge about their values are given.

The following chapter introduces the concept of renormalization and outlines the calculation of the renormalization group equations governing the running. After that, these techniques are applied to lepton mass parameters in ch. 4. The first part of this chapter deals with the running below the see-saw scale in the Standard Model and MSSM. Differential equations are derived that approximately describe the running of the mass eigenvalues and mixing parameters directly rather than that of the neutrino mass matrix. Thus, it is possible to gain a qualitative understanding of the dependence of the running on the various parameters, for instance the absolute neutrino mass scale and the CP phases. To a reasonable accuracy, the formulae can also be used to determine the size of quantum corrections quantitatively. Thus, one can quickly estimate if they are important in a particular model. In the second part of ch. 4, the running above the see-saw scale in the Standard Model and MSSM extended by heavy singlet neutrinos is studied. Special emphasis is placed on the evolution between the see-saw scales for non-degenerate singlet masses.

In the next chapter, various applications of the running of lepton mass parameters are presented. It is pointed out that the size of the radiative corrections to the mixing angles is quite likely to be within the reach of future precision measurements, which provides an additional motivation for these experiments. Besides, the implications of the change of the neutrino masses under the renormalization group for leptogenesis calculations and for the experimental bounds on the absolute mass scale are addressed. After that, the possible reconciliation of the observed bi-large neutrino mixing pattern with the more symmetric bi-maximal mixing scenario by radiative corrections is studied. Eventually, the idea of texture zeros, one of the above-mentioned approaches towards an understanding of the leptonic flavour structure, is considered in connection with the running of the neutrino mass matrix. In particular, modifications of statements about the compatibility of textures with experimental data are discussed.

Finally, after the summary chapter of the main part, formulae which are important for this work are listed in the appendix, in particular all relevant renormalization group equations. Parts of this work have been published in [17–23].

Chapter 2

Framework for Neutrino Masses

2.1 Neutrino Mass Terms

We will start the description of the theoretical and experimental framework for massive neutrinos by discussing the possible neutrino mass terms. Afterwards, we will define the mixing parameters that are derived from them. We will also review the experimental knowledge about these quantities and briefly describe some theoretical attempts for their explanation.

With the particle content of the Standard Model (SM) or its minimal supersymmetric extension (MSSM), extended by a number of right-handed neutrino fields ν_{R}^{i} which are singlets under the SM gauge groups, there are two possibilities for constructing a mass term in the Lagrangian.

1. The usual Dirac mass term, which is analogous to the mass terms of the other fermions, reads

$$\mathscr{L}_{\mathrm{Dirac}} = -\overline{\nu_{\mathrm{R}}} m_{\mathrm{D}} \nu_{\mathrm{L}} + \mathrm{h.c.}\ . \tag{2.1}$$

2. In addition, there can be the Majorana mass terms

$$\mathscr{L}_{\mathrm{Majorana}} = -\frac{1}{2}\overline{\nu_{\mathrm{L}}^{\mathcal{C}}} m_{\mathrm{L}} \nu_{\mathrm{L}} - \frac{1}{2}\overline{\nu_{\mathrm{R}}} m_{\mathrm{R}} \nu_{\mathrm{R}}^{\mathcal{C}} + \mathrm{h.c.}\ . \tag{2.2}$$

$\nu_{\mathrm{L}} = (\nu_{\mathrm{L}}^{1}, \nu_{\mathrm{L}}^{2}, \nu_{\mathrm{L}}^{2})^{T}$ and $\nu_{\mathrm{R}} = (\nu_{\mathrm{R}}^{1}, \nu_{\mathrm{R}}^{2}, \nu_{\mathrm{R}}^{3})^{T}$ are vectors in flavour space, and m_{D}, m_{L} as well as m_{R} are 3×3 matrices, which are complex in general. The Majorana mass matrices have to be symmetric, since the Lagrangian is a scalar and thus e.g.

$$(\overline{\nu_{\mathrm{L}}^{\mathcal{C}}} m_{\mathrm{L}} \nu_{\mathrm{L}})^{T} = (-\nu_{\mathrm{L}}^{T} \mathcal{C}^{-1} m_{\mathrm{L}} \nu_{\mathrm{L}})^{T} = \overline{\nu_{\mathrm{L}}^{\mathcal{C}}} m_{\mathrm{L}}^{T} \nu_{\mathrm{L}} \overset{!}{=} \overline{\nu_{\mathrm{L}}^{\mathcal{C}}} m_{\mathrm{L}} \nu_{\mathrm{L}}\ ,$$

where we have used the anticommutation property of fermion fields and eq. (A.2b). The superscript $\mathcal{C}$ denotes charge conjugation, as defined in app. A. Although the number of right-handed neutrinos is arbitrary, we restrict ourselves to the most commonly

considered case where there are three of them. If we take all possibilities together, we arrive at the most general neutrino mass term

$$\mathscr{L}^{\nu}_{\text{Mass}} = -\frac{1}{2}\overline{\nu^{\mathcal{C}}_{\text{L}}} m_{\text{L}} \nu_{\text{L}} - \overline{\nu_{\text{R}}} m_{\text{D}} \nu_{\text{L}} - \frac{1}{2}\overline{\nu_{\text{R}}} m_{\text{R}} \nu^{\mathcal{C}}_{\text{R}} + \text{h.c.} \,. \tag{2.3}$$

It can be rewritten in the compact form

$$\mathscr{L}^{\nu}_{\text{Mass}} = -\frac{1}{2}\overline{\Psi^{\mathcal{C}}} M \Psi + \text{h.c.} \,, \tag{2.4}$$

where

$$\Psi := \begin{pmatrix} \nu_{\text{L}} \\ \nu^{\mathcal{C}}_{\text{R}} \end{pmatrix} \quad \text{and} \quad M := \begin{pmatrix} m_{\text{L}} & m_{\text{D}}^{T} \\ m_{\text{D}} & m_{\text{R}} \end{pmatrix} \,.$$

As the 6×6 mass matrix M is (blockwise) symmetric, it can be block-diagonalized by substituting

$$\Psi = U\chi := U \begin{pmatrix} \chi_1 \\ \chi_2 \end{pmatrix} \quad , \quad M_{\text{diag}} = \begin{pmatrix} m_1 & 0 \\ 0 & m_2 \end{pmatrix} = U^{T} M \, U \,, \tag{2.5}$$

where U is a unitary matrix. Then the Lagrangian becomes

$$\mathscr{L}_{\text{Mass}} = -\frac{1}{2}\overline{\chi^{\mathcal{C}}_1} m_1 \chi_1 - \frac{1}{2}\overline{\chi^{\mathcal{C}}_2} m_2 \chi_2 + \text{h.c.} \,, \tag{2.6}$$

i.e. we have obtained two fields with pure Majorana mass terms. In the special case $m_{\text{L}} = m_{\text{R}} = 0$, $m_{\text{D}} \neq 0$, these can be combined to form one field with a Dirac mass term. If m_{R} is non-zero, there is no symmetry in the SM or MSSM that could force it to be small. Hence, it is natural to assume that its eigenvalues are of the order of magnitude of a very high energy scale where the SM or MSSM is embedded into a more fundamental theory, such as a GUT. In contrast, m_{D} is proportional to a Yukawa coupling times the Higgs vacuum expectation value (VEV) and thus has eigenvalues of the order of the electroweak scale or smaller. Besides, m_{L} has to be much smaller than m_{D}[1] in order to avoid too large neutrino masses. Then, we have $m_{\text{L}} \ll m_{\text{D}} \ll m_{\text{R}}$, and approximate block-diagonalization is achieved by

$$U = \begin{pmatrix} 1 & m_{\text{D}}^{\dagger} m_{\text{R}}^{*\,-1} \\ -m_{\text{R}}^{-1} m_{\text{D}} & 1 \end{pmatrix}, \tag{2.7}$$

yielding the fields

$$\chi_1 \approx \nu_{\text{L}} \quad \text{and} \quad \chi_2 \approx \nu^{\mathcal{C}}_{\text{R}} \tag{2.8a}$$

[1] By this we mean that all eigenvalues of m_{L} are much smaller than those of m_{D}.

with masses

$$m_1 \approx m_{\mathrm{L}} - m_{\mathrm{D}}^T m_{\mathrm{R}}^{-1} m_{\mathrm{D}} \quad \text{and} \quad m_2 \approx m_{\mathrm{R}} \; . \tag{2.8b}$$

The corrections are suppressed by powers of $m_{\mathrm{D}} m_{\mathrm{R}}^{-1}$. Thus, the mass eigenstates are three very light neutrinos predominantly composed of the left-handed states that participate in the weak interactions, and three very heavy ones which are singlets under the SM gauge groups to a good approximation. This is the see-saw mechanism [13–16], which is currently the most popular explanation for the smallness of neutrino masses.

2.2 Definition of the Leptonic Mass Parameters

In order to define the parameters describing the masses and mixing of the leptons, let us consider the SM with small Majorana masses for the left-handed neutrinos. As we do not want to restrict ourselves to a particular scenario, we do not specify how the neutrino masses are generated. This is not necessary for our discussion, since the physics responsible for this must work at some high energy beyond the current experimental capabilities, and therefore the particles involved decouple from the low-energy physics we are interested in at the moment. Of course, the discussion is analogous in the MSSM.

The lepton flavour eigenstates e'_{L} and ν'_{L} (which are both vectors in flavour space, e.g. $\nu'_{\mathrm{L}} = (\nu'_{e_{\mathrm{L}}}, \nu'_{\mu_{\mathrm{L}}}, \nu'_{\tau_{\mathrm{L}}})^T$) are defined by the requirement that the charged currents of the weak interaction be flavour-diagonal, i.e. an electron only interacts with an electron neutrino but not with a muon neutrino. In the flavour eigenstate basis, the mass matrices in

$$\mathscr{L}_{\mathrm{Mass}} = -\overline{e'_{\mathrm{R}}} m_e e'_{\mathrm{L}} - \frac{1}{2} \overline{\nu'^{\mathcal{C}}_{\mathrm{L}}} m_\nu \nu'_{\mathrm{L}} + \mathrm{h.c.} \tag{2.9}$$

are not diagonal in general. The change to the mass eigenstate basis is attained by the transformations

$$\nu_{\mathrm{L}} = U^{\nu\dagger} \nu'_{\mathrm{L}} \; , \tag{2.10a}$$

$$e_{\mathrm{L}} = U_{\mathrm{L}}^{e\dagger} e'_{\mathrm{L}} \; , \tag{2.10b}$$

$$e_{\mathrm{R}} = U_{\mathrm{R}}^{e\dagger} e'_{\mathrm{R}} \; , \tag{2.10c}$$

where the unitary matrices U^ν, U^e_{L} and U^e_{R} are determined from

$$U^{\nu\dagger}\, m_\nu^\dagger m_\nu\, U^\nu = \mathrm{diag}(m_1^2, m_2^2, m_3^2) \; , \tag{2.11a}$$

$$U_{\mathrm{L}}^{e\dagger}\, m_e^\dagger m_e\, U_{\mathrm{L}}^e = U_{\mathrm{R}}^{e\dagger}\, m_e m_e^\dagger\, U_{\mathrm{R}}^e = \mathrm{diag}(m_e^2, m_\mu^2, m_\tau^2) \tag{2.11b}$$

and therefore satisfy

$$U^{\nu T} m_\nu\, U^\nu = \mathrm{diag}(m_1, m_2, m_3) \; , \tag{2.12a}$$

$$U_{\mathrm{R}}^{e\dagger} m_e\, U_{\mathrm{L}}^e = \mathrm{diag}(m_e, m_\mu, m_\tau) \; . \tag{2.12b}$$

The real and positive numbers m_i are the mass eigenvalues of the neutrinos and charged leptons. For the diagonalization of the neutrino mass matrix, a single unitary matrix is sufficient, since m_ν is a Majorana mass matrix and thus symmetric. Due to the unitarity of the transformation matrices, every term of the Lagrangian that is proportional to $\overline{\psi}\psi$ ($\psi \in \{\nu_\mathrm{L}, e_\mathrm{R}, e_\mathrm{L}\}$), i.e. the diagonal part of the $\mathrm{SU}(2)_\mathrm{L}$ structure, is invariant under the transformations (2.10). The only change occurs in the term describing the charged current weak interactions,

$$\mathscr{L}_\mathrm{cc} = -\frac{g_2}{\sqrt{2}}\overline{e'_\mathrm{L}}\gamma^\mu W^-_\mu \nu'_\mathrm{L} + \mathrm{h.c.} = -\frac{g_2}{\sqrt{2}}\overline{e_\mathrm{L}}\, V_\mathrm{MNS}\, \gamma^\mu W^-_\mu \nu_\mathrm{L} + \mathrm{h.c.}\,, \tag{2.13}$$

where

$$V_\mathrm{MNS} := U^{e\dagger}_\mathrm{L} U^\nu \tag{2.14}$$

is the Maki-Nakagawa-Sakata (MNS) matrix. In the mass eigenstate basis, $\mathscr{L}_\mathrm{cc}$ is the only flavour non-diagonal term in the leptonic sector. Consequently, lepton mixing is uniquely characterized by V_MNS and only the elements of this matrix are experimentally accessible.

Being a 3×3 unitary matrix, V_MNS can be parameterized by 3 angles $\theta_{12}, \theta_{13}, \theta_{23}$ and 6 phases $\delta, \varphi_1, \varphi_2, \delta_e, \delta_\mu, \delta_\tau$. We use the parameterization

$$V_\mathrm{MNS} = \mathrm{diag}(e^{i\delta_e}, e^{i\delta_\mu}, e^{i\delta_\tau}) \cdot V \cdot \mathrm{diag}(e^{-i\varphi_1/2}, e^{-i\varphi_2/2}, 1) \tag{2.15a}$$

with

$$V = \begin{pmatrix} c_{12}c_{13} & s_{12}c_{13} & s_{13}e^{-i\delta} \\ -c_{23}s_{12} - s_{23}s_{13}c_{12}e^{i\delta} & c_{23}c_{12} - s_{23}s_{13}s_{12}e^{i\delta} & s_{23}c_{13} \\ s_{23}s_{12} - c_{23}s_{13}c_{12}e^{i\delta} & -s_{23}c_{12} - c_{23}s_{13}s_{12}e^{i\delta} & c_{23}c_{13} \end{pmatrix}, \tag{2.15b}$$

where $s_{12} := \sin\theta_{12}$, $c_{12} := \cos\theta_{12}$ etc. The phases δ_e, δ_μ and δ_τ can be removed by a global phase transformation of the charged lepton fields and are thus unphysical. Unlike in the quark sector, this is not possible for φ_1 and φ_2, since the Majorana mass term (2.9) does not allow to change the phases of the neutrino fields, as otherwise the mass eigenvalues would become complex. Hence, these phases are observable in principle and called Majorana phases. If at least one of them is different from 0 and π, the MNS matrix becomes complex, leading to CP violation in the lepton sector. The same is true for the Dirac phase δ, unless θ_{13} is zero. In the latter case, δ is undefined, since the MNS matrix contains only the combinations $s_{13}e^{\pm i\delta}$.

Note that the mixing angles are undefined if the neutrino masses are exactly degenerate, since then any unitary matrix U^ν satisfies eq. (2.11a). Analogously, one of the angles is undefined if two masses are degenerate. We know from oscillation experiments that this is not the case at low energy, but it might occur at high energies due to quantum corrections.

We use the convention where $0 \leq \theta_{12} \leq \frac{\pi}{4}$ and $0 \leq \theta_{13}, \theta_{23} \leq \frac{\pi}{2}$. This implies that the neutrino mass eigenvalues are not ordered in general, i.e. $m_1 < m_2 < m_3$ does *not* hold. All phases are chosen to lie between 0 and 2π.[2]

If one defines the flavour eigenstates of the charged leptons to equal the mass eigenstates, $V_{\rm MNS}$ connects the corresponding eigenstates of the left-handed neutrinos,

$$\nu'_{\rm L} = V_{\rm MNS}\, \nu_{\rm L} \ , \tag{2.16}$$

thus characterizing neutrino mixing. We will often work in this basis in the following.

2.3 Experimental Knowledge about Neutrino Mass Parameters

2.3.1 Neutrino Oscillations

A lot of experimental effort has been under way in recent years to observe neutrino oscillations, which occur if neutrinos mix and have non-degenerate masses. The progress has been remarkable, most notably the first evidence for flavour transitions of atmospheric neutrinos by Super-Kamiokande [1], the solution of the solar neutrino puzzle by SNO [2, 3], and the confirmation of the LMA solution by KamLAND [4]. Just recently, the Super-Kamiokande collaboration has reported that the dependence of the atmospheric neutrino data on L/E, the ratio of the baseline and the energy, disfavors the possibility that the observed flavour transitions are caused by any other mechanism than oscillations [5]. This result is also backed by the latest data from the K2K long-baseline experiment [6].

The probability for neutrino oscillations depends on the mixing angles and the Dirac CP phase as well as the mass squared differences $\Delta m^2_{\odot} := m_2^2 - m_1^2$ and $\Delta m^2_{\rm a} := m_3^2 - m_2^2$. Hence, these parameters can be determined by oscillation experiments in principle, while such measurements are not sensitive to the Majorana phases and the absolute neutrino masses. Today, we know that the mixing angles θ_{12} and θ_{23} are large, while the third one, θ_{13}, is small. As the most sensitive limit on θ_{13} has been obtained by an oscillation experiment at the CHOOZ reactor [24], it is often called CHOOZ or reactor angle. Due to its smallness, the oscillations of solar and atmospheric neutrinos are almost decoupled, so that to a good approximation they can be treated as independent two-flavour oscillations governed by the parameters θ_{12}, $\Delta m^2_{\odot}$ and θ_{23}, $\Delta m^2_{\rm a}$, respectively. The favored region for the solar angle and mass squared difference is usually referred to as the Large Mixing Angle (LMA) solution.

[2] One might wonder whether the physically meaningful range for the Majorana phases actually reaches up to 4π, as they are multiplied by $1/2$ in eq. (2.15a). However, by inverting eq. (2.12a) and plugging in (2.15a), one sees that only $m_{1,2}\, e^{i\varphi_{1,2}}$ are relevant for the neutrino mass matrix, so that the given range is sufficient.

The sign of the mass differences is not relevant for neutrino oscillations in vacuum, but it influences the oscillation probability in matter, so that it is measurable. From the solar neutrino experiments, we already know that $\Delta m^2_\odot$ is positive, since the LMA solution relies on a resonance effect inside the sun known as the MSW effect, which has to occur for neutrinos rather than for anti-neutrinos. The sign of Δm^2_{a} is yet unknown and remains to be determined by long-baseline experiments which are sensitive to matter effects inside the earth. Therefore, two orderings of the neutrino mass eigenvalues are allowed at the moment, either $m_1 < m_2 < m_3$ or $m_3 < m_1 < m_2$. They are referred to as normal and inverted hierarchy, respectively.

An open question remains the validity of the LSND evidence for oscillations [11,12], which is only compatible with the other observations, if light sterile neutrinos exist or if the masses of neutrinos and antineutrinos are different, implying CPT violation [25]. Even with one sterile neutrino, there is a conflict with the other data [26], so that at least two of them are needed for a good global fit of all data [27]. Besides, a part of the region in parameter space that is favored by LSND is excluded by the KARMEN experiment [28]. A test of the LSND result will be provided by the MiniBooNE experiment [29]. In this work, we will not take into account this result and stick to the conventional picture with three light neutrinos.

2.3.2 Measurements of the Absolute Neutrino Mass

Tritium Decay

One method that is sensitive to the absolute value of the neutrino masses rather than only the difference involves the β^- decay of tritium. If neutrinos are massive, the energy spectrum of the produced electrons has to end slightly below the energy of 18.6 keV that is released in the decay, since the neutrino has to carry at least its rest energy. Due to neutrino mixing, the quantity measured in this process is not one of the mass eigenvalues itself but the linear combination

$$m^2(\nu_e) = \sum_{i=1}^{3} |U_{1i}|^2 \, m_i^2 \; . \tag{2.17}$$

The current experimental limit is $m(\nu_e) < 2.2$ eV at the 95% CL [7].

Neutrinoless Double Beta Decay

In a double beta decay, the atomic number of a nucleus changes by two units, and two electrons as well as two anti-neutrinos (or two positrons and two neutrinos) are emitted. This process has an extremely long half-life, but it can be observed in certain nuclei where the usual beta decay is energetically forbidden, for instance ^{76}Ge. If neutrinos have non-vanishing Majorana masses, a neutrinoless decay mode becomes possible. It can be distinguished from the conventional one via the spectrum of the sum of the

electron energies. While it is continuous if neutrinos are emitted, it becomes discrete if this is not the case. For $0\nu\beta\beta$ decay, the relevant effective neutrino mass is the 11-element of the mass matrix,

$$\langle m_\nu \rangle = \left| \sum_{i=1}^{3} U_{1i}^2 \, m_i \right| = \left| m_1 \, c_{12}^2 c_{13}^2 \, e^{i\varphi_1} + m_2 \, s_{12}^2 c_{13}^2 \, e^{i\varphi_2} + m_3 \, s_{13}^2 \, e^{2i\delta} \right| \; . \tag{2.18}$$

Unfortunately, the decay amplitude also depends on a nuclear matrix element, which is only known up to a factor of about 2. This places an additional limit on the experimental sensitivity that can be reached. With an optimistic estimate of the precision of the matrix element, the current best upper limit as obtained by the Heidelberg-Moscow and IGEX experiments is about $\langle m_\nu \rangle < 0.35$ eV at the 90% CL [8, 9]. Some members of the Heidelberg-Moscow collaboration have reported evidence for the observation of $0\nu\beta\beta$ decay with a best-fit effective mass of $\langle m_\nu \rangle \approx 0.44$ eV [30], but this result is highly controversial.

As eq. (2.18) also depends on the Majorana phases, $0\nu\beta\beta$ experiments are sensitive to them in principle. However, it is unlikely that the experimental and theoretical precision will become good enough to make a measurement of them possible in practice.

Cosmology

Neutrinos contribute to the dark matter and thus play a role in the formation of structure in the universe. As they are relativistic particles, they act as hot dark matter, which means that they tend to wash out structure on small scales. By comparing the structures observed in galaxy surveys and via the Lyman α forest with model calculations and measurements of the cosmic microwave background (CMB), one can place an upper limit on the fraction of hot dark matter in the total energy density of the universe. This translates into an upper bound on the neutrino mass, because the number density of neutrinos produced after the big bang can be calculated.

At the moment, the most precise data stem from the WMAP satellite, which measured the CMB, and the 2dF galaxy redshift survey. They restrict the sum of the neutrino masses to be smaller than 0.69 eV at the 95% CL [10]. As the mass differences are much smaller, the bound implies $m_i < 0.23$ eV. Using a more conservative analysis, the limit $m_i < 0.34$ eV was found in [31].

An overview of the current experimental knowledge about the neutrino mass parameters is given in tab. 2.1. For the oscillation parameters, we quote the results from [32], which are in good agreement with other global fits of the data [33–37]. The latest best-fit value of θ_{13} is non-zero, but the goodness of fit for $\theta_{13} = 0$ is virtually the same, so that this result cannot be regarded as a statistically significant evidence for a non-vanishing CHOOZ angle yet.

Experiment	Parameter	Best-fit value	Allowed range	CL
Oscillations	θ_{12}	33.2°	28.7° .. 38.6°	3σ
(global fit) [32]	θ_{23}	46.1°	34.4° .. 56.8°	3σ
	θ_{13}	4.1°	0° .. 14.3°	3σ
	$\Delta m^2_\odot$	$6.9 \cdot 10^{-5}$ eV^2	$(5.4$ .. $9.4) \cdot 10^{-5}$ eV^2	3σ
	$\lvert\Delta m^2_{\rm a}\rvert$	$2.3 \cdot 10^{-3}$ eV^2	$(1.1$ .. $3.4) \cdot 10^{-3}$ eV^2	3σ
Tritium decay [7]	$m(\nu_e)$		< 2.2 eV	95%
$0\nu\beta\beta$ decay [8, 9]	$\langle m_\nu \rangle$		< 0.35 eV	90%
[30]	$\langle m_\nu \rangle$	0.44 eV	(0.24 .. 0.58) eV	3σ
Cosmology [10]	m_i		< 0.23 eV	95%

Table 2.1: Overview of experimental results for neutrino mass parameters.

2.3.3 Potential of Future Experiments

In the coming years, progress in pinning down the values of the oscillation parameters will come primarily from long-baseline experiments, where neutrino beams produced at accelerators are sent to underground detectors several hundred kilometers away. The first of these projects, K2K has already produced data, and experiments like MINOS, ICARUS and OPERA are to follow. The next generation of experiments will be the so-called superbeams, for example JPARC-SK and NuMI. Finally, the ultimate precision could be reached with a neutrino factory. Besides the long-baseline experiments, measurements with neutrinos produced at nuclear reactors will play an important role in constraining the small mixing angle θ_{13}.

From the point of view of theory, precise determinations of θ_{13} and θ_{23} are especially interesting, since current data are compatible with the values 0 and $\pi/4$, respectively, which correspond to a very special flavour configuration. If confirmed, it would point towards an underlying symmetry and rule out a lot of the models for fermion masses and mixings that have been proposed so far. Furthermore, θ_{13} is of interest because one can only hope to measure CP violation in the lepton sector if this parameter is not too small. Therefore, an overview of the attainable experimental precisions on these parameters is given in tabs. 2.2 and 2.3.

Apart from that, the results of MiniBooNE, which are expected rather soon, are naturally extremely important, as they will either confirm or rule out the LSND anomaly and thus answer the question whether the conventional picture of three light neutrinos is correct.

As far as the absolute neutrino mass scale is concerned, the bound from tritium decay will be significantly lowered by the KATRIN experiment. The planned sensitivity limit is about 0.3 eV. Several experiments have been proposed to continue the search for $0\nu\beta\beta$ decay, see e.g. [41]. If the planned sensitivities of around 50 meV on the effective neutrino mass are reached, these experiments will be able to rule out the inverted mass hierarchy, if the neutrinoless decay mode is not discovered.

Experiment	$\sin^2 2\theta_{13}$	θ_{13}
Current limit (CHOOZ)	0.14	11.0°
Conventional beams	0.061	7.5°
Reactor (Double-CHOOZ)	0.032	5.2°
Superbeams (JPARC-SK, NuMI)	0.023	4.4°
Reactor-II	0.014	3.4°
JPARC-HK, NuFact-I	10^{-3}	0.9°
NuFact-II (magic baseline)	$6 \cdot 10^{-5}$	0.2°

Table 2.2: Sensitivity limits of proposed neutrino oscillation experiments on the small mixing angle θ_{13} at the 90% CL [38–40]. The conventional beam experiments include MINOS, ICARUS and OPERA. The last entry refers to an advanced stage neutrino factory with experiments at two different baselines. For a description of the experiments and the assumptions used in the analysis, see [38–40] and references therein. The numbers should be treated with some care, since they depend on the true values of the other oscillation parameters, in particular Δm^2_{a}.

Experiment	$\lvert 0.5 - \sin^2\theta_{23}\rvert$	$\lvert 45° - \theta_{23}\rvert$
Current limit (SK) [5]	0.16	9.2°
Conventional beams	0.100	5.8°
JPARC-SK	0.057	3.3°
NuMI	0.079	4.6°
Combination	0.050	2.9°
JPARC-HK	0.020	1.2°
NuFact-II	0.055	3.2°

Table 2.3: Potential of proposed experiments to measure deviations from maximal atmospheric mixing. Listed are the minimal values of $|0.5 - \sin^2\theta_{23}|$ and $|45° - \theta_{23}|$ required to exclude maximal mixing at the 90% CL [22]. The entry "Combination" refers to the combined potential of the experiments in the first 3 lines. See [22] and references therein for a description of the experiments and the analysis methods. As in tab. 2.2, the results depend on the true values of the other oscillation parameters.

2.4 Generation of Neutrino Masses

2.4.1 SM and MSSM as Effective Theories

So far we have assumed that neutrinos have Majorana masses without specifying any mechanism for their generation. The SM (or MSSM) by itself cannot accommodate massive neutrinos. A Dirac mass term is not possible due to the lack of right-handed neutrinos, and a Majorana mass term would break $\mathrm{U}(1)_\mathrm{Y}$ as well as the accidental lepton number symmetry explicitly.

However, neither the SM nor the MSSM can be valid up to arbitrarily high energies because of the Landau pole in the running of the U(1) gauge coupling constant, to say nothing of the need to include gravity at the Planck scale in a complete theory. They rather have to be viewed as effective field theories (EFTs) describing the infrared limit of some high-energy theory, which involves new particles and interactions, including ones that allow for massive neutrinos. In the effective theory, this new physics manifests itself in the form of new operators, which may be non-renormalizable. In principle, one expects all Lorentz and gauge invariant terms compatible with the assumed symmetries to appear, in general including lepton and baryon number violating ones, since the latter quantities are only conserved due to accidental symmetries in the SM. Whenever we refer to neutrino masses in the SM or MSSM (without extended particle content) in this work, we implicitly assume this EFT approach. The coupling constants of operators with a mass dimension higher than 4 are suppressed by powers of the scale at which the SM is embedded into the more fundamental theory. Hence, to first order it is sufficient to consider only the lowest-dimensional of the new operators. In the context of neutrino masses, this is the dimension 5 operator

$$\mathscr{L}_\kappa = \frac{1}{4}\kappa_{gf}\,\overline{\ell^{\mathrm{C}}_{\mathrm{L}c}}^{g}\varepsilon_{cd}\phi_d\;\ell^{f}_{\mathrm{L}b}\varepsilon_{ba}\phi_a + \mathrm{h.c.}\,, \tag{2.19}$$

where ℓ_L denotes the left-handed lepton doublets, ϕ is the Higgs, and ε is the totally antisymmetric tensor in 2 dimensions. Besides, $f, g \in \{1,2,3\}$ and $a, b, c, d \in \{1,2\}$ are generation and SU(2) indices, respectively. They will only be written explicitly where it is necessary for clarity. Summation over repeated indices will be implied throughout this work. The coupling κ is a complex symmetric matrix with a mass dimension of -1, thus suppressed by the embedding scale, which we will often call the see-saw scale in the following.

The operator (2.19) is compatible with all SM symmetries except for lepton number conservation and yields Majorana neutrino masses after the spontaneous breaking of the electroweak symmetry. The mass term is obtained from $\mathscr{L}_\kappa$ by replacing the neutral component of the Higgs field by its VEV, $\langle\phi^0\rangle = v/\sqrt{2} \approx 246\ \mathrm{GeV}/\sqrt{2}$,

$$\mathscr{L}^{\nu}_{\mathrm{Mass}} = \frac{v^2}{8}\,\overline{\nu^{\mathrm{C}}_{\mathrm{L}}}\kappa\nu_\mathrm{L} + \mathrm{h.c.}\,. \tag{2.20}$$

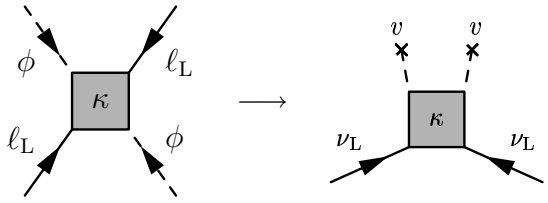

Figure 2.1: Majorana neutrino mass term arising from the dimension 5 operator (2.19) after electroweak symmetry breaking.

This is visualized in fig. 2.1. Hence, the neutrino mass matrix is given by

$$m_\nu = -\frac{v^2}{4}\kappa \,. \tag{2.21}$$

In the MSSM, the neutrino mass operator is also given by eq. (2.19), if ϕ is replaced by $\phi^{(2)}$, the Higgs field coupling to the up-type quarks. It arises from the F-term of the relevant part of the superpotential,

$$\mathscr{W}_\kappa = -\frac{1}{4}\kappa_{gf}\, \mathbf{l}_c^g \varepsilon^{cd} \mathbf{h}_d^{(2)}\; \mathbf{l}_b^f \varepsilon^{ba} \mathbf{h}_a^{(2)}\big|_{\theta\theta} + \text{h.c.} \,. \tag{2.22}$$

The bold-face letters $\mathbf{l}$ and $\mathbf{h}^{(2)}$ denote the left-handed lepton doublet and the up-type Higgs superfields. Note that in this case the VEV needed to calculate the mass matrix from κ contains an additional factor of $\sin\beta$, i.e. $v \approx \sin\beta \cdot 246$ GeV, where $\tan\beta$ is the ratio of the two Higgs VEVs.

The EFT point of view has the advantage of being relatively model-independent. Whatever the high-energy theory is, it always leads to the described effective operator at low energies, as long as lepton number is not conserved and as long as the SM or MSSM is indeed the correct low-energy theory.[3] The operator can then be used to study effects up to the scale at which new physics becomes important. Before we address this, we will discuss the two most straightforward possibilities for its generation.

2.4.2 Addition of Right-Handed Neutrinos

The simplest extension of the SM that accommodates neutrino masses is the addition of right-handed neutrino fields which are singlets under all gauge symmetries. Then the neutrinos acquire Dirac masses after spontaneous electroweak symmetry breaking, typically comparable to the masses of the other fermions, and in general we also expect large Majorana masses for the singlets, as argued in sec. 2.1. Thus, the see-saw formula (2.8b) (with $m_{\mathrm{L}} = 0$) holds and produces very light masses for the active neutrinos. This is often referred to as the type I see-saw scenario. Note that lepton number is no

[3] In some models, κ is forced to vanish by a symmetry, so that neutrino masses arise from different effective operators, see e.g. [42, 43].

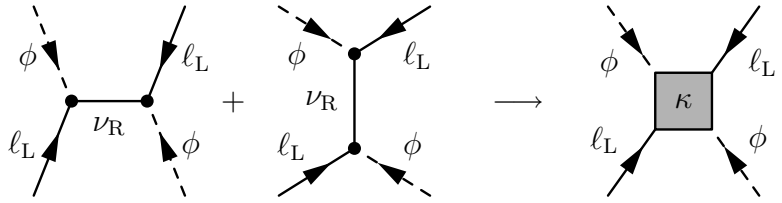

Figure 2.2: Generation of the effective neutrino mass operator via the exchange of heavy singlet neutrinos ν_R (type I see-saw mechanism).

longer conserved, if both Dirac and Majorana mass terms are present, no matter which lepton number is assigned to the singlet neutrinos.

At energies below the masses of the singlets, they can be integrated out, leading to the effective operator (2.19), as visualized in fig. 2.2. This procedure and the matching conditions that determine the coupling κ from the Yukawa couplings and the singlet mass matrix will be described in more detail in sec. 4.2.2. In the MSSM, the situation is completely analogous, but of course one has to add the superpartners of the right-handed neutrinos as well in order to avoid breaking supersymmetry.

2.4.3 Extension of the Higgs Sector

If no right-handed neutrinos are introduced, only the possibility of constructing a Majorana mass term from the left-handed ones remains. In order to respect the $SU(2)_L$ symmetry, it has to be made up of the doublets ℓ_L that include the left-handed charged leptons besides the neutrinos. The combination of the doublets $\overline{\ell_L^C}$ and ℓ_L is either an $SU(2)_L$ singlet or a triplet and has a weak hypercharge of -1. To obtain a singlet Lagrangian, we have to introduce a new Higgs particle with a coupling to this combination and a weak hypercharge of $+1$. The two options are a singlet S^+ and a triplet Δ. Such a singlet has an electric charge after electroweak symmetry breaking, so that it cannot couple to two neutrinos alone. Hence, only a triplet can be used. If its electrically neutral component develops a VEV v_Δ, lepton number conservation is violated, and a Majorana mass term for the left-handed neutrino fields arises.

However, this VEV breaks the custodial SU(2) symmetry of the SM at the tree level and thus causes a change of the ρ parameter. As the deviation of ρ from its SM value is strongly restricted by experiments [44], v_Δ is constrained to be very small. Furthermore, if lepton number conservation was broken spontaneously by v_Δ, this would lead to a massless Goldstone boson, the triplet Majoron [45], which is excluded by the measurement of the Z decay width at LEP. Both problems can be elegantly solved in models with asymptotic parity conservation, for example left-right symmetric theories. In this case, the Higgs potential contains a large mass term for the triplet as well as a lepton number violating coupling to the other Higgs fields. Minimizing the potential then leads to a naturally small induced VEV v_Δ after electroweak symmetry breaking. This is usually called the type II see-saw mechanism [46–49]. Again, the effective

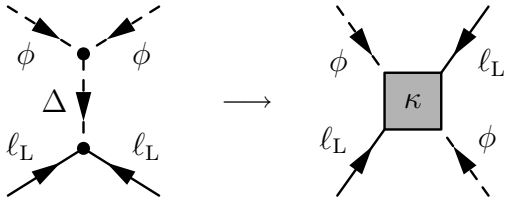

Figure 2.3: Generation of the effective neutrino mass operator employing a Higgs triplet Δ in the type II see-saw mechanism.

neutrino mass operator arises from integrating out the heavy new particles, in this case the triplet, as shown in fig. 2.3.

Of course, the type I and type II see-saw scenarios can be combined. There are also alternative mechanisms for explaining the smallness of neutrino masses, for example radiative generation at the one- or two-loop level [50,51], and models with Dirac neutrino masses only [52–57].

2.5 Theoretical Models for Fermion Masses

While the smallness of the neutrino mass eigenvalues is elegantly explained by the see-saw mechanism, there is no comparable "standard model" for explaining the mixing parameters yet. In order to give an impression of the ideas that are being considered, we describe a few examples in this section.

2.5.1 Textures

If one assumes certain patterns for the mass matrices, the number of free parameters is reduced, so that a simpler structure is obtained and often predictions in the form of correlations between observables become possible. For example, it is often assumed that some matrix elements are zero in a certain basis. This idea was first used to explain the structure of the quark Yukawa couplings [58–60] and later applied to the lepton sector as well. If the texture zeros are specified in the basis where the charged lepton Yukawa couplings are diagonal, it has been shown that there are 9 textures with two independent zeros for the neutrino mass matrix which are allowed by experimental data, while three-zero textures are not possible [61, 62].

The origin of such textures is usually left open and should be explained by some symmetry, see e.g. [63]. In this respect, the texture approach can be viewed as an intermediate step helping to identify the possible symmetries.

2.5.2 Right-Handed Lepton Dominance

In the simplest version of this mechanism, single right-handed neutrino dominance [64], one of the heavy singlet neutrinos is much lighter than the other two, so that according

to the see-saw formula (2.8b) its contribution to the light neutrino mass matrix is dominant. For instance, if the singlet mass matrix and the neutrino Yukawa couplings are of the form $m_{\rm R} = \mathrm{diag}(X', X, Y)$ and $Y_\nu = \begin{pmatrix} \times & \times & d \\ \times & \times & e \\ \times & \times & f \end{pmatrix}$ with $Y \ll X, X'$ and the crosses "$\times$" denoting arbitrary entries not larger than d, e, f, the mass matrix of the light neutrinos is approximately given by

$$m_\nu \approx \begin{pmatrix} \frac{d^2}{Y} & \frac{de}{Y} & \frac{df}{Y} \\ \frac{de}{Y} & \frac{e^2}{Y} & \frac{ef}{Y} \\ \frac{df}{Y} & \frac{ef}{Y} & \frac{f^2}{Y} \end{pmatrix}. \tag{2.23}$$

This yields a large atmospheric mixing angle for $d \ll e \approx f$, and a hierarchy between the neutrino mass eigenvalues m_2 and m_3 due to the small 23-subdeterminant. The idea can be extended to sequential right-handed neutrino [65] or lepton [66] dominance, which can also account for the large solar angle and the small CHOOZ angle. The scenario is not considered a separate model but rather a mechanism that is an important ingredient in various classes of models.

2.5.3 Grand Unified Theories

GUTs unify the SM gauge groups in a simple group such as SU(5) or SO(10). Quarks and leptons are both contained in common multiplets of this group, so that their Yukawa couplings are related, which makes predictions possible. The exact relations depend on the employed Higgs multiplets.

While the symmetry between quarks and leptons is an attractive feature, it makes it harder to explain the striking difference between their mixings. One way around this problem, used in lopsided models [67,68], is that in SU(5) the left-handed leptons share a multiplet with the right-handed down quarks. Thus, a large mixing between the left-handed charged leptons only implies a large mixing between right-handed quarks, which is unobservable.

Another approach uses SO(10), with fermion masses obtained from Yukawa couplings to Higgs fields in the representations **10** and **126**. If the type II see-saw contribution dominates, the neutrino mass matrix satisfies the sum rule $m_\nu \propto Y_d - Y_e$ [69]. As the bottom and the tau mass are roughly equal at the GUT scale in supersymmetric models, we have $Y_{d33} \approx Y_{e33}$, so that the 33-element of m_ν becomes small, typically of the same order as $m_{\nu 22}$ and $m_{\nu 23}$. This leads to large atmospheric mixing. A large θ_{12} and a small θ_{13} can be accommodated as well [70]. However, it is a bit more difficult to obtain the correct CP phase in the quark mixing matrix [71].

2.5.4 Flavour Symmetries

A lot of models impose symmetries to relate the different families of fermions. The used groups can be divided into Abelian and non-Abelian as well as continuous and

discrete. A simple example for a continuous Abelian symmetry is the conservation of $L_e - L_\mu - L_\tau$ [72,73], corresponding to invariance under a U(1) transformation. It leads to the light neutrino mass matrix and charged lepton Yukawa couplings

$$m_\nu = \begin{pmatrix} 0 & a & b \\ a & 0 & 0 \\ b & 0 & 0 \end{pmatrix} \quad , \quad Y_e = \begin{pmatrix} \times & 0 & 0 \\ 0 & \times & \times \\ 0 & \times & \times \end{pmatrix} , \tag{2.24}$$

where the crosses again stand for non-zero entries. The predictions are $\theta_{12} = \pi/4$, $\theta_{13} = 0$ as well as an inverted hierarchy with one massless neutrino and two degenerate masses, i.e. $\Delta m^2_\odot = 0$. The atmospheric angle is large if $a \sim b$. In order to obtain a non-maximal solar mixing angle and a non-zero mass squared difference, the symmetry has to be broken, for example by a small entry $m_{\nu_{11}}$.

Another widely used application of flavour symmetries is the Froggatt-Nielsen mechanism [74], where all Yukawa couplings are forbidden by a U(1) at the tree level. This symmetry is broken by the VEVs of scalar "flavon" fields Θ. Non-zero Yukawa couplings suppressed by powers of the small parameter $\lambda := \frac{\langle\Theta\rangle}{M_V}$ are then generated by the exchange of vector-like fields with a large mass M_V, similarly to the generation of the effective neutrino mass operator in the type I see-saw scenario. The resulting Yukawa matrices are hierarchical and of the form

$$Y = \begin{pmatrix} * \, \lambda^{q_1+q'_1} & * \, \lambda^{q_1+q'_2} & * \, \lambda^{q_1+q'_3} \\ * \, \lambda^{q_2+q'_1} & * \, \lambda^{q_2+q'_2} & * \, \lambda^{q_2+q'_3} \\ * \, \lambda^{q_3+q'_1} & * \, \lambda^{q_3+q'_2} & * \, \lambda^{q_3+q'_3} \end{pmatrix} , \tag{2.25}$$

where the asterisks "$*$" denote $\mathcal{O}(1)$ parameters, and q_i are the charges of the fermions under the flavour symmetry. If the third family is uncharged, i.e. $q_3 = q'_3 = 0$, the entry Y_{33} can also be allowed at the tree level and thus be of the order of 1. Further variations of the scenario are possible, for instance replacing U(1) by a non-Abelian symmetry.

Needless to say, a vast number of models exist that combine the approaches mentioned in this section or employ further ideas. Examples are anarchy, supersymmetric theories with R-parity violation, radiative generation or enhancement of masses and mixings, and models with additional spacetime dimensions such as orbifold GUTs or dimensional deconstruction. Describing them in detail would be far beyond the scope of this work. Instead, we will now turn to radiative corrections in quantum field theories, which are very important for model building, since they imply that the flavour structure observed in experiments is not necessarily identical to the structure that has to be explained in fermion mass models.

Chapter 3

Renormalization and Renormalization Group Equations

3.1 Introduction

When calculating quantum corrections to physical processes due to loops, one inevitably encounters infinities. As a simple example, consider the following self-energy diagram for a real scalar field in ϕ^4 theory:

$$i\Sigma_\phi := \quad = \frac{1}{2}\lambda \int \frac{\mathrm{d}^4k}{(2\pi)^4}\,\frac{1}{k^2-m^2} = \frac{i\lambda}{2}\int \frac{\mathrm{d}^4k_E}{(2\pi)^4}\,\frac{1}{-k_E^2-m^2} =$$

$$= -\frac{i\lambda}{32\pi^2}\left[k_E^2 - m^2\ln\!\left(1+\tfrac{k_E^2}{m^2}\right)\right]_0^\infty \,, \tag{3.1}$$

where k is the 4-momentum of the particle in the loop and where we have Wick-rotated to Euclidean space by changing variables to $k^0 := ik_E^4$, $\vec{k} := \vec{k}_E$ and defining $k_E^2 := \vec{k}_E^{\,2} + (k_E^4)^2$. The result shows that the diagram is divergent. The same problem occurs on a regular basis when other loop diagrams are computed. Consequently, it is necessary to find a way to deal with these divergences. It consists of the two steps regularization and renormalization.

3.2 Regularization

3.2.1 Ultraviolet Cutoff

There are several methods of regularization, which all involve introducing some parameter, or regulator, that makes all diagrams finite. The divergence is then recovered in an appropriate limit of the regulator.

The simplest procedure is cutting off the integration over the loop momentum at some value Λ which is much larger than all other relevant energy scales. In our example, this

corresponds to changing the upper limit of the integration over $|k_E|$ in eq. (3.1) from ∞ to Λ. Then we find

$$\Sigma_\phi = -\frac{\lambda}{32\pi^2}\left[\Lambda^2 - m^2 \ln\bigl(1+\tfrac{\Lambda^2}{m^2}\bigr)\right]. \tag{3.2}$$

The Λ^2-term shows that the diagram in eq. (3.1) is quadratically divergent, which causes the hierarchy problem in the SM: the loop correction drives the Higgs mass towards the high-energy scale where the model is embedded into some other theory, such as a GUT. Hence, a severe fine-tuning is necessary to obtain a Higgs mass of the order of the electroweak scale and to stabilize it against quantum corrections. One way to solve the second task is supersymmetry, where the additional contributions by superparticles in the loops cancel all quadratic divergences. Therefore, the MSSM contains only logarithmic divergences of the form $\ln \frac{\Lambda^2}{m^2}$ if an ultraviolet cutoff is used. Alternative approaches towards the hierarchy problem employ large extra dimensions [75] or the dynamical breaking of the electroweak symmetry [76–78], and neutrinos may play a special role here as well [79].

Cutoff regularization has the serious disadvantage of breaking local gauge invariance, which makes it inadequate for gauge theories. Because of this, we will use a different method in the following, which is called dimensional regularization.

3.2.2 Dimensional Regularization

Here divergences are removed by reducing the number of spacetime dimensions to $d := 4 - \epsilon$. Defining this in a mathematically clean way involves some subtleties, including the fact that one actually has to work in an infinite-dimensional vector space [80], but for practical purposes this is not a problem. After evaluating the d-dimensional integrals, the results are expanded in powers of ϵ. Terms of order ϵ and higher are not relevant, because they will vanish when one finally goes back to 4 spacetime dimensions.

Compared to the 4-dimensional case, the mass dimensions of the fields are changed. They are determined by the condition that the action $\int \mathrm{d}^d x\, \mathscr{L}$ be dimensionless, which means that the Lagrangian has mass dimension d. For instance, we can use the fact that the kinetic term of a real scalar field is $\frac{1}{2}(\partial_\mu\phi)(\partial^\mu\phi)$ to derive $[\phi] = \frac{d-2}{2}$. In order to keep the coupling constants dimensionless, we add appropriate powers of an arbitrary energy scale μ, the renormalization scale, to the interaction terms. In the above example, we replace $\lambda \to \mu^\epsilon \lambda$ and then find

$$\Sigma_\phi = -\frac{i}{2}\mu^\epsilon\lambda \int \frac{\mathrm{d}^d k}{(2\pi)^d}\,\frac{1}{k^2 - m^2} = \frac{\lambda}{32\pi^2}\, m^2 \left[\frac{2}{\epsilon} + \ln 4\pi - \gamma_\mathrm{E} + 1 + \ln\frac{\mu^2}{m^2} + \mathscr{O}(\epsilon)\right], \tag{3.3}$$

where $\gamma_\mathrm{E} = 0.5772\ldots$ is Euler's constant.

Several other regularization schemes exist, for instance the Pauli-Villars method and lattice regularization. Results for physical quantities such as cross sections have to be

independent of the choice of the regularization prescription. It is even possible to avoid regularization completely by using the BPHZ scheme, as long as one is not considering non-Abelian gauge theories [80].

3.3 Renormalization

Calculating higher orders in the perturbative expansion, corresponding to Feynman diagrams with loops, yields quantum corrections of the parameters of a theory. For example, the diagram in eq. (3.1) is responsible for a shift in the particle mass. What is measured in an experiment, are the parameters that result after including corrections from all orders in perturbation theory. They are called renormalized parameters, in contrast to the bare ones that one would obtain if the quantum corrections were removed. In the following, bare quantities will be indicated by a subscript B, while those without this subscript will be considered to be renormalized.

In a relativistic field theory, only the renormalized quantities can be measured, since they differ from the bare ones due to interactions with virtual particles that cannot be "switched off". Consequently, we may assume that the unobservable bare parameters are infinite in such a way that their divergences cancel those of the quantum corrections, thus producing finite renormalized parameters. This is the basic idea of renormalization.

It should be noted that even without divergences quantum corrections produce differences between bare and renormalized parameters. For example, an electron in a solid behaves like a particle with an effective mass that is different from its mass in vacuum. Therefore, the need for renormalization is a rather general phenomenon in quantum field theory, independent of the appearance of infinities.

To implement it in calculations, bare and renormalized parameters are related using renormalization constants which contain the divergences, for instance $\lambda_\mathrm{B} = \mu^\epsilon Z_\phi^{-2} Z_\lambda \lambda$ in ϕ^4 theory if dimensional regularization is used. This has also to be done for the fields, in this example $\phi_\mathrm{B} = Z_\phi^{1/2}\phi$, in order to obtain finite Green's functions. Z_ϕ is called wavefunction renormalization constant. After expanding the renormalization constants in powers of the deviation from 4 dimensions,

$$Z_i := 1 + \delta Z_i = 1 + \sum_{k\geq 1} \delta Z_{i,k} \frac{1}{\epsilon^k} \,, \tag{3.4}$$

where the $\delta Z_{i,k}$ are independent of ϵ, the bare Lagrangian is split into a renormalized and a counterterm part, for instance

$$\begin{aligned} \mathscr{L}_\phi = {} & \frac{1}{2}(\partial_\mu\phi)(\partial^\mu\phi) - \frac{m^2}{2}\phi^2 - \frac{1}{4!}\mu^\epsilon \lambda\, \phi^4 + \\ & + \frac{\delta Z_\phi}{2}(\partial_\mu\phi)(\partial^\mu\phi) - \frac{\delta m^2}{2}\phi^2 - \frac{1}{4!}\mu^\epsilon \delta Z_\lambda \lambda\, \phi^4. \end{aligned} \tag{3.5}$$

Both parts would yield infinities if considered separately, but the counterterms (the terms on the second line) are chosen in such a way that the divergences cancel exactly.

This procedure can be applied successfully, if the number of divergent Green's functions is finite. Otherwise, an infinite number of counterterms would be needed, implying an infinite number of physical parameters and thus destroying the predictivity of the theory. In this case, the theory is called non-renormalizable. It can be shown that this happens if one or more coupling constants have a negative mass dimension. Conversely, if all couplings are dimensionless or have a positive dimension, renormalization is possible in principle. However, there are special cases where it fails although the mass dimensions of all coupling constants are non-negative, for example if counterterms are needed that do not correspond to any terms in the bare Lagrangian. Therefore, a rigorous proof of renormalizability is non-trivial.

The SM and MSSM with massless neutrinos as well as their extensions by right-handed neutrinos or additional Higgs fields have been proven to be renormalizable [81–83]. Effective theories, on the other hand, are non-renormalizable, since their Lagrangians contain all terms that are not excluded for symmetry reasons, including irrelevant operators with coupling constants of negative mass dimension. Nevertheless, effective theories can give useful physical predictions, since they are only valid up to a certain energy and the effects of irrelevant operators are suppressed by powers of this energy scale. To obtain a given accuracy, one performs an expansion in inverse powers of this scale and keeps only as many terms as needed, discarding all higher-order contributions. Consequently, merely a finite number of terms appear in the Lagrangian, and a finite number of counterterms are sufficient, so that the effective theory can be treated like a renormalizable one.

In the EFTs we consider in this work, the scale responsible for the suppression of irrelevant operators is the see-saw scale. As we restrict ourselves to the leading order, only one effective operator has to be taken into account, the dimension 5 neutrino mass operator of eq. (2.19) or (2.22), respectively, and only terms proportional to κ are kept in loop calculations.

3.4 Renormalization Schemes

In eq. (3.4), we have already applied a particular renormalization scheme, minimal subtraction (MS). Different definitions of the renormalization constants are possible by including additional finite parts in δZ_i, because this implies only a finite change of the unobservable bare parameters without affecting the cancellation of infinities. This corresponds to different renormalization schemes.

Regardless of the choice of a renormalization scheme, calculations of physical quantities, which are directly accessible by experiment, must always yield the same result.[1]

[1] Strictly speaking, this is not true for calculations up to a finite order in perturbation theory, since only the complete perturbative series would be renormalization scheme independent.

This means that renormalized quantities cannot necessarily be identified with physical ones, because they are scheme-dependent. However, they can be calculated from physical quantities once a scheme is picked, and in this sense they are measurable as well.

Minimal subtraction is particularly simple, since it defines the counterterms in such a way that only the divergences are canceled. Another advantage is that the renormalization constants are independent of particle masses in this scheme, as long as only logarithmic divergences appear. This is because the counterterms have no finite parts but depend only on the divergences, which arise at very large momenta, where the effects of masses are negligible. As the renormalization constants are dimensionless, they do not depend explicitly on the renormalization scale either. The same is true for the β-functions defined below. For dimensionless quantities, they are mass-independent as well.

Today, the most commonly used renormalization scheme is modified minimal subtraction, or $\overline{\text{MS}}$ [84]. Compared to MS, the finite term $\ln 4\pi - \gamma_\text{E}$ is subtracted in addition to the divergence by changing the renormalization scale to $\mu_{\overline{\text{MS}}} = \mu\, e^{\gamma_\text{E}/2}\,(4\pi)^{-1/2}$. We nevertheless adhere to the MS scheme, because in our calculations we will only need the infinite parts of the renormalization constants, which are equal in MS and $\overline{\text{MS}}$ at the one-loop level.

3.5 Renormalization Group Equations

One of the most interesting consequences of renormalization is the running or renormalization group (RG) evolution of the parameters such as coupling constants and masses of a theory, which means that they depend on energy. This can be seen from the relation between the bare and the renormalized quantities. It can always be cast into the form

$$Q_\text{B} = \left(\prod_{i\in I} Z_{\phi_i}^{n_i}\right) [Q + \delta Q]\, \mu^{D_Q \epsilon} \left(\prod_{j\in J} Z_{\phi_j}^{n_j}\right) , \tag{3.6}$$

where $I := \{1, \ldots, M\}$ and $J := \{M+1, \ldots, N\}$. Z_{ϕ_i} are wavefunction renormalization constants. In general, all quantities in eq. (3.6) except $\mu^{D_Q\epsilon}$ are tensors, for example Yukawa coupling matrices. We explicitly include the possibility that Q cannot be multiplicatively renormalized, which is the case for the coupling of the effective neutrino mass operator. All bare quantities are independent of the choice of the renormalization scheme. In particular, they remain constant under a change of the renormalization scale μ. For an infinitesimal change, this means that their total derivatives with respect to μ have to be zero. Consequently, the total derivative of the right hand side of eq. (3.6) with respect to μ vanishes. This is only possible if Q depends on μ. Thus, coupling constants and masses are actually no constants, but instead depend on the renormalization scale, which translates into a dependence on the energy scale at which an experiment is done.

An often cited analogy is the screening of an electric charge in a medium due to the surrounding atomic dipoles. This effect becomes weaker at decreasing distance from the charge, corresponding to increasing energy of the particles in a scattering experiment. Consequently, one obtains a larger value for the charge, if the measurement is done at a higher energy. In the case of QED, the screening is caused by the polarization of the vacuum due to virtual particle-antiparticle pairs. For the coupling constants of non-Abelian gauge theories like QCD, the opposite running is observed, i.e. they decrease with increasing energy and hence are asymptotically free. This is caused by virtual gauge particles, which lead to an antiscreening effect, comparable to that in a paramagnetic medium.

The running is determined by the renormalization group equations (RGEs),

$$\mu \frac{\mathrm{d}Q}{\mathrm{d}\mu} = \beta_Q \,, \tag{3.7}$$

where β_Q is called the β-function of Q. A method for calculating β-functions in MS-like renormalization schemes has been derived in [17, 85, 86]. Therefore, we give only the final result,

$$\beta_Q = \beta_Q^{(0)} - D_Q Q\, \epsilon \,, \tag{3.8a}$$

where

$$\begin{aligned}\beta_Q^{(0)} = {} & D_Q \left\langle \frac{\mathrm{d}\,\delta Q_{,1}}{\mathrm{d}Q} \middle| Q \right\rangle + \sum_A D_{V_A} \left\langle \frac{\mathrm{d}\,\delta Q_{,1}}{\mathrm{d}V_A} \middle| V_A \right\rangle - D_Q\, \delta Q_{,1} + \\ & + \sum_{i\in I} n_i \left[D_Q \left\langle \frac{\mathrm{d}\,\delta Z_{\phi_i,1}}{\mathrm{d}Q} \middle| Q \right\rangle + \sum_A D_{V_A} \left\langle \frac{\mathrm{d}\,\delta Z_{\phi_i,1}}{\mathrm{d}V_A} \middle| V_A \right\rangle \right] Q + \\ & + Q \sum_{j\in J} n_j \left[D_Q \left\langle \frac{\mathrm{d}\,\delta Z_{\phi_j,1}}{\mathrm{d}Q} \middle| Q \right\rangle + \sum_A D_{V_A} \left\langle \frac{\mathrm{d}\,\delta Z_{\phi_j,1}}{\mathrm{d}V_A} \middle| V_A \right\rangle \right] . \end{aligned} \tag{3.8b}$$

The second expression is the relevant part of the β-function, because the terms proportional to ϵ vanish in 4 dimensions. V_A are the parameters of the theory besides Q, and

$$\delta Q := \sum_{k\geq 1} \delta Q_{,k}\, \frac{1}{\epsilon^k} \,. \tag{3.9}$$

The brackets stand for the abbreviation

$$\left\langle \frac{\mathrm{d}F}{\mathrm{d}x} \middle| y \right\rangle := \begin{cases} \dfrac{\mathrm{d}F}{\mathrm{d}x}\, y & \text{for scalars } x, y \\ \dfrac{\mathrm{d}F}{\mathrm{d}x_{mn}}\, y_{mn} & \text{for matrices } x = (x_{mn}), y = (y_{mn}) \end{cases} \tag{3.10}$$

etc. A nice feature of eq. (3.8) is that it only depends on the $\frac{1}{\epsilon}$-poles of the renormalization constants, which simplifies calculations beyond one-loop order. It also shows that the β-functions do not explicitly depend on masses and on the renormalization scale, because the same is true for the renormalization constants. Moreover, they are gauge-independent.

The RG evolution of several quantities, for example the coupling constants of QED and QCD, can be measured in collider experiments. For neutrino mass parameters, this is not possible as the current experimental uncertainties are much larger than the effects of renormalization in the experimentally accessible energy range. Nevertheless, they are also important in this context because theoretical predictions from theories beyond the SM, such as GUTs, are typically valid at some very high energy scale, while experimental data are taken at lower energies. For example, the energies of solar and reactor neutrinos are of the order of 1–10 MeV, those of atmospheric ones reach up to about 100 GeV, and energies in accelerator neutrino experiments are in the GeV range. Therefore, it is essential to allow for the running of the parameters between these energies and the high scale when comparing experimental results and theoretical predictions.

Chapter 4

Running of Lepton Masses and Mixings

4.1 RG Evolution below the See-Saw Scale

In this chapter, we apply the methods of renormalization described in the previous sections to calculate the change of the lepton flavour structure due to quantum corrections. We start by considering the SM and MSSM in the effective field theory approach of sec. 2.4.1 involving the dimension 5 neutrino mass operators (2.19) and (2.22). This approach can be used for energies below the see-saw scale, where these operators are generated. Later on, we will also discuss the running above this scale in the type I see-saw scenario.

It should be pointed out that using the effective theory for calculating the evolution of the lepton mass parameters below the see-saw scale is not just a matter of convenience, but essential in order to obtain meaningful results. This is due to the Appelquist-Carazzone theorem [87], which states that heavy particles decouple at energies much smaller than their masses, so that physics is independent of them at these energies, except for the possible appearance of effective operators like $\mathscr{L}_\kappa$. In particular, heavy particles do not contribute to the β-functions at low energy. This behavior can clearly be seen, if the β-functions are calculated in a mass-dependent renormalization scheme. However, it is not contained in MS β-functions, since they are independent of masses. Hence, the β-functions of the high-energy theory cannot produce the correct RG running at low energies. Consequently, it is necessary to remove the heavy particles from the theory by hand, i.e. to integrate them out and to use the EFT [88].

4.1.1 Beta-Functions for the Neutrino Mass Operator

In order to find the one-loop RGEs for the dimension 5 neutrino mass operator, one has to calculate the divergent parts of all one-loop corrections to the effective vertex. In the SM, this involves Feynman diagrams like the one shown in fig. 4.1, which evaluates to

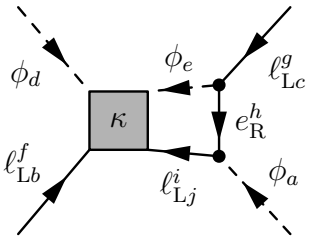

Figure 4.1: Example for a one-loop diagram contributing to the renormalization of the effective neutrino mass operator in the SM. ℓ_{L} denotes the left-handed lepton doublets, ϕ the Higgs, and e_{R} the right-handed charged leptons.

$$\begin{aligned}
i\mu^\epsilon(\Gamma^{e(4)}_\kappa)^{abcd}_{gf} &= \left[-i\mu^{\frac{\epsilon}{2}}(Y_e^T)_{gh}\delta_{ce}\right]\left[-i\mu^{\frac{\epsilon}{2}}(Y_e^*)_{hi}\delta_{aj}\right]\left[i\mu^\epsilon\kappa_{if}\tfrac{1}{2}(\varepsilon_{je}\varepsilon_{bd}+\varepsilon_{be}\varepsilon_{jd})\right]\times \\
&\quad\times\int\frac{\mathrm{d}^dk}{(2\pi)^d}\,P_{\mathrm{L}}\frac{-i(\not p+\not k)}{(p+k)^2}P_{\mathrm{R}}\frac{-i(\not p-\not q'+\not k)}{(p-q'+k)^2}P_{\mathrm{L}}\frac{i}{k^2-m^2} \\
&= -\frac{i}{16\pi^2}\mu^\epsilon(Y_e^TY_e^*\kappa)_{gf}\tfrac{1}{2}(\varepsilon_{ac}\varepsilon_{bd}+\varepsilon_{bc}\varepsilon_{ad})\times \\
&\quad\times\frac{\mu^\epsilon}{i\pi^2}\int\mathrm{d}^dk\,\frac{\not p+\not k}{(p+k)^2}\frac{\not p-\not q'+\not k}{(p-q'+k)^2}\frac{1}{k^2-m^2}P_{\mathrm{L}} \\
&= \frac{i}{8\pi^2}\mu^\epsilon(Y_e^TY_e^*\kappa)_{gf}\tfrac{1}{2}(\varepsilon_{ca}\varepsilon_{bd}-\varepsilon_{cb}\varepsilon_{da})P_{\mathrm{L}}\frac{1}{\epsilon}+\text{UV finite}\,, \qquad (4.1)
\end{aligned}$$

where "UV finite" stands for terms that are finite as $\varepsilon\to 0$ and thus not relevant for the calculation of the β-function. p, p', q, q' are the momenta of the external particles, k is the loop momentum, and $P_{\mathrm{R,L}}$ denote the chirality projectors $\frac{1}{2}(1\pm\gamma_5)$. The Feynman rules used for the calculation can be found in [85]. In addition to the vertex corrections, the wavefunction renormalization constants of the external particles are needed. As the calculations have been described in detail in [17,18,85,86,89], we immediately give the result here. The MSSM β-function has been first derived in [90,91].

The RGEs for the effective neutrino mass operator in the SM and MSSM read

$$16\pi^2\,\frac{\mathrm{d}\kappa}{\mathrm{d}t} = C\,(Y_e^\dagger Y_e)^T\,\kappa + C\,\kappa\,(Y_e^\dagger Y_e) + \alpha\,\kappa\,, \qquad (4.2)$$

where we have introduced the abbreviation $t := \ln(\mu/\mu_0)$ with an arbitrary energy scale μ_0. The first two terms contain the matrix of charged lepton Yukawa couplings Y_e and thus distinguish between the generations. Hence, they are responsible for the running of the mixing parameters. They are multiplied by the factors

$$C = -\frac{3}{2} \quad \text{in the SM}, \qquad (4.3a)$$

$$C = 1 \quad \text{in the MSSM}. \qquad (4.3b)$$

The last term contains

$$\alpha_{\mathrm{SM}} = -3g_2^2 + 2\left(y_\tau^2 + y_\mu^2 + y_e^2\right) + 6\left(y_t^2 + y_b^2 + y_c^2 + y_s^2 + y_d^2 + y_u^2\right) + \lambda \,, \tag{4.4a}$$

$$\alpha_{\mathrm{MSSM}} = -\frac{6}{5}g_1^2 - 6g_2^2 + 6\left(y_t^2 + y_c^2 + y_u^2\right) \,, \tag{4.4b}$$

where g_1, g_2 are the gauge couplings of $\mathrm{U}(1)_\mathrm{Y}$ and $\mathrm{SU}(2)_\mathrm{L}$, respectively, y_i are Yukawa couplings, and λ is the quartic Higgs self-coupling. We use GUT charge normalization for g_1, i.e. it is related to the conventional SM coupling $\tilde{g}_1$ by $g_1^2 = \frac{5}{3}\tilde{g}_1^2$. The α's consist only of real numbers and are thus flavour-blind. Hence, they influence the running of the mass eigenvalues but not that of the mixings.

In order to calculate the evolution of the neutrino mass matrix, eq. (4.2) is not sufficient, since all the couplings it contains are running quantities themselves. Their RGEs are listed in app. B. Hence, one needs to solve a rather complex system of coupled differential equations, which can only be done numerically. Nevertheless, it is possible to gain an analytic insight into the running of the neutrino masses and mixings by employing suitable approximations. To this aim, we will translate eq. (4.2) into differential equations for these quantities next [21, 92, 93].

4.1.2 RGEs for the Lepton Mass Parameters

Derivation

The derivation of the RGEs for the neutrino mass eigenvalues and mixing parameters is similar to the analogous calculation in the quark sector [94]. For briefness, we define $P := C\left(Y_e^\dagger Y_e\right)$. We work in the basis where Y_e is diagonal. In this basis, we have $V_{\mathrm{MNS}} = U^\nu$. As can be seen from the RGE (B.3f) or (B.5f), respectively, the running does not create off-diagonal entries in Y_e in the energy region below the see-saw scale, where the neutrino Yukawa couplings do not contribute. We start from the inverted form of eq. (2.12a),

$$U^{\nu *} D\, U^{\nu \dagger} = m_\nu \,, \tag{4.5}$$

where $D := \mathrm{diag}(m_1, m_2, m_3)$. Differentiating with respect to t yields in combination with eq. (4.2)[1]

$$\dot{U}^{\nu *} D\, U^{\nu \dagger} + U^{\nu *} D\, \dot{U}^{\nu \dagger} + U^{\nu *} \dot{D}\, U^{\nu \dagger} = \frac{1}{16\pi^2}\left(P^T U^{\nu *} D\, U^{\nu \dagger} + U^{\nu *} D\, U^{\nu \dagger}\, P + \alpha\, U^{\nu *} D\, U^{\nu \dagger}\right). \tag{4.6}$$

[1] We do not take into account the running of the Higgs VEV. We *define* the neutrino mass matrix as $m_\nu(t) := -\frac{v(0)^2}{4}\kappa(t)$ with $v(0) = 246$ GeV or $v(0) = \sin\beta \cdot 246$ GeV. In principle, v runs as well, but its evolution depends on the renormalization scheme and on the definition of the Higgs mass, see e.g. [95], so that there is no straightforward definition of a neutrino mass with a running VEV.

Multiplying with $U^{\nu T}$ from the left and with U^ν from the right and exploiting the unitarity of U^ν, we obtain

$$U^{\nu T}\dot{U}^{\nu *} D + D\,\dot{U}^{\nu\dagger}U^\nu + \dot{D} = \frac{1}{16\pi^2}\left[\alpha\, D + P'^T D + D\, P'\right], \tag{4.7}$$

where we have introduced $P' := U^{\nu\dagger} P\, U^\nu$. Next, we define the anti-Hermitian matrix T by

$$\dot{U}^\nu = U^\nu\, T\ . \tag{4.8}$$

With this definition, we find

$$\dot{D} = \frac{1}{16\pi^2}\left(\alpha\, D + P'^T D + D\, P'\right) - T^* D + D\, T\ , \tag{4.9}$$

where the anti-hermiticity of T has been used in the last term. For the diagonal elements, this implies

$$\dot{m}_i = \frac{1}{16\pi^2}\left(\alpha + 2P'_{ii}\right) m_i + \left(T_{ii} - T^*_{ii}\right) m_i\ . \tag{4.10}$$

Note that here and in the following equations, no sum over repeated indices is implied. As the mass eigenvalues are real by definition, the imaginary part of the right hand side of eq. (4.10) has to be zero, i.e.

$$2\,\mathrm{Im}\, T_{ii} = -\frac{1}{16\pi^2}\left(\mathrm{Im}\,\alpha + 2\,\mathrm{Im}\, P'_{ii}\right). \tag{4.11}$$

The real part of eq. (4.10) yields eq. (15) of [93], the RGE for the mass eigenvalues, which reads with our conventions

$$16\pi^2\,\dot{m}_i = \left(\mathrm{Re}\,\alpha + 2\,\mathrm{Re}\, P'_{ii}\right) m_i\ . \tag{4.12}$$

Eq. (4.11) differs from Eq. (19) of [93], where the imaginary part of α is not present; however, this difference is irrelevant in the SM and the MSSM, where α is real. Note that only the moduli of U^ν_{ij} enter into the diagonal elements of P', if P is diagonal, $P = \mathrm{diag}(P_1, P_2, P_3)$ (which is the case in the SM and MSSM in the basis we use), since

$$P'_{ii} = \sum_{jk} (U^{\nu\dagger})_{ij} P_{jk} U^\nu_{ki} = \sum_{jk} U^{\nu *}_{ji} P_j \delta_{jk} U^\nu_{ki} = \sum_j |U^\nu_{ji}|^2 P_j\ . \tag{4.13}$$

Together with eq. (4.12), this implies that the running of the mass eigenvalues does not directly depend on the Majorana phases.

To determine the evolution of the mixing parameters, we use the off-diagonal parts of eq. (4.9),

$$m_i\, T_{ij} - T^*_{ij}\, m_j = -\frac{1}{16\pi^2}\left(m_j P'_{ji} + m_i\, P'_{ij}\right) \tag{4.14}$$

for $i \neq j$. Adding and subtracting this equation and its complex conjugate, we obtain

$$16\pi^2 \operatorname{Re} T_{ij} = -\frac{m_j \operatorname{Re} P'_{ji} + m_i \operatorname{Re} P'_{ij}}{m_i - m_j} , \tag{4.15a}$$

$$16\pi^2 \operatorname{Im} T_{ij} = -\frac{m_j \operatorname{Im} P'_{ji} + m_i \operatorname{Im} P'_{ij}}{m_i + m_j} . \tag{4.15b}$$

Note that this step is not possible if the states ν_i and ν_j have degenerate masses, so that our results cannot be applied then. For a discussion of RG effects in this case, see for example [96–100]. Using eqs. (4.15) together with eqs. (4.8) and (2.15), one can now determine the differential equations for the running of the mixing angles and phases in terms of T and the MNS matrix elements [93]. In order to obtain expressions which are as short as possible and show the dependence on the mixing parameters explicitly, we extend the derivation by an additional step. As P and P' are Hermitian, we can use $\operatorname{Re} P'_{ji} = \operatorname{Re} P'^*_{ij} = \operatorname{Re} P'_{ij}$ and $\operatorname{Im} P'_{ji} = \operatorname{Im} P'^*_{ij} = -\operatorname{Im} P'_{ij}$ to simplify eqs. (4.15) to

$$16\pi^2 \operatorname{Re} T_{ij} = -\frac{m_i + m_j}{m_i - m_j} \operatorname{Re} P'_{ij} , \tag{4.16a}$$

$$16\pi^2 \operatorname{Im} T_{ij} = -\frac{m_i - m_j}{m_i + m_j} \operatorname{Im} P'_{ij} . \tag{4.16b}$$

Plugging this result as well as the standard parameterization (2.15) into the inverted form of eq. (4.8),

$$U^{\nu\dagger} \dot{U}^{\nu} = T , \tag{4.17}$$

we can write the left hand side of the resulting equation as a function of the mixing parameters and their derivatives. If we combine the mixing parameters in the vector $(\xi_k) := (\theta_{12}, \theta_{13}, \theta_{23}, \delta, \delta_e, \delta_\mu, \delta_\tau, \varphi_1, \varphi_2)^T$, the expression is linear in $\dot{\xi}_k$. Therefore, by solving the corresponding system of linear equations, we can express the derivatives of the mixing parameters by the mixing parameters, the mass eigenvalues and the charged lepton Yukawa couplings. The resulting formulae are too long to be presented here, but can be obtained from `http://www.ph.tum.de/~mratz/AnalyticFormulae/` [21].

Approximations

The RGEs derived above can be simplified considerably by neglecting the small Yukawa couplings of the electron and muon against the one of the tau and by keeping only the leading terms in an expansion in the small angle θ_{13} [21]. These approximations turn out to be accurate enough to understand the RG evolution qualitatively and in many cases also quantitatively. We will use the abbreviation

$$\zeta := \frac{\Delta m^2_\odot}{\Delta m^2_{\mathrm{a}}} \tag{4.18}$$

for the ratio of the solar and atmospheric mass squared differences. The current best-fit value is about 0.03. For the mixing angles, we obtain the approximate RGEs

$$\dot{\theta}_{12} = -\frac{Cy_\tau^2}{32\pi^2}\,\sin 2\theta_{12}\, s_{23}^2\,\frac{|m_1\, e^{i\varphi_1} + m_2\, e^{i\varphi_2}|^2}{\Delta m_\odot^2} + \mathscr{O}(\theta_{13})\,, \tag{4.19}$$

$$\begin{aligned}\dot{\theta}_{13} = {} & \frac{Cy_\tau^2}{32\pi^2}\,\sin 2\theta_{12}\,\sin 2\theta_{23}\,\frac{m_3}{\Delta m_{\rm a}^2\,(1+\zeta)}\,\times \\ & \times\left[m_1\cos(\varphi_1-\delta) - (1+\zeta)\,m_2\,\cos(\varphi_2-\delta) - \zeta m_3\,\cos\delta\right] + \mathscr{O}(\theta_{13})\,,\end{aligned} \tag{4.20}$$

$$\dot{\theta}_{23} = -\frac{Cy_\tau^2}{32\pi^2}\,\sin 2\theta_{23}\,\frac{1}{\Delta m_{\rm a}^2}\left[c_{12}^2\,|m_2\, e^{i\varphi_2} + m_3|^2 + s_{12}^2\,\frac{|m_1\, e^{i\varphi_1} + m_3|^2}{1+\zeta}\right] + \mathscr{O}(\theta_{13})\,. \tag{4.21}$$

If θ_{13} is exactly zero, one has to use eq. (4.20) together with the analytic continuation eq. (4.33) for the Dirac phase, which will be explained later in this section. The $\mathscr{O}(\theta_{13})$ terms in the above equations can become important if θ_{13} is not too small and in particular if cancellations appear in the leading terms. For example, in (4.19) this is the case for $|\varphi_1 - \varphi_2| = \pi$, as we will discuss below in more detail. The RGE for the Dirac phase is given by

$$\dot{\delta} = \frac{Cy_\tau^2}{32\pi^2}\frac{\delta^{(-1)}}{\theta_{13}} + \frac{Cy_\tau^2}{8\pi^2}\delta^{(0)} + \mathscr{O}(\theta_{13}) \tag{4.22a}$$

with

$$\begin{aligned}\delta^{(-1)} = {} & \sin 2\theta_{12}\,\sin 2\theta_{23}\,\frac{m_3}{\Delta m_{\rm a}^2\,(1+\zeta)}\,\times \\ & \times\left[m_1\sin(\varphi_1-\delta) - (1+\zeta)\,m_2\,\sin(\varphi_2-\delta) + \zeta m_3\,\sin\delta\right],\end{aligned} \tag{4.22b}$$

$$\begin{aligned}\delta^{(0)} = {} & \frac{m_1 m_2\, s_{23}^2\,\sin(\varphi_1-\varphi_2)}{\Delta m_\odot^2} + \\ & + m_3\, s_{12}^2\left[\frac{m_1\,\cos 2\theta_{23}\,\sin\varphi_1}{\Delta m_{\rm a}^2(1+\zeta)} + \frac{m_2\, c_{23}^2\,\sin(2\delta-\varphi_2)}{\Delta m_{\rm a}^2}\right] \\ & + m_3\, c_{12}^2\left[\frac{m_1\, c_{23}^2\,\sin(2\delta-\varphi_1)}{\Delta m_{\rm a}^2(1+\zeta)} + \frac{m_2\,\cos 2\theta_{23}\,\sin\varphi_2}{\Delta m_{\rm a}^2}\right].\end{aligned} \tag{4.22c}$$

For the Majorana phases, we find

$$\begin{aligned}\dot{\varphi}_1 = {} & \frac{Cy_\tau^2}{4\pi^2}\left\{m_3\,\cos 2\theta_{23}\,\frac{m_1 s_{12}^2\,\sin\varphi_1 + (1+\zeta)\,m_2\, c_{12}^2\,\sin\varphi_2}{\Delta m_{\rm a}^2\,(1+\zeta)} + \right. \\ & \left. + \frac{m_1 m_2\, c_{12}^2\, s_{23}^2\,\sin(\varphi_1-\varphi_2)}{\Delta m_\odot^2}\right\} + \mathscr{O}(\theta_{13})\,,\end{aligned} \tag{4.23}$$

$$\begin{aligned}\dot{\varphi}_2 = {} & \frac{Cy_\tau^2}{4\pi^2}\left\{m_3\,\cos 2\theta_{23}\,\frac{m_1 s_{12}^2\,\sin\varphi_1 + (1+\zeta)\,m_2\, c_{12}^2\sin\varphi_2}{\Delta m_{\rm a}^2\,(1+\zeta)} + \right. \\ & \left. + \frac{m_1 m_2\, s_{12}^2\, s_{23}^2\,\sin(\varphi_1-\varphi_2)}{\Delta m_\odot^2}\right\} + \mathscr{O}(\theta_{13})\,.\end{aligned} \tag{4.24}$$

In many cases, the above expressions can be simplified further by neglecting ζ against 1 without losing much accuracy. However, we have not made use of this approximation, since ζ may become sizable at high energies due to the running of the mass squared differences, as we will see later. Note that singularities can appear in the $\mathscr{O}(\theta_{13})$-terms at points in parameter space where the phases are not well-defined. For the mass eigenvalues, the results for $y_e = y_\mu = 0$ are relatively short, hence we show the full dependence on θ_{13},

$$16\pi^2\,\dot{m}_1 = \left[\alpha + C y_\tau^2 \left(2 s_{12}^2\, s_{23}^2 + F_1\right)\right] m_1 \;, \tag{4.25a}$$
$$16\pi^2\,\dot{m}_2 = \left[\alpha + C y_\tau^2 \left(2 c_{12}^2\, s_{23}^2 + F_2\right)\right] m_2 \;, \tag{4.25b}$$
$$16\pi^2\,\dot{m}_3 = \left[\alpha + 2C y_\tau^2\, c_{13}^2\, c_{23}^2\right] m_3 \;, \tag{4.25c}$$

where F_1 and F_2 contain the terms proportional to $\sin\theta_{13}$,

$$F_1 = -s_{13}\,\sin 2\theta_{12}\,\sin 2\theta_{23}\,\cos\delta + 2 s_{13}^2\, c_{12}^2\, c_{23}^2 \;, \tag{4.26a}$$
$$F_2 = \;\; s_{13}\,\sin 2\theta_{12}\,\sin 2\theta_{23}\,\cos\delta + 2 s_{13}^2\, s_{12}^2\, c_{23}^2 \;. \tag{4.26b}$$

These formulae can be translated into RGEs for the mass squared differences,

$$8\pi^2\,\frac{\mathrm{d}}{\mathrm{d}t}\Delta m_\odot^2 = \alpha\,\Delta m_\odot^2 + C y_\tau^2 \left[2 s_{23}^2 \left(m_2^2\, c_{12}^2 - m_1^2\, s_{12}^2\right) + F_\odot\right] , \tag{4.27a}$$
$$8\pi^2\,\frac{\mathrm{d}}{\mathrm{d}t}\Delta m_\mathrm{a}^2 = \alpha\,\Delta m_\mathrm{a}^2 + C y_\tau^2 \left[2 m_3^2\, c_{13}^2\, c_{23}^2 - 2 m_2^2\, c_{12}^2\, s_{23}^2 + F_\mathrm{a}\right] , \tag{4.27b}$$

where

$$F_\odot = \left(m_1^2 + m_2^2\right) s_{13}\,\sin 2\theta_{12}\,\sin 2\theta_{23}\,\cos\delta + 2 s_{13}^2\, c_{23}^2 \left(m_2^2\, s_{12}^2 - m_1^2\, c_{12}^2\right) , \tag{4.28a}$$
$$F_\mathrm{a} = -m_2^2\, s_{13}\,\sin 2\theta_{12}\,\sin 2\theta_{23}\,\cos\delta - 2 m_2^2\, s_{13}^2\, s_{12}^2\, c_{23}^2 \;. \tag{4.28b}$$

These expressions determine the slope of the RG evolution at a given energy scale and thus yield an insight into the energy dependence of the masses and mixing parameters. Note that a simple linear interpolation, i.e. assuming the right hand sides of the equations to be constant, will not always give the correct RG evolution. This is mainly due to large changes of θ_{12} and the mass squared differences.

Generic Size of the RG Effects

Let us next try a rough estimate of the generic size of the RG effects on the mixing angles and phases. All RGEs contain a factor involving the tau Yukawa coupling, which evaluates to

$$\frac{3 y_\tau^2}{64\pi^2} \approx 0.5 \cdot 10^{-6} \tag{4.29a}$$

	$\dot{\theta}_{12}$	$\dot{\theta}_{13}$	$\dot{\theta}_{23}$	$\dot{\delta}$	$\dot{\varphi}_i$
n.h.	1	$\sqrt{\zeta}$	1	$\sqrt{\zeta}\,\theta_{13}^{-1}$	$\sqrt{\zeta}$
p.d.(n.)	$\dfrac{m_1^2}{\Delta m_\odot^2}$	$\dfrac{m_1}{\sqrt{\Delta m_\mathrm{a}^2}}$	1	$\dfrac{m_1}{\sqrt{\Delta m_\mathrm{a}^2}}\theta_{13}^{-1} + \dfrac{m_1^2}{\Delta m_\odot^2}$	$\dfrac{m_1^2}{\Delta m_\odot^2}$
i.h.	ζ^{-1}	$\mathscr{O}(\theta_{13})$	1	ζ^{-1}	ζ^{-1}
p.d.(i.)	ζ^{-1}	$\dfrac{m_3}{\sqrt{\Delta m_\mathrm{a}^2}}$	1	$\dfrac{m_3}{\sqrt{\Delta m_\mathrm{a}^2}}\theta_{13}^{-1} + \zeta^{-1}$	ζ^{-1}
d.	$\dfrac{m^2}{\Delta m_\odot^2}$	$\dfrac{m^2}{\Delta m_\mathrm{a}^2}$	$\dfrac{m^2}{\Delta m_\mathrm{a}^2}$	$\dfrac{m^2}{\Delta m_\mathrm{a}^2}\theta_{13}^{-1} + \dfrac{m^2}{\Delta m_\odot^2}$	$\dfrac{m^2}{\Delta m_\odot^2}$

Table 4.1: Generic enhancement and suppression factors for the RG evolution of the mixing angles and phases. A '1' indicates that there is no generic enhancement or suppression. In this case, the running is usually insignificant. 'n.h.' and 'p.d.(n.)' denote the hierarchical and partially degenerate mass spectra in the case of a normal mass ordering, i.e. $m_1^2 \ll \Delta m_\odot^2$ or $\Delta m_\odot^2 \ll m_1^2 \lesssim \Delta m_\mathrm{a}^2$. 'i.h.' and 'p.d.(i.)' stand for the analogous spectra in the inverted case, i.e. $m_3^2 \ll \Delta m_\odot^2$ or $\Delta m_\odot^2 \ll m_3^2 \lesssim \Delta m_\mathrm{a}^2$. Finally, 'd.' means nearly degenerate masses, $\Delta m_\mathrm{a}^2 \ll m_1^2 \sim m_2^2 \sim m_3^2 \sim m^2$.

in the SM and

$$\frac{y_\tau^2}{32\pi^2} \approx 0.3 \cdot 10^{-6} \left(1 + \tan^2\beta\right) \tag{4.29b}$$

in the MSSM. If the running was linear on a logarithmic scale, it would yield a factor of e.g.

$$\ln \frac{M_1}{M_Z} = \ln \frac{10^{13}}{10^2} \approx 25 \tag{4.30}$$

for $M_1 = 10^{13}$ GeV. Clearly, these factors are too small to cause sizable changes by themselves even in the MSSM with a large $\tan\beta$. The necessary further enhancement can come from the mass-dependent terms, since they contain the mass squared differences in their denominators, so that large factors can arise if the absolute neutrino masses in the numerators are large enough. On the other hand, these terms can also cause a further suppression of the running. Under the assumption that the solar and atmospheric angles are large and that the CP phases do not cause severe cancellations, we find the generic enhancement and suppression factors listed in tab. 4.1. Denoting them by Γ_enh and using eqs. (4.29) and (4.30), we obtain an estimate for the change of the mixing angles and phases due to the RG evolution,

$$\Delta_\mathrm{RG} \sim 10^{-5} \left(1 + \tan^2\beta\right) \Gamma_\mathrm{enh}\ . \tag{4.31}$$

Of course, the factor $1 + \tan^2\beta$ has to be omitted in the SM. As an example, let us estimate the size of the absolute neutrino mass scale (the "amount of degeneracy")

needed for a sizable RG change of θ_{12}, say $0.1 \approx 6^\circ$. In the SM, this requires $\Gamma_{\rm enh} \sim 10^4$, corresponding to a neutrino mass of the order of 1 eV, which is excluded by cosmology and double beta decay experiments. On the other hand, in the MSSM this mass scale can easily be lowered to about 0.1 eV with $\tan\beta$ as small as 8. Thus, we conclude that the running of the mixing parameters is negligible for most purposes in the SM and in the MSSM with a small $\tan\beta$ or a strong normal mass hierarchy. Vice versa, significant RG effects are possible in the MSSM, if $\tan\beta$ is large and if the masses are at least partially degenerate or inversely hierarchical.

Even for a large enhancement factor, the RG evolution can be suppressed by the Majorana phases. For example, an opposite CP parity of the first and second mass eigenstate, i.e. $|\varphi_1 - \varphi_2| = \pi$, results in a maximal suppression of the running of the solar mixing angle [93,101–103]. Nevertheless, tab. 4.1 allows to determine which angles or phases have the potential for a significant RG evolution. Obviously, the expressions for $\dot{\delta}$ are not applicable for $\theta_{13} = 0$. This special case will be discussed later on.

After these general considerations, let us now discuss the running of the mixing angles, CP phases and masses in more detail. In order to check the reliability of the approximate RGEs, we compare their predictions to the results of a numerical solution of the RGE (4.2) for the neutrino mass operator and the RGEs for all the other couplings (cf. app. B). For the numerics we use the "run and diagonalize" approach, i.e. we first compute the running of the mass matrix and then extract the mass eigenvalues and mixing parameters at each energy between M_Z and the see-saw scale. In most examples, we consider the MSSM with $\tan\beta = 50$, a normal mass hierarchy, $m_1 = 0.1$ eV for the mass of the lightest neutrino, and a mass of about 120 GeV for the light Higgs. Besides, we use the best-fit values for the oscillation parameters. These boundary conditions are applied at the electroweak scale, i.e. we calculate the evolution from low to high energies. Below the SUSY-breaking scale, which we take to be $M_{\rm SUSY} = 1.5$ TeV, we assume the SM to be valid as an effective theory and use the corresponding RGEs.

RG Evolution of θ_{12}

From eq. (4.19), we can easily derive some important properties of the running of the solar angle which have been found – usually with considerably more effort – in earlier studies. Firstly, in the MSSM the solar angle always decreases when running upwards for $\theta_{13} = 0$ [104] due to the minus sign in the RGE. Secondly, a non-zero difference of the Majorana phases damps the running by decreasing $|m_1\, e^{i\varphi_1} + m_2\, e^{i\varphi_2}|$. This effect becomes maximal for $\varphi_1 - \varphi_2 = \pi$, which corresponds to opposite CP parities of the states with masses m_1 and m_2 [93,101–103]. In this case, the mass-dependent factor in eq. (4.19) is $(m_2 - m_1)/(m_2 + m_1)$, which is always smaller than 1 and becomes tiny for quasi-degenerate masses.

In addition to that, from tab. 4.1 we expect θ_{12} to experience the strongest RG effects among the mixing angles in general, since $\Delta m^2_\odot$ appears in the denominator of the enhancement factor, as opposed to the much larger atmospheric mass splitting

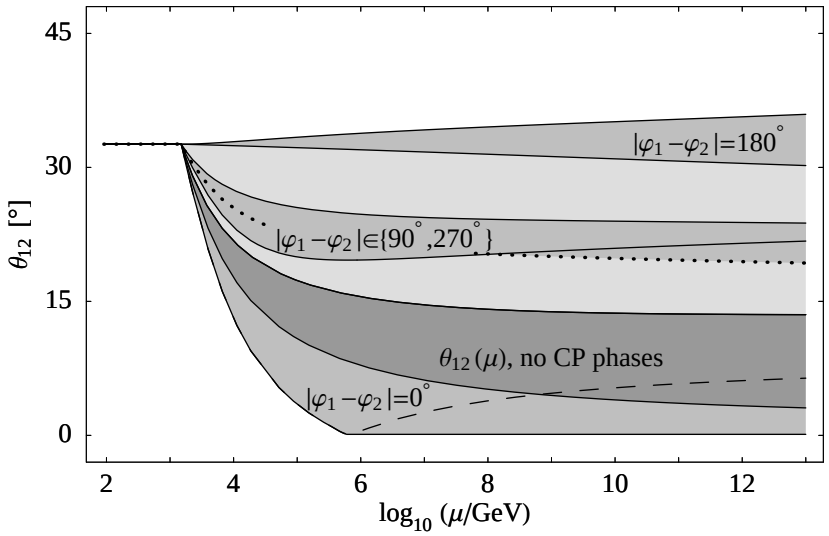

Figure 4.2: RG evolution of θ_{12} in the MSSM with $\tan\beta = 50$, a normal mass hierarchy and $m_1 = 0.1$ eV for the mass of the lightest neutrino. The dark-gray region shows the evolution with best-fit values for the neutrino oscillation parameters, $\theta_{13} \in [0°, 9°]$ and all CP phases equal to zero. The medium- and light-gray regions emerge from varying the phases, as explained in the text. The dashed line shows the RG evolution with $|\varphi_1 - \varphi_2| = 0$, $\theta_{13} = 9°$ and $\delta = 180°$. The dotted line is obtained for $|\varphi_1 - \varphi_2| = 90°$ and $\theta_{13} = 0°$.

which is relevant for θ_{13} and θ_{23}. An enhanced running generically occurs even if the lightest neutrino is massless, provided that the hierarchy is inverted, since in this case $m_1^2 \approx m_2^2 = \Delta m_{\rm a}^2$.

For comparison, fig. 4.2 shows the numerically determined running. The dark-gray region has been obtained using the LMA best-fit values as input parameters at low energy, varying the initial θ_{13} in the interval $[0°, 9°]$ and setting all CP phases equal to zero. The medium-gray regions show the evolution for $|\varphi_1 - \varphi_2| \in \{0°, 90°, 180°, 270°\}$, $\theta_{13} \in [0°, 9°]$ and $\delta \in \{0°, 90°, 180°, 270°\}$. Finally, the light-gray regions correspond to intermediate values of the phases. The damping influence of φ_1 and φ_2 is clearly visible. The horizontal line at low energies stems from the SM running below $M_{\rm SUSY}$, which is negligible as we have seen above.

As demonstrated by the relatively broad dark-gray band in the figure, the $\mathscr{O}(\theta_{13})$-term in the RGE is quite important here. The dominant part of this term is

$$\Upsilon = \frac{C y_\tau^2}{32\pi^2} \frac{m_2 + m_1}{m_2 - m_1} \sin 2\theta_{23} \cos\frac{\varphi_1 - \varphi_2}{2} \times \\ \times \left(\cos 2\theta_{12} \cos\delta \cos\frac{\varphi_1 - \varphi_2}{2} + \sin\delta \sin\frac{\varphi_1 - \varphi_2}{2} \right) \theta_{13} \,. \tag{4.32}$$

The most drastic running, where θ_{12} can even become zero, occurs for maximal θ_{13}, $\delta = \pi$ and $\varphi_1 - \varphi_2 = 0$. In this case, the leading and the next-to-leading term add up constructively. It also turns out that θ_{12} can run to slightly larger values than its

starting value at the electroweak scale. The damping due to the Majorana phases is maximal in this case, i.e. $|\varphi_1 - \varphi_2| = \pi$, which almost eliminates the leading term and causes Υ to vanish exactly. Then, virtually all the running is caused by the other next-to-leading terms that we have not shown explicitly.

The strong curvature of the lines in the figure also shows that it is not a good approximation to assume the right hand sides of eqs. (4.19) and (4.32) to be constant (which would yield straight lines in the plot) in order to estimate θ_{12} at a high energy scale. The reason are non-linear effects, chiefly from the change of $\sin 2\theta_{12}$ and $\Delta m^2_\odot$, which cannot be neglected here.

Finally, we point out that the numerical calculation never yields negative values of θ_{12}, as it takes into account that the angle lies between 0 and 45° by definition (cf. sec. 2.2). When determining the running from eq. (4.19), one has to apply this restriction manually, since it was not included in the derivation. An example is given by the dashed line in fig. 4.2, which shows that θ_{12} is "reflected" to positive values when it reaches 0. Analogous considerations hold for the other mixing parameters.

RG Evolution of θ_{13}

A notable difference between the running of θ_{13} and that of the other mixing angles is that it is not always damped by non-zero Majorana phases. To the contrary, the strongest damping occurs if they are equal, in particular zero. In this case, the first two terms in the second line of eq. (4.20) nearly cancel, since the masses m_1 and m_2 are very close to each other. Vice versa, the fastest running occurs if $\varphi_1 - \varphi_2 = \pi$ and $\varphi_1 - \delta \in \{0, \pi\}$, so that these two terms are maximal and add up. The suppressed evolution for equal Majorana phases is in agreement with earlier studies, for instance [101, 105], where it was discussed for the CP-conserving case $\varphi_1 = \varphi_2 = \pi$. Such cancellations do not occur for a strong normal mass hierarchy, since then $m_1 \approx 0$ and the evolution is dominated by the term proportional to m_2. For an inverted hierarchy, the RG effect becomes tiny if the lightest mass eigenvalue m_3 is small, since the leading term is proportional to m_3. Then the dominant contribution comes from the $\mathscr{O}(\theta_{13})$-term unless θ_{13} is very small.

Whether the running increases or decreases θ_{13} depends both on the values of the phases and on the mass hierarchy. With zero phases, θ_{13} decreases with increasing energy for a normal hierarchy in the MSSM, because the second line of the RGE is negative due to $m_1 < m_2$. This yields the dark-gray region in fig. 4.3 where the numerical result for the running is plotted.[2] For an inverted hierarchy Δm^2_{a} is negative, so that the direction of the evolution is reversed. As θ_{13} can always be made positive by a suitable redefinition of parameters, the sign of $\dot{\theta}_{13}$ is irrelevant for $\theta_{13} = 0$. The comparison with the numerical results also shows that θ_{13} runs linearly on a logarithmic scale to a good approximation. Thus, using eq. (4.20) with a constant right hand side

[2] The relatively large slope of its upper boundary is due to the $\mathscr{O}(\theta_{13})$ contribution to the RGE.

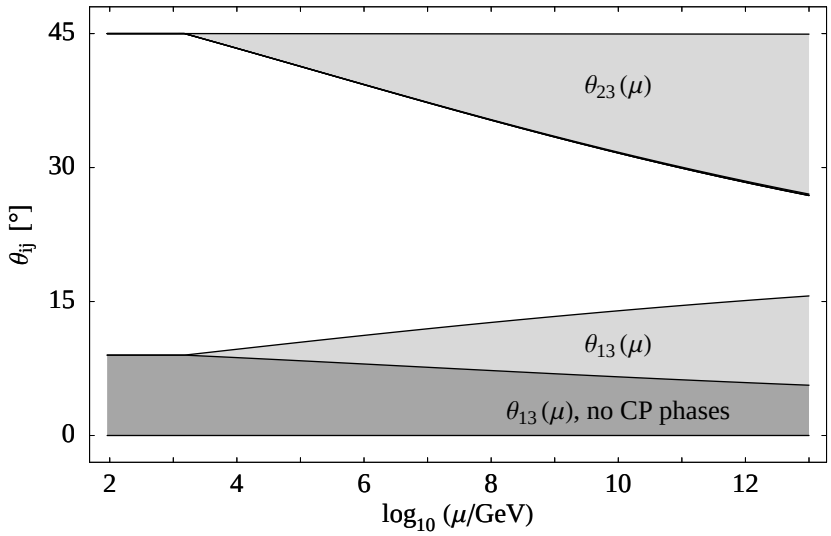

Figure 4.3: RG evolution of θ_{13} and θ_{23} in the MSSM with $\tan\beta = 50$, a normal mass hierarchy and $m_1 = 0.1$ eV. The dark-gray regions show the evolution with best-fit values for the neutrino oscillation parameters, $\theta_{13} \in [0°, 9°]$ and zero CP phases at low energies. In the case of θ_{23}, the corresponding region reduces to a thick line at the bottom of the gray-shaded area. The light-gray regions can be reached if arbitrary CP phases are allowed.

yields pretty accurate results.

With $\varphi_1 \neq \varphi_2$, significant RG effects occur for nearly degenerate masses, as confirmed by the light-gray region in fig. 4.3. However, since long-baseline experiments will be able to probe very small values of θ_{13} (cf. tab. 2.2), even small effects could be important, since a low-energy value smaller than the RG change would appear unnatural. This will be discussed in more detail in sec. 5.1.

RG Evolution of θ_{23}

Similarly to θ_{13}, the atmospheric angle runs linearly on a logarithmic scale to a good approximation, as demonstrated by the numerical results, which are also shown in fig. 4.3. Another similarity is that the direction of the running depends on the mass ordering. In this case, the phases do not play a role, so that θ_{23} always decreases with energy in the MSSM for a normal hierarchy and always increases for an inverted one. The evolution is very well described by the leading term in eq. (4.21), as we see from the very narrow dark-gray band at the bottom of the gray-shaded area in the figure which implies that varying θ_{13} has virtually no effect.

From the approximate RGE we expect that non-zero Majorana phases always reduce the running for nearly degenerate masses. This is confirmed by the light-gray region in fig. 4.3. The damping is much less severe for a hierarchical mass spectrum, since either m_1 and m_2 or m_3 are very small then.

RG Evolution of the Dirac Phase

Let us next discuss the running of the CP phases. In general, a significant change is expected for quasi-degenerate and inverted hierarchical mass patterns, since the RGEs (4.22)–(4.24) contain the ratio $m_1 m_2/\Delta m^2_\odot$. This is important for studies about possible connections between the phases in the light neutrino mass matrix and those relevant for leptogenesis, e.g. [106–111].

We will first consider the Dirac phase δ, whose evolution is approximately described by eqs. (4.22). The RGE diverges for $\theta_{13} \to 0$. This is a consequence of the fact that δ is not defined for vanishing θ_{13}, since only the combination $s_{13}e^{\pm i\delta}$ appears in the MNS matrix. However, one can show that a well-defined analytic continuation exists for δ and $\dot\delta$: the derivative of the MNS matrix U^ν is given by eq. (4.8), $\dot U^\nu = U^\nu\, T$, where U^ν and T are continuous. Hence, $U^\nu_{13}(t) = s_{13}(t)\, e^{-i\delta(t)}$ describes a continuously differentiable curve in the complex plane. Consequently, $\theta_{13}(t)$ and $\delta(t)$ are continuously differentiable even for $\theta_{13} = 0$, if δ is extended continuously at this point. This continuation for δ is determined by the requirement that $\dot\delta$ remain finite. Then the divergence of θ_{13}^{-1} has to be canceled by $\delta^{(-1)} = 0$. For $\varphi_1 = \varphi_2 = 0$, this obviously implies $\delta = 0$ or $\delta = \pi$. In the general case, a short calculation yields

$$\cot\delta = \frac{m_1 \cos\varphi_1 - (1+\zeta)\, m_2\, \cos\varphi_2 - \zeta m_3}{m_1 \sin\varphi_1 - (1+\zeta)\, m_2\, \sin\varphi_2}\,. \tag{4.33}$$

This value of δ uniquely determines the slope of θ_{13} for $\theta_{13} = 0$.[3] If θ_{13} is small but non-zero, the term proportional to θ_{13}^{-1} in the RGE can become very large. This is one of the few examples where a significant RG evolution is possible even for a strong normal mass hierarchy. However, one has to keep in mind that a measurement of δ is very hard in this case.

Another interesting possibility is the radiative generation of a Dirac phase by Majorana phases [93]: if at least one of the Majorana phases is non-zero, a non-zero δ is produced by RG effects, since some of the terms in the RGE do not vanish for $\delta = 0$. Fig. 4.4 shows an example. The most important term in this context is the first one in $\delta^{(0)}$. As it is proportional to $\sin(\varphi_1 - \varphi_2)$, the effect is suppressed for $\varphi_1 = \varphi_2$. For small but non-zero values of θ_{13}, the term involving $\delta^{(-1)}$ also contributes significantly because of the factor θ_{13}^{-1}. For $\varphi_1 = \varphi_2$, this contribution is suppressed as well, since the parts proportional to m_1 and m_2, respectively, nearly cancel.

In this context, one can observe some non-trivial subleading effects which once again demonstrate the potential of the approximate RGEs for the mixing parameters. Hence,

[3] Due to the periodicity of cot, there are two solutions of eq. (4.33) differing by π. As changing δ by π changes the sign of $\dot\theta_{13}$ and as we use the convention $0 \le \theta_{13} \le \pi/2$, it is clear that the solution with $\dot\theta_{13} < 0$ is valid to the left of a node of θ_{13} and the one with $\dot\theta_{13} > 0$ to the right. This implies that the evolution of δ does actually exhibit a jump if θ_{13} runs through zero. However, this is an "artificial" discontinuity caused by our requirement of a positive θ_{13}, and there are still finite one-sided limits for δ and $\dot\delta$ as θ_{13} approaches 0.

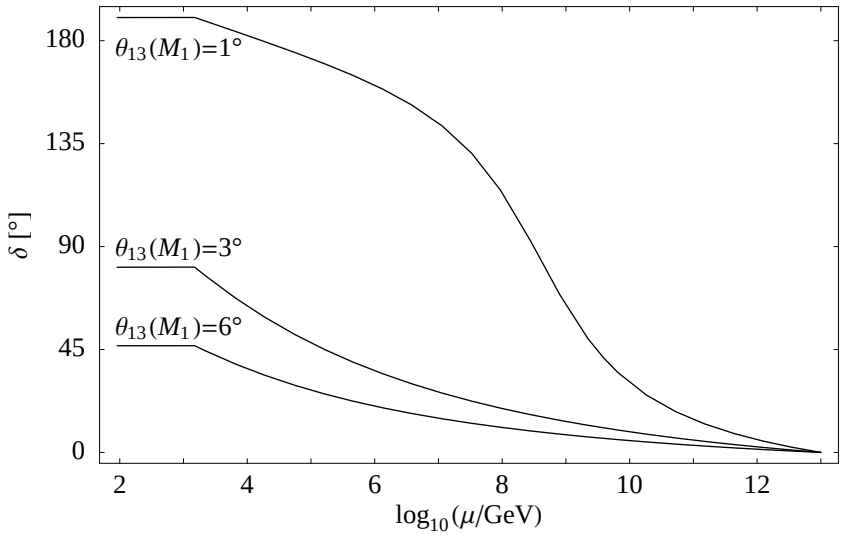

Figure 4.4: Radiative generation of a Dirac phase in the MSSM with $\tan\beta = 30$ and a normal mass hierarchy. Here the running is to be viewed from high to low energies, i.e. the boundary conditions are given at the see-saw scale $M_1 = 10^{13}$ GeV. δ is zero there but large at the electroweak scale. The other starting values are $\theta_{12} = 18°$, $\theta_{13} \in \{1°, 3°, 6°\}$, $\theta_{23} = 34°$, $m_1 = 0.17$ eV, $\Delta m^2_{\mathrm{a}} = 3.8 \cdot 10^{-3}$ eV^2, $\Delta m^2_{\odot} = 5.7 \cdot 10^{-4}$ eV^2, $\varphi_1 = 16°$, $\varphi_2 = 140°$.

let us discuss the radiative generation of δ in some more detail.[4] As the most important term in $\dot{\delta}$ depends only on the difference of the Majorana phases, the evolution is expected to stay roughly the same if both phases change by the same value. Fig. 4.5(a) demonstrates that this is true only to a first approximation. In this example, $\theta_{13} = 5°$, $\varphi_1 - \varphi_2 = 70°$ and φ_2 is incremented step by step. Thereby, the running of δ is increasingly damped. The main reason for this is the second term in square brackets in $\delta^{(-1)}$ (the one proportional to m_2), whose sign is opposite to that of the leading term for $\delta < \varphi_2$. This term grows with φ_2, while the previous one (proportional to m_1) does not change much as long as φ_1 is close to 90°.

Fig. 4.5(b) shows that the situation can be very different for smaller values of θ_{13} (4° in this example). Now the initial rise of δ is enhanced, so that it can become larger than φ_2. Then the sign of the aforementioned second term in square brackets changes, so that it no longer damps the evolution but amplifies it. This happens here for $\varphi_2 = 30°$. For larger values, the Dirac phase never reaches φ_2 in this example, resulting in the same damping as before (but now intensified by the larger θ_{13}^{-1}).

In the case of an inverted hierarchy with $\tan\beta$ varying between 30 and 50, Dirac phases of about 15° to 30° can be generated. Now the term involving $\delta^{(-1)}$ receives an additional suppression from the small value of m_3, so that the described subleading effects become unimportant. Hence, the running of δ is independent of θ_{13} and depends

[4] To simplify the numerical calculations, we return to considering the running from low to high energies, i.e. the Dirac phase now vanishes at the electroweak scale.

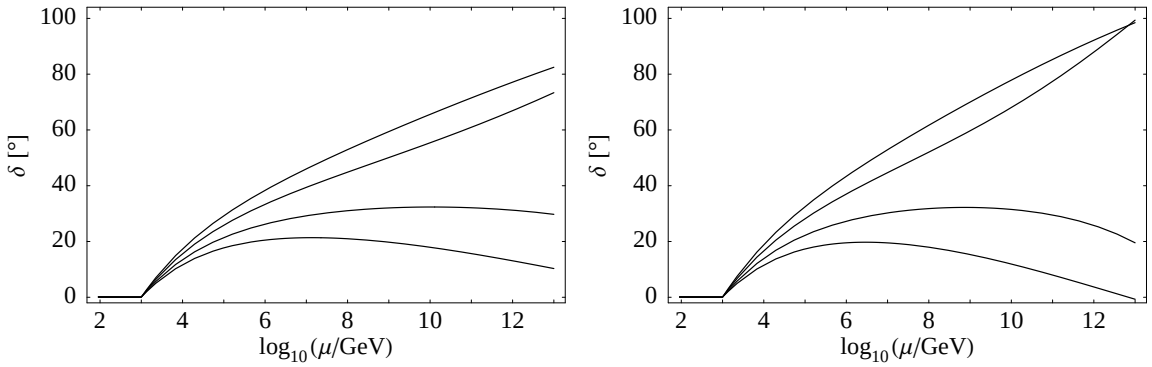

(a) $\theta_{13} = 5°$ (b) $\theta_{13} = 4°$

Figure 4.5: RG evolution of the Dirac phase in the MSSM with a normal hierarchy for a constant difference of the Majorana phases, $\varphi_1 - \varphi_2 = 70°$, and $\varphi_2 \in \{0, 30°, 60°, 90°\}$ (0 corresponding to the top curves). The initial conditions for θ_{13} at M_Z are given below the plots, and for the remaining parameters we chose $\tan\beta = 30$, $\delta = 0$, $m_1 = 0.14$ eV, as well as the best-fit values for the mass squared differences, θ_{12} and θ_{23}.

only on the difference of the Majorana phases to a very good approximation.

RG Evolution of the Majorana Phases

While the RGEs for the Majorana phases are somewhat lengthy, there is a simple expression for the running of their difference for small θ_{13},

$$\dot{\varphi}_1 - \dot{\varphi}_2 = \frac{C y_\tau^2}{4\pi^2} \frac{m_1 m_2}{\Delta m_\odot^2} \cos 2\theta_{12} \sin^2\theta_{23} \sin(\varphi_1 - \varphi_2) + \mathcal{O}(\theta_{13}) \,. \tag{4.34}$$

It shows that for $\theta_{13} = 0$, the phases remain equal, if they are equal at some scale. Obviously, in the MSSM $\dot{\varphi}_1 - \dot{\varphi}_2 > 0$ for $\varphi_1 > \varphi_2$ and vice versa, which means that the difference between the phases tends to increase with increasing energy. In other words, a large difference at the see-saw scale becomes smaller at low energy. An example is shown in fig. 4.6. If $\varphi_1 - \varphi_2$ is not too small, a non-zero θ_{13} tends to damp its running. This is due to a term in the RGE for φ_1 whose sign is opposite to that of the leading one in eq. (4.34) and which is proportional to $\sin\theta_{13} \cot\theta_{12}$. This term can grow important if θ_{12} becomes small with increasing energy.

For $\varphi_1 = \varphi_2$ the evolution of the Majorana phases is suppressed, since the leading terms in the RGEs (4.23) and (4.24) vanish. For $\theta_{13} = 5°$, the first line in the RGE and the terms proportional to $\sin\theta_{13}$ are about equally important for the running of φ_1. Non-linear effects caused by the decrease of the solar and atmospheric mixing angles are essential here, as the initial slope of the curves is extremely small due to the suppression by $\sin\theta_{13}$ and $\cos 2\theta_{23}$. The evolution of φ_2 is virtually independent of θ_{13}, since the respective terms are not multiplied by $\cot\theta_{12}$, which again can become large

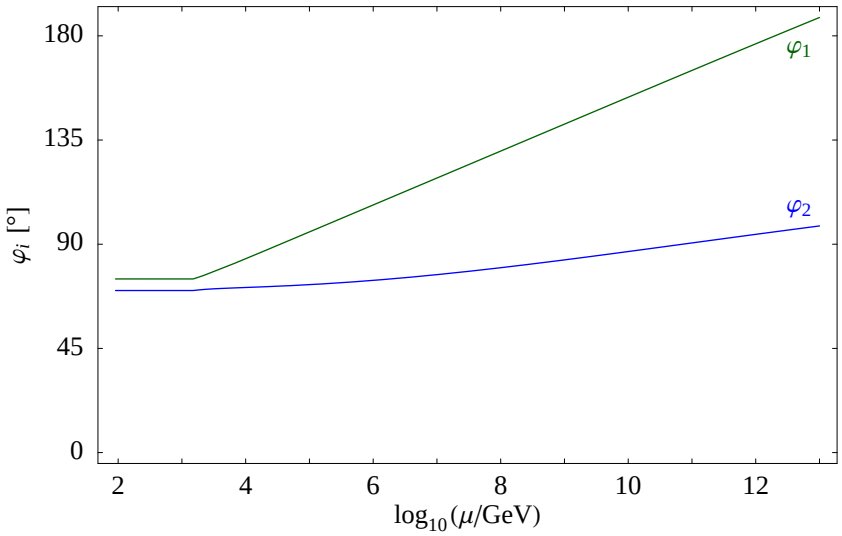

Figure 4.6: Running of the Majorana phases in the MSSM with a normal mass hierarchy, $\tan\beta = 50$, $\varphi_1 = 75°$, $\varphi_2 = 70°$, $m_1 = 0.15$ eV, $\theta_{13} = 0$, and current best-fit values for the other oscillation parameters at the electroweak scale. The RG effects are significant, and the difference $\varphi_1 - \varphi_2$ increases with increasing energy.

at higher energies because of the decreasing θ_{12}, but by $\tan\theta_{12}$, which remains smaller than 1.

In principle, it is also possible to generate Majorana phases radiatively, if the CP phase is non-zero. This demonstrates that vanishing Majorana phases do not correspond to any symmetry which could protect them against radiative corrections. However, it follows from the discussion in the previous paragraph that the generation of Majorana phases only happens via terms proportional to $\sin\theta_{13}$.

RG Evolution of the Neutrino Mass Eigenvalues

The RGEs (4.25) for the mass eigenvalues also depend on the flavour-blind factor α in the β-function of the effective neutrino mass operator. It causes a common rescaling of all three masses. As α contains large quantities such as the top Yukawa coupling and (in the SM) the Higgs self-coupling, the evolution is substantial even in the SM or for a strong mass hierarchy. It is virtually independent of the mixing parameters unless y_τ^2 is comparable to α, which is only possible in the MSSM with large $\tan\beta$. Thus, in most cases the running is well approximated by the common scaling of the mass eigenvalues [103], which can be calculated by neglecting y_τ and integrating eqs. (4.25),

$$m_i(t) \approx \exp\left[\frac{1}{16\pi^2}\int_{t_0}^{t} \mathrm{d}\tau\, \alpha(\tau)\right] m_i(t_0) =: s(t,t_0)\, m_i(t_0)\ . \tag{4.35}$$

Fig. 4.7 shows the scaling factor s in the SM and in the MSSM for various combinations of the parameters. Notably, the masses change more in the SM than in the MSSM in

most cases. This is due to the contribution of the Higgs self-coupling that is absent in the MSSM. The three SM curves correspond to different values of this parameter or, equivalently, different Higgs masses in the current experimentally allowed region at the 95% CL, 114 GeV $\lesssim m_H \lesssim$ 251 GeV [112]. In the MSSM, we use only one value, $m_H = 120$ GeV, for the light Higgs mass, since the allowed range is further restricted by the upper limit at about 130 GeV here, and since it influences the RG evolution only marginally as long as M_{SUSY} and M_Z differ by not more than a few orders of magnitude. Moreover, further uncertainties due to threshold corrections [113] and the unknown value of the SUSY-breaking scale can be equally important as the one due to the unknown Higgs mass.

In those cases where the terms proportional to y_τ^2 in the RGEs (4.25) are large enough to influence the running, the values of the mixing angles and the Dirac phase become relevant. However, as we have seen above from eq. (4.13), the Majorana phases still do not play a direct role [93]. Besides, $\dot{m}_3$ does not depend on δ, since only the moduli of the elements of the third column of the MNS matrix are relevant in this case. Nevertheless, an indirect dependence on the phases remains, because these influence the running of the mixing angles.

RG Evolution of the Mass Squared Differences

Clearly, in the SM and the MSSM with small $\tan\beta$ the running of the mass squared differences is dominated by the universal rescaling described in the previous section. Therefore, it is very similar to fig. 4.7, except that the scaling factor is now s^2.

Interesting new effects are found in the MSSM with a large $\tan\beta$ and nearly degenerate masses. The running of $\Delta m^2_\odot$ and Δm^2_{a} can be significantly faster than that of the squares of the mass eigenvalues, since the RGEs (4.27) contain terms that are proportional to the absolute masses rather than the differences. From eqs. (4.28) as well as the extensive light-gray regions in fig. 4.8, as usual obtained by varying all CP phases, we also see that the influence of the phases, in particular the Dirac phase, is crucial. The numerical example furthermore shows that $\Delta m^2_\odot$ runs dramatically in most cases. On the one hand, it can grow by more than an order of magnitude. For an inverted mass hierarchy and an absolute mass scale somewhat above the one used in the plot, $\Delta m^2_\odot$ can even become larger than $|\Delta m^2_{\text{a}}|$ which means that the hierarchy appears to be normal at high energies. Thus, the mass ordering is not always preserved by the RG evolution. On the other hand, $\Delta m^2_\odot$ can run to 0 at energy scales slightly beyond the maximum of 10^{13} GeV shown in the figure. For large $\tan\beta$, $\Delta m^2_\odot \ll m_1^2$, and not too small θ_{13}, the first term in $F_\odot$ of eq. (4.28a) is essential for understanding these effects, since it is proportional to the sum of the masses squared. For $\delta = \pi$ and θ_{13} near the CHOOZ bound, its sign is negative and its absolute value maximal, which causes the evolution of $\Delta m^2_\odot$ towards zero. For $\delta = 0$, the sign becomes positive, so that the running towards larger values is enhanced, which explains the upper boundary of the light-gray region in the first plot of fig. 4.8.

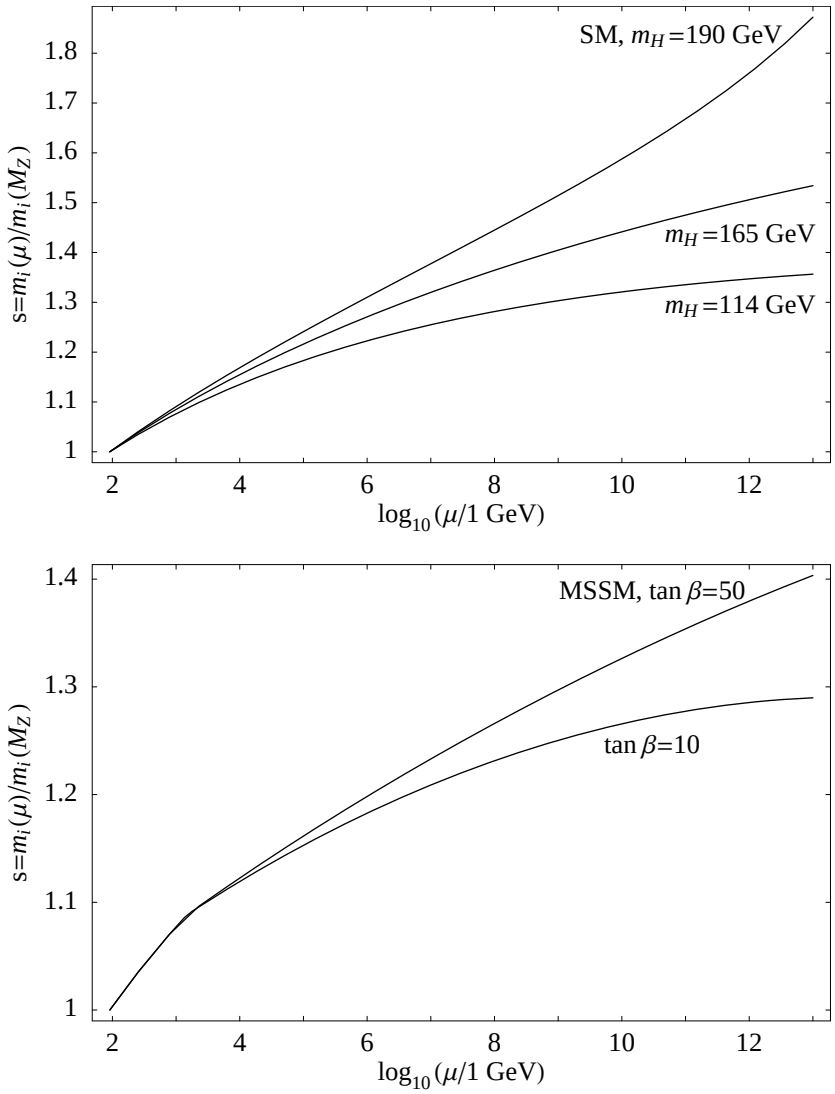

Figure 4.7: Scaling of the neutrino mass eigenvalues under the RG in the SM and MSSM. The three curves in the upper plot show the evolution in the SM for different Higgs masses. The lower plot illustrates the running in the MSSM with $m_H = 120$ GeV as well as $\tan\beta = 10$ and $\tan\beta = 50$, respectively. The rescaling is the same for all mass eigenvalues and virtually independent of the mixing parameters, except for the MSSM example with $\tan\beta = 50$, where the scaling of m_3 for a strong normal mass hierarchy, $\theta_{13} = 0$, zero CP phases, and experimental best-fit values for the other oscillation parameters at low energy is displayed.

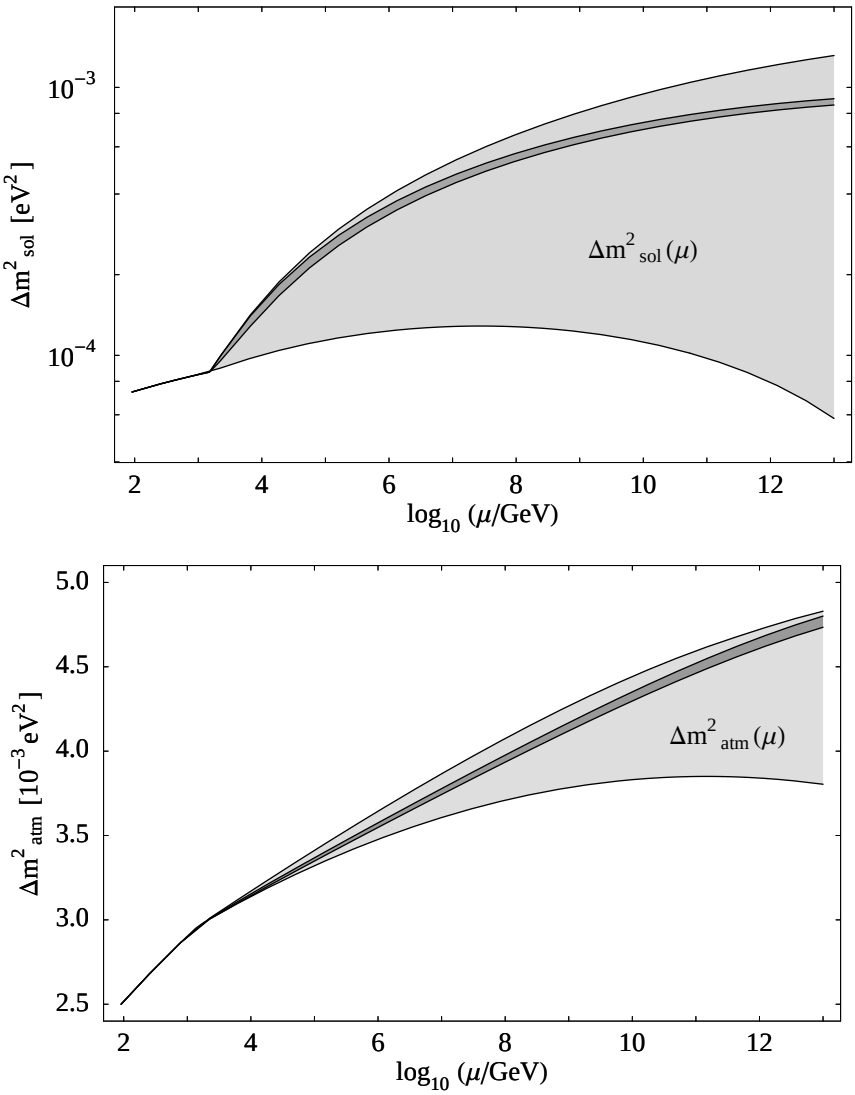

Figure 4.8: RG evolution of the neutrino mass squared differences in the MSSM with $\tan\beta = 50$, a normal mass hierarchy and $m_1 = 0.1$ eV. The dark-gray regions show the evolution with LMA best-fit values for the neutrino parameters, $\theta_{13} \in [0°, 9°]$ and all CP phases equal to zero. The light-gray regions show the evolution which is possible if arbitrary phases are allowed.

Such an enhancement does not occur for the atmospheric mass squared difference, as we see from the lower plot in fig. 4.8. In this case the phases can only cause a damping of the RG evolution. Depending on their values, $\Delta m^2_{\rm a}$ grows by about 50% – 95%. Analogously to above, the maximal damping is mainly due to the first term in $F_{\rm a}$, so that it occurs for large θ_{13} and $\delta = 0$. Compared to the case of the solar mass squared difference, both the RG change and the influence of δ are generically smaller here, because $\Delta m^2_{\rm a}/m_i^2$ is larger.

4.2 RG Evolution above the See-Saw Scale

4.2.1 Effective Mass Matrix of the Light Neutrinos

Let us now turn to a specific example for a high-energy theory of neutrino masses and lepton number violation, the type I see-saw scenario. As described in sec. 2.4.2, this is the straightforward extension of the SM or MSSM by three neutrino fields which are gauge singlets and are therefore assumed to have very large Majorana masses. The Lagrangian which yields the neutrino mass terms of eq. (2.3) after spontaneous symmetry breaking is given by

$$\mathscr{L}^{\nu} = -\overline{\nu_{\rm R}} Y_\nu \ell_{\rm L} \widetilde{\phi}^\dagger - \frac{1}{2} \overline{\nu_{\rm R}} M_{\rm R} \nu_{\rm R}^{\mathcal{C}} + \text{h.c.} \,, \tag{4.36}$$

where $\widetilde{\phi} = i\tau^2 \phi^*$ is the charge conjugate of the Higgs field. In the MSSM, it is replaced by $\phi^{(2)}$. As we are assuming the type I see-saw, there is no direct Majorana mass term for the left-handed neutrinos. The quantity relevant for the masses of the light neutrinos in the energy region above the highest see-saw scale is the effective light neutrino mass matrix

$$m_\nu = -\frac{v^2}{2} Y_\nu^T M_{\rm R}^{-1} Y_\nu \,, \tag{4.37}$$

which is obtained from block-diagonalizing the 6×6 neutrino mass matrix as described in sec. 2.1. For analytical considerations, it is useful to calculate the RGE for this composite quantity from those for Y_ν and $M_{\rm R}$ [97, 98, 114, 115]. We obtain

$$16\pi^2 \frac{{\rm d}m_\nu}{{\rm d}t} = (C_e\, Y_e^\dagger Y_e + C_\nu\, Y_\nu^\dagger Y_\nu)^T\, m_\nu + m_\nu\, (C_e\, Y_e^\dagger Y_e + C_\nu\, Y_\nu^\dagger Y_\nu) + \alpha'\, m_\nu \tag{4.38}$$

with

$$C_e = -\frac{3}{2},\ C_\nu = \frac{1}{2} \quad \text{in the SM,} \tag{4.39a}$$

$$C_e = C_\nu = 1 \qquad \text{in the MSSM,} \tag{4.39b}$$

and

$$\alpha'_{\mathrm{SM}} = -\frac{9}{10}g_1^2 - \frac{9}{2}g_2^2 + 2\,\mathrm{Tr}(Y_\nu^\dagger Y_\nu) + 2\,(y_\tau^2 + y_\mu^2 + y_e^2) + \\ + 6\,(y_t^2 + y_b^2 + y_c^2 + y_s^2 + y_d^2 + y_u^2)\,, \tag{4.40a}$$

$$\alpha'_{\mathrm{MSSM}} = -\frac{6}{5}g_1^2 - 6g_2^2 + 2\,\mathrm{Tr}(Y_\nu^\dagger Y_\nu) + 6\,(y_t^2 + y_c^2 + y_u^2)\,. \tag{4.40b}$$

In numerical calculations, we determine the running of Y_ν and M_{R} instead and use it to calculate m_ν afterwards. Note that the RG evolution now produces off-diagonal entries in the charged lepton Yukawa couplings unless Y_e and Y_ν are simultaneously diagonal. This means that unlike in the region below the see-saw scale, there is no basis where the MNS matrix is determined by m_ν alone at all energies.

4.2.2 Effect of Non-Degenerate Singlet Masses

Important complications arise, if the masses of the heavy singlets are non-degenerate. As argued in the beginning of this chapter, each has to be integrated out at its own mass scale in order to obtain reliable results for the RG evolution in the MS renormalization scheme. Hence, we have to use a series of EFTs rather than just the full theory with all three singlets and the low-energy EFT without any of them [19, 116]. Thus, the contributions to the dimension 5 neutrino mass operator are generated at several different see-saw scales.

We will denote the singlet masses, i.e. the eigenvalues of the Majorana mass matrix M_{R}, by $M_1 < M_2 < M_3$. Successively integrating out the heavy neutrinos at the thresholds M_i results in effective theories valid in certain energy ranges as depicted in fig. 4.9. By integrating out all singlet neutrinos, one obtains the dimension 5 operator (2.19). In the intermediate region between the $(n-1)$th and the nth threshold, the singlets $\{\nu_{\mathrm{R}}^n, \ldots, \nu_{\mathrm{R}}^3\}$ are integrated out, leading to an effective operator analogous to (2.19), but with the coupling constant $\overset{(n)}{\kappa}$, where $\overset{(1)}{\kappa}$ is identical to κ. In this energy region, the neutrino Yukawa matrix is a $(n-1)\times 3$ matrix and will be denoted by $\overset{(n)}{Y}_\nu$. Likewise, the Majorana mass matrix for the remaining singlet neutrinos is the $(n-1)\times(n-1)$ matrix $\overset{(n)}{M}_{\mathrm{R}}$.

RGEs between the See-Saw Scales

The running of the effective neutrino mass operators is determined by the RGEs [19, 86, 89]

$$16\pi^2\,\frac{\mathrm{d}\overset{(n)}{\kappa}}{\mathrm{d}t} = \left(C_e\,Y_e^\dagger Y_e + C_\nu\,\overset{(n)}{Y}{}_\nu^\dagger \overset{(n)}{Y}_\nu\right)^T \overset{(n)}{\kappa} + \overset{(n)}{\kappa}\left(C_e\,Y_e^\dagger Y_e + C_\nu\,\overset{(n)}{Y}{}_\nu^\dagger \overset{(n)}{Y}_\nu\right) + \overset{(n)}{\alpha}\,\overset{(n)}{\kappa} \tag{4.41}$$

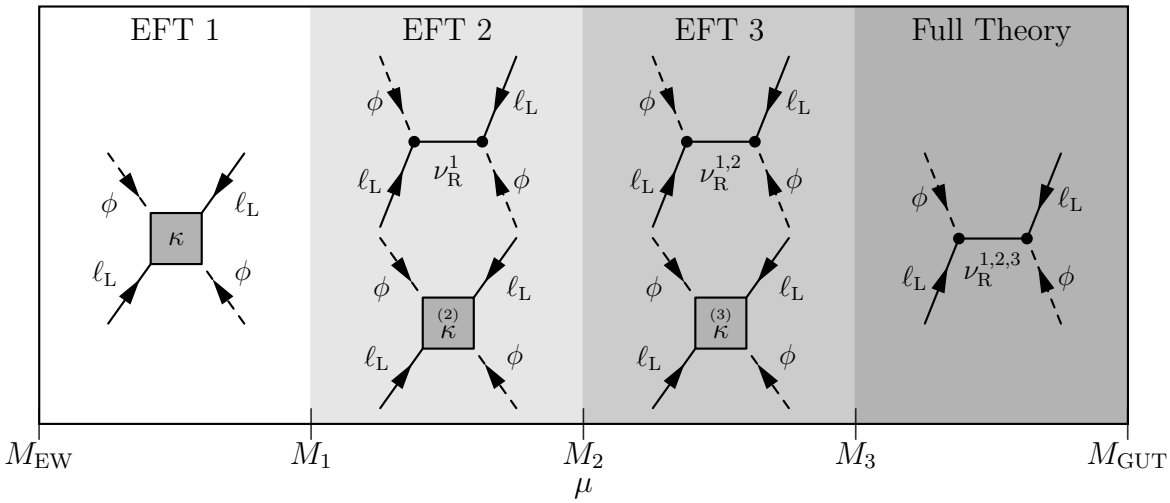

Figure 4.9: Illustration of the ranges of the different theories and the diagrams relevant for neutrino masses in each of them. The EFTs emerge from successively integrating out the heavy singlet neutrinos ν_R^i. "EFT 1" corresponds to the SM or MSSM with the additional dimension 5 operator for neutrino masses. "Full Theory" refers to the SM or MSSM, extended by 3 singlets.

with

$$C_e = -\frac{3}{2},\ C_\nu = \frac{1}{2} \quad \text{in the SM,} \tag{4.42a}$$

$$C_e = C_\nu = 1 \qquad \text{in the MSSM,} \tag{4.42b}$$

and

$$\begin{aligned} \overset{(n)}{\alpha}_{\text{SM}} = &-3g_2^2 + 2\,\text{Tr}\big(\overset{(n)}{Y_\nu^\dagger}\overset{(n)}{Y_\nu}\big) + 2\,(y_\tau^2 + y_\mu^2 + y_e^2) + \\ &+ 6\,(y_t^2 + y_b^2 + y_c^2 + y_s^2 + y_d^2 + y_u^2) + \lambda\,, \end{aligned} \tag{4.43a}$$

$$\overset{(n)}{\alpha}_{\text{MSSM}} = -\frac{6}{5}g_1^2 - 6g_2^2 + 2\,\text{Tr}\big(\overset{(n)}{Y_\nu^\dagger}\overset{(n)}{Y_\nu}\big) + 6\,(y_t^2 + y_c^2 + y_u^2)\,. \tag{4.43b}$$

The β-functions for the Yukawa couplings and the singlet mass matrix are listed in app. B. These RGEs have been calculated in a basis in which the Majorana mass matrix M_R (omitting the superscript (n) for briefness) is diagonal. Therefore, one could worry that the running, which spoils the diagonal structure of M_R, might require a constant re-diagonalization while solving the RGEs. However, this is not necessary because they are invariant under the transformation that diagonalizes M_R, $M_R \to U^T M_R\, U$, $Y_\nu \to U^T Y_\nu$, and $\nu_R \to U^T \nu_R$.

Calculation of the Low-Energy Neutrino Mass Matrix

Using the RGEs given above and in app. B, the low-energy neutrino mass matrix can now be calculated numerically: at the GUT scale, we start with the Yukawa matrices Y_ν,

the Majorana mass matrix M_{R} for the singlet neutrinos, and suitable initial conditions for the remaining parameters of the theory. By solving the set of coupled differential equations for all these quantities, we calculate their RG running to the highest mass threshold, the largest eigenvalue M_3 of M_{R}.

At this energy we integrate out the heaviest singlet neutrino. This leads to an EFT including the dimension 5 mass operator with coupling $\overset{(3)}{\kappa}$, whose value at M_3 is determined by the tree-level matching condition

$$\overset{(3)}{\kappa}_{gf}\big|_{M_3} = 2\,(Y_\nu^T)_{g3}\,M_3^{-1}(Y_\nu)_{3f}\big|_{M_3}\,, \tag{4.44}$$

which is found from evaluating the diagrams in fig. 2.2. The Yukawa coupling $\overset{(3)}{Y}_\nu$ at the threshold is determined simply by removing the last row of Y_ν. Note that this procedure is only possible in the mass eigenstate basis of the singlets at the threshold, which is different from the original one at the GUT scale, since the RG evolution produces non-zero off-diagonal entries in M_{R}. Therefore, the mass matrix has to be diagonalized by the unitary transformation described above.

Next, $\overset{(3)}{\kappa}$, $\overset{(3)}{Y}_\nu$, $\overset{(3)}{M}_{\mathrm{R}}$ and the other parameters are evolved down to the threshold M_2. The RGE that determines the running of the dimension 5 mass operator between the thresholds is given by eq. (4.41). Integrating out the next singlet neutrino yields the second EFT, valid between M_1 and M_2. This time, the matching condition for the neutrino mass operator reads

$$\overset{(2)}{\kappa}_{gf}\big|_{M_2} = \overset{(3)}{\kappa}_{gf}\big|_{M_2} + 2\,\big(\overset{(3)}{Y}_\nu^T\big)_{g2}\,M_2^{-1}\big(\overset{(3)}{Y}_\nu\big)_{2f}\big|_{M_2}\,. \tag{4.45}$$

For the matrix of the neutrino Yukawa couplings, the procedure is the same as before. The quantities in the resulting effective theory are now run to the last threshold M_1, where the lightest singlet neutrino is integrated out. The matching is completely analogous to the one done at M_2. Thus, we finally arrive at the SM or MSSM with the effective neutrino mass operator (2.19) or (2.22) and no additional particles, where the RG evolution is calculated as discussed in sec. 4.1.

Note that between the thresholds the effective light neutrino mass matrix is made up of two contributions, one from the dimension 5 operator and one from the singlets that are still contained in the theory. Explicitly, the analog of eq. (4.37) between the $(n-1)$th and the nth threshold is given by

$$\overset{(n)}{m}_\nu = -\frac{v^2}{4}\big(\overset{(n)}{\kappa} + 2\,\overset{(n)}{Y}_\nu^T\,\overset{(n)}{M}_{\mathrm{R}}^{-1}\overset{(n)}{Y}_\nu\big)\,. \tag{4.46}$$

Running of the Mixing Angle in a Two-Flavour Example

As the procedure of using several EFTs is rather involved, an obvious question is whether it can be simplified by integrating out all singlets at some common intermediate mass scale. To check whether this yields an acceptable approximation, we

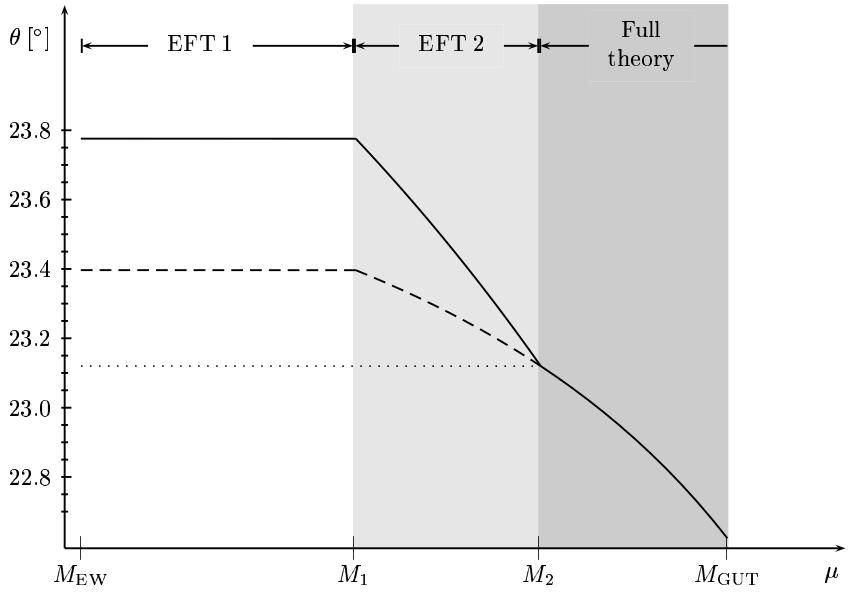

Figure 4.10: RG evolution of the leptonic mixing angle θ in the SM with 2 generations, extended by 2 singlet neutrinos with masses of 10^8 GeV and 10^{12} GeV. We chose the initial values of the Yukawa coupling matrices Y_ν at the high-energy scale $M_{\rm GUT} = 10^{16}$ GeV to be real with (untuned) entries between 0.025 and 1.

study the running in a simple example with two generations. We choose singlet masses $M_1(M_{\rm GUT}) = 10^8$ GeV, $M_2(M_{\rm GUT}) = 10^{12}$ GeV, and real Yukawa couplings $Y_\nu(M_{\rm GUT})$ with (untuned) entries between 0.025 and 1. The resulting RG evolution of the leptonic mixing angle θ is shown as solid lines in fig. 4.10 for the SM and in fig. 4.11 for the MSSM.

The transitions to the effective theories at the mass thresholds lead to pronounced kinks in the evolution. For comparison, the dotted and dashed lines show the results when both heavy neutrinos are integrated out at the higher or the lower threshold, respectively. Obviously, this produces large deviations from the true evolution, and the correct result need not even lie between the two extreme cases. Although this occurs only in the SM in our example, the same is possible in the MSSM, depending on the initial values of the Yukawa couplings. We will see an explicit example later in sec. 5.4. Consequently, the correct running of the mixing angle cannot be reproduced by integrating out all heavy neutrinos at some intermediate mass scale $M_{\rm int} \in [M_1, M_2]$ in general.

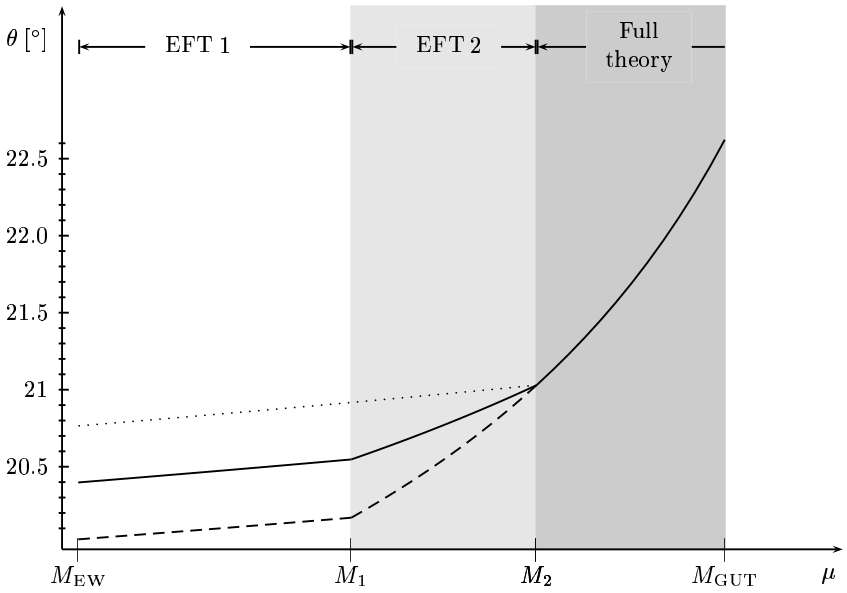

Figure 4.11: RG evolution of the mixing angle θ in the MSSM with 2 generations and 2 additional singlet neutrinos. We chose $\tan\beta = 35$ as well as $M_{\mathrm{SUSY}} \approx M_{\mathrm{EW}}$ for the SUSY breaking scale. The other parameters are the same as in fig. 4.10.

Chapter 5

Applications

Apart from causing corrections to the predictions of high-energy models, RG effects have several interesting model-independent applications. In this chapter, we will present some examples, starting with implications of the running below the see-saw scale and afterwards turning to the evolution in the full theory with singlet neutrinos.

5.1 Prospects for Precision Neutrino Experiments

As described in sec. 2.3.3, significant progress is expected in the precision of oscillation experiments in the coming years. This can open up new vistas for the study of RG effects as well, if their size is comparable to the experimental sensitivities. We will show in this section that this is indeed the case for the mixings θ_{13} and θ_{23}. An application of the running of the solar angle will be discussed in a different context in sec. 5.4.

5.1.1 Radiative Generation of a Non-Zero CHOOZ Angle

To get a first impression of the typical size of RG corrections to the CHOOZ angle, let us use the estimate (4.31) for the MSSM with quasi-degenerate neutrinos. Comparing the result to the sensitivities of planned experiments listed in tab. 2.2, we find that the enhancement factor $m^2/\Delta m^2_{\text{a}}$ leads to changes exceeding the experimental detection limits already for moderate values of $\tan\beta$. For example, $m_1 = 0.1$ eV and $\tan\beta = 30$ yield a change of $\sin^2 2\theta_{13}$ by about $0.5 \cdot 10^{-2}$. This number is further enhanced by a factor of 4 if the Majorana phases are aligned properly.

Thus, a more detailed study appears worthwhile. For this purpose, we use the RGE (4.20) in the linear approximation $\dot{\theta}_{13} \approx$ const., which yields an evolution with a constant slope on a logarithmic scale and is a rather good approximation as we have found out in sec. 4.1.2. This also allows us to use the best-fit values of the oscillation parameters. We assume θ_{13} to vanish at the GUT scale. In this case, the initial value of the Dirac phase δ is determined by the analytic continuation eq. (4.33). The remaining free parameters are the mass of the lightest neutrino m_1 (for a normal hierarchy), $\tan\beta$, and the Majorana phases φ_1 and φ_2. In fig. 5.1 we show the results for the change of $\sin^2 2\theta_{13}$ as a function of these parameters. In the left plot, the phases are

fixed at $\varphi_1 = 0$, $\varphi_2 = \pi$, and m_1 as well as $\tan\beta$ are varied. The resulting pattern is easy to understand from eq. (4.20): the RG effects grow monotonously with m_1 and $\tan\beta$. Note that the gray-shaded region corresponding to the sensitivity of a neutrino factory in the most optimistic scenario extends to zero m_1. Hence, RG effects could be experimentally relevant even for hierarchical neutrino masses in this case.

The right diagram in fig. 5.1 was obtained by setting m_1 to 0.075 eV and $\tan\beta$ to 50, and varying the Majorana phases. The result can be explained by the approximate RGE for θ_{13}, too. Consider partially or quasi-degenerate neutrino masses. Then eq. (4.20) yields to a reasonably good approximation

$$\begin{aligned}\dot{\theta}_{13} &\approx \frac{Cy_\tau^2}{32\pi^2}\,\sin 2\theta_{12}\,\sin 2\theta_{23}\,\frac{m^2}{\Delta m^2_{\mathrm{a}}}\,[\cos(\varphi_1-\delta)-\cos(\varphi_2-\delta)] \\ &\propto \sin\frac{\varphi_1+\varphi_2-2\delta}{2}\,\sin\frac{\varphi_1-\varphi_2}{2}\,. \end{aligned} \tag{5.1}$$

Applying an analogous approximation to eq. (4.33), it can be shown that the first term in the second line is always ± 1, so that the running is completely determined by the difference of the Majorana phases. This leads to the diagonal bands in fig. 5.1, in particular the white and light-gray ones corresponding to $\varphi_1 - \varphi_2 \approx 0$, where the RG change is very small. The white region is actually deformed to an ellipse due to the non-zero mass splittings, which cause corrections to eq. (5.1) that can yield a change of $\sin^2 2\theta_{13}$ larger than $6 \cdot 10^{-5}$ even for equal Majorana phases. If one starts with a small but non-zero θ_{13}, which allows an arbitrary δ, it turns out that the RG evolution quickly drives δ to a value satisfying eq. (4.33), so that the final pattern of fig. 5.1 is unchanged.

The cancellation for $\varphi_1 = \varphi_2$ does not appear with a strong normal mass hierarchy, since the running is dominated by the term proportional to m_2 in eq. (4.20) then. In the case of a strong inverted hierarchy, $\dot{\theta}_{13}$ is proportional to the smallest mass eigenvalue, so that it can become arbitrarily small. To reach $\Delta\sin^2 2\theta_{13} \gtrsim 10^{-4}$, this eigenvalue has to be larger than about 0.01 eV for $\tan\beta = 50$. If the masses are at least partially degenerate, the running is basically the same as for a normal mass ordering, as expected.

Thus, the change of $\sin^2 2\theta_{13}$ due to the RG evolution between the GUT and the electroweak scale in the MSSM lies above the sensitivity limit of planned experiments in a large part of the parameter space, often even for the next-generation reactor experiments. Generically, we expect the low-energy value of $\sin^2 2\theta_{13}$ to be at least as large as the change due to the RG. Although it is possible that the combination of a non-zero θ_{13} at high energy and radiative corrections could yield a nearly vanishing angle at low energy, this appears unnatural since it requires a conspiracy between two effects that are not related in general. Note also that our estimate is conservative, since we have not taken into account the contributions of neutrino Yukawa couplings above the see-saw scale [20, 97, 98, 116–118] and possible corrections from physics above the GUT scale [119].

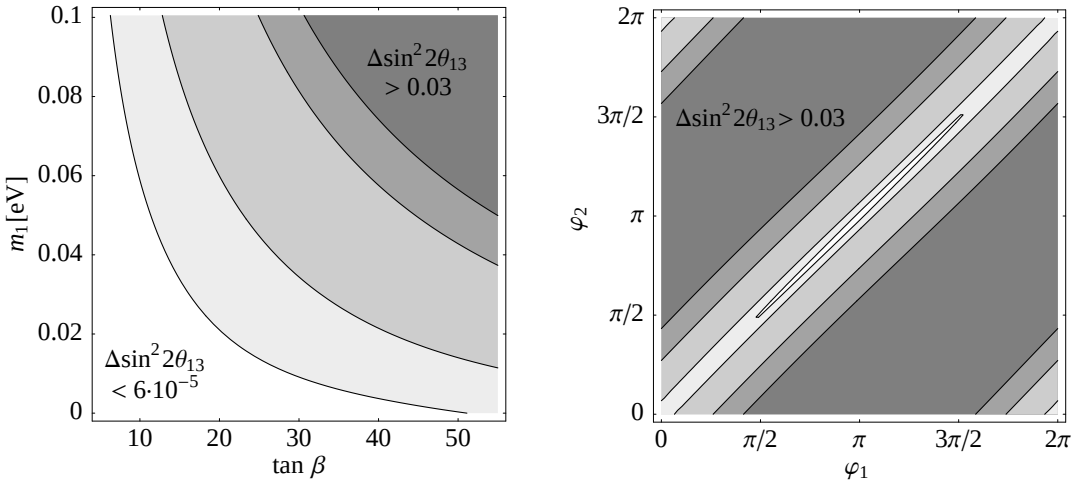

Figure 5.1: Change of $\sin^2 2\theta_{13}$ due to the RG evolution from $2 \cdot 10^{16}$ GeV to 100 GeV in the MSSM, calculated from eq. (4.20) in linear approximation with initial conditions $\theta_{13} = 0$ and LMA best-fit values for the remaining oscillation parameters. The left diagram shows the dependence on $\tan\beta$ and on the mass of the lightest neutrino for a normal mass hierarchy and Majorana phases $\varphi_1 = 0$ and $\varphi_2 = \pi$. In the right plot, the dependence on the Majorana phases is shown for $\tan\beta = 50$ and $m_1 = 0.075$ eV. The contour lines correspond to the expected sensitivities of some future experiments as given in tab. 2.2, $\Delta\sin^2 2\theta_{13} = 6 \cdot 10^{-5}$, 10^{-3}, 0.014 and 0.032, respectively. The plots look rather similar for an inverted mass hierarchy.

5.1.2 Deviations from Maximal Atmospheric Mixing

An analogous discussion can be performed for the atmospheric mixing angle. In this case, we are interested in deviations from $\theta_{23} = \pi/4$. We assume that this maximal mixing is realized at a high energy scale and calculate the running of θ_{23} down to 100 GeV in the MSSM from eq. (4.21). As before, we use the linear approximation and the best-fit values for the oscillation parameters as initial conditions. Besides, we set θ_{13} to 0, so that the evolution is independent of the Dirac CP phase.

The resulting deviations from maximal atmospheric mixing for a normal mass hierarchy are displayed in fig. 5.2. In the left diagram, the free parameters are the mass of the lightest neutrino and $\tan\beta$, while both Majorana phases are set to 0. The pattern looks very similar to the one in fig. 5.1 and is of course explained by the same reasoning. The right diagram shows the RG change as a function of the Majorana phases for $m_1 = 0.075$ eV and $\tan\beta = 50$. The result can easily be understood from eq. (4.21): in the region with $\varphi_1 \approx \varphi_2 \approx \pi$, the terms $|m_2\, e^{i\varphi_2} + m_3|^2$ and $|m_1\, e^{i\varphi_1} + m_3|^2$ are small for quasi-degenerate neutrinos, which yields the ellipse with small radiative corrections in the center of the diagram. The ellipse is wider in the φ_1-direction, since the partial derivative of $\dot{\theta}_{23}$ with respect to φ_1 is smaller than the one with respect to φ_2, mainly because of $s_{12}^2 < c_{12}^2$.

For strongly hierarchical masses, we have $m_3^2 \approx \Delta m_{\mathrm{a}}^2 \gg m_{1,2}^2$, so that eq. (4.21) simplifies to $\dot{\theta}_{23} \approx -\frac{C y_\tau^2}{32\pi^2}$, which is independent of the CP phases and the masses.

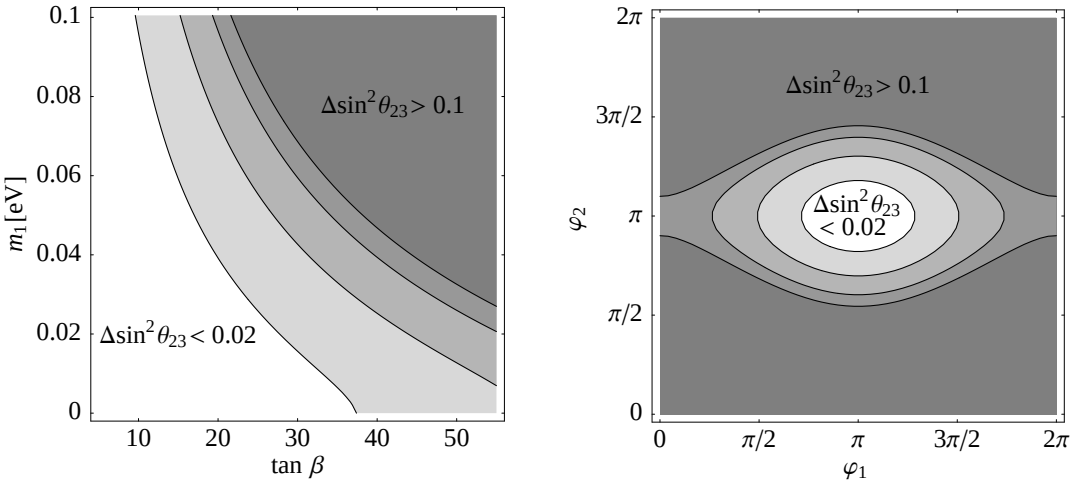

Figure 5.2: Corrections to $\sin^2\theta_{23}$ caused by the RG evolution from $2 \cdot 10^{16}$ GeV to 100 GeV in the MSSM with a normal mass hierarchy, calculated from the analytical approximation (4.21). The initial conditions were $\theta_{23} = \pi/4$, $\theta_{13} = 0$ and the best-fit values for θ_{12} and the mass squared differences. The left diagram shows the dependence on $\tan\beta$ and on the mass m_1 of the lightest neutrino for vanishing Majorana phases. In the right diagram, the dependence on the Majorana phases φ_1 and φ_2 is displayed for $m_1 = 0.075$ eV and $\tan\beta = 50$. The contour lines correspond to the expected experimental sensitivities listed in tab. 2.3, $\Delta\sin^2\theta_{23} = 0.02$, 0.05, 0.08 and 0.1, respectively. The plots are virtually unchanged for an inverted mass hierarchy.

Hence, no cancellations occur. The deviation from maximal mixing is accessible by the most sensitive experiment, in this case the superbeam JPARC-HyperKamiokande, for large $\tan\beta$. All results are virtually unchanged in the case of an inverted mass hierarchy, except that the sign of the change of θ_{23} changes.

Analogously to the discussion in the previous section, we generically expect the deviation of the low-energy $\sin^2\theta_{23}$ from 0.5 to be at least as large as the change due to the running. The comparison of fig. 5.2 with the precision of future experiments (cf. tab. 2.3) shows that in a large part of the parameter space the RG change of θ_{23} is experimentally accessible, too.

The results of this section provide an additional motivation for precision measurements of θ_{13} and $\theta_{23} - \pi/4$. Quantum corrections on their own make measurable values likely. Vice versa, even if non-zero values cannot be found experimentally, significantly improved upper bounds will serve as valuable input for theory, disfavoring parameter space regions where RG corrections are larger and pointing towards a symmetry explanation for such a special flavour structure.

5.2 Running of the Input Parameters for Leptogenesis

The see-saw scenario makes a very attractive explanation of the observed baryon asymmetry of the universe possible, which is called leptogenesis [120]. In this theory, a

lepton asymmetry is generated by the decays of the heavy singlet neutrinos[1] into lepton doublets and Higgs bosons as well as their antiparticles. This lepton asymmetry is later partially converted into a baryon asymmetry by the electroweak sphaleron processes [121, 122].

The maximal baryon asymmetry that can be generated in thermal leptogenesis is [123, 124]

$$\eta_B^{\max} \approx 0.96 \cdot 10^{-2}\, \varepsilon_1^{\max}\, \kappa_f \ , \tag{5.2}$$

where $\kappa_f \leq 1$ is an efficiency factor determined by a set of coupled Boltzmann equations, see e.g. [125]. It approaches 1 for a thermal initial abundance of singlets and no washout of the asymmetry by inverse decays and scatterings. $\varepsilon_1^{\max}$ stands for the maximal CP asymmetry in the decays of the lightest singlet, which is reached for a proper alignment of the CP phases. It can be expressed as [126]

$$\varepsilon_1^{\max}(m_1, m_3, \widetilde{m}_1) = \frac{3}{16\pi}\, \frac{M_1\, m_3}{(v/\sqrt{2})^2} \left[1 - \frac{m_1}{m_3}\left(1 + \frac{m_3^2 - m_1^2}{\widetilde{m}_1^2}\right)^{1/2}\right] \tag{5.3}$$

for a normal mass hierarchy,[2] where

$$\widetilde{m}_1 := \frac{(m_{\rm D}^\dagger m_{\rm D})_{11}}{M_1} \tag{5.4}$$

with the neutrino Dirac mass $m_{\rm D} \propto Y_\nu$. Typically, $\widetilde{m}_1$ lies between m_1 and m_3. Eq. (5.3) improves the older bound [127]

$$\varepsilon_1^{\max}(m_1, m_3) = \frac{3}{16\pi}\, \frac{M_1}{(v/\sqrt{2})^2}\, \frac{\Delta m_{\rm a}^2 + \Delta m_\odot^2}{m_3} \ . \tag{5.5}$$

As shown in [126], successful thermal leptogenesis is possible in a certain region in the $\widetilde{m}_1$-M_1 plane, which depends on the absolute neutrino mass scale via the combination $\overline{m} := \sqrt{m_1^2 + m_2^2 + m_3^2}$. If $\overline{m}$ is too large, the allowed region vanishes, so that the requirement of successful thermal leptogenesis places an upper bound on the neutrino mass, which is about $m_1 \lesssim 0.12$ eV.

The calculations relevant for leptogenesis, however, involve processes at very high energies, and therefore the RG evolution of the input parameters has to be taken into account [21, 128]. The correct procedure would be to assume specific values for the neutrino mass parameters at low energy, taking into account the experimental input, evolve them to the scale M_1 and test the leptogenesis mechanism using these values. As the full calculation is beyond the scope of this work, we give an estimate of the influence of RG effects by considering the change of the maximal CP asymmetry due

[1] In the MSSM, the decays of their superpartners play a role as well.

[2] For an inverted hierarchy, one has to replace (m_1, m_2, m_3) by (m_3, m_1, m_2).

to the running of the neutrino masses. A general discussion for $\varepsilon_1^{\max}$ in eq. (5.3) is difficult, since the relation between $\widetilde{m}_1$ and the mass eigenvalues is model-dependent. Therefore, we consider the older expression (5.5) instead, assuming that the qualitative behavior will be similar for the newer bound.

As we have seen in sec. 4.1.2, the running of the neutrino mass eigenvalues amounts to a common rescaling in the SM and in the MSSM with a small $\tan\beta$. Then, the maximal CP asymmetry in eq. (5.5) experiences the same scaling, so that it is enhanced by between 20% and 80%, cf. fig. 4.7. This is also true for the refined bound (5.3), if $\widetilde{m}_1$ is a linear combination of the light mass eigenvalues. On the other hand, the efficiency factor κ_f decreases if larger mass eigenvalues imply larger Yukawa couplings and thus a larger $\widetilde{m}_1$, which makes washout processes more efficient. In numerical studies, it was found that this actually leads to a stronger bound on the light neutrino masses [125, 129]. It also turned out that corrections from different sources happen to cancel approximately, so that the final result $m_1 \lesssim 0.12$ eV remains essentially unchanged.

In the MSSM with a large $\tan\beta$ and hierarchical neutrino masses, the evolution of $\varepsilon_1^{\max}$ is determined by the one of the largest mass eigenvalue to a good approximation, as can be seen most easily from eq. (5.3). Consequently, we have to consider the running of m_3 for a normal hierarchy, which is shown in fig. 4.7, and that of m_2 for an inverted hierarchy, which turns out to be very similar. In order to illustrate the magnitude of the RG effects and its dependence on $\tan\beta$, we pick a leptogenesis scale of $M_1 = 10^{10}$ GeV and plot $\overline{m}_{\text{rel}} := \overline{m}(M_1)/\overline{m}(M_Z)$ in fig. 5.3(a), also including small values of $\tan\beta$ for completeness. The results depend on the mixing angles now, for which we use the experimental best-fit values and $\theta_{13} = 0$. As $\overline{m}$ is roughly equal to the largest mass eigenvalue for hierarchical masses, the relative change of the maximal CP asymmetry is the same as that of $\overline{m}$.

For large $\tan\beta$ and nearly degenerate masses, $\varepsilon_1^{\max}$ runs faster than $\overline{m}$, since the change of the mass squared differences under the RG is larger than the one of the squares of the mass eigenvalues, as we have seen in sec. 4.1.2. Fig. 5.3(b) shows the relative change $\varepsilon_{\text{rel}} := \varepsilon_1^{\max}(M_1)/\varepsilon_1^{\max}(M_Z)$, calculated using eq. (5.5), as a function of the mass of the lightest neutrino for a normal mass hierarchy and fixed $\tan\beta = 50$. In this case, the CP phases play a role and damp the running of $\varepsilon_1^{\max}$. The figure shows the maximal evolution obtained for vanishing phases. The growth of the CP asymmetry becomes rather large for neutrino masses above 0.1 eV, which may compensate the decrease of the efficiency factor. Hence, for a large $\tan\beta$ and quasi-degenerate masses the RG evolution might be able to raise the upper bound on the neutrino mass from thermal leptogenesis.

Finally, we remark that the baryon asymmetry can also be created by non-thermal mechanisms [130], in which the masses of the light neutrinos may be almost degenerate [131]. In such scenarios, the RG evolution is expected to be even more important than in thermal leptogenesis, because it increases the CP asymmetry, while the effects due to the decreasing efficiency factor do not occur.

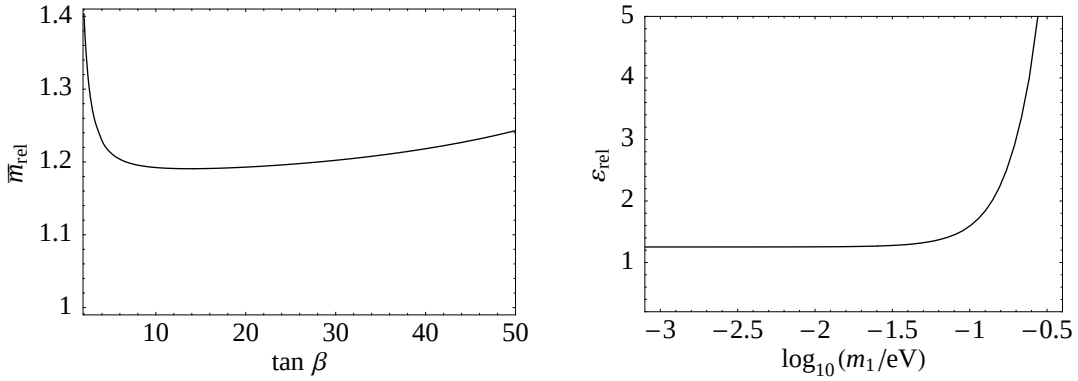

(a) Increase of $\overline{m}$ for hierarchical masses.

(b) Growth of $\varepsilon_1^{\max}$ for $\tan\beta = 50$.

Figure 5.3: Relative increase of the average neutrino mass scale $\overline{m}_{\rm rel} := \overline{m}(M_1)/\overline{m}(M_Z)$ and the maximal CP asymmetry $\varepsilon_{\rm rel} := \varepsilon_1^{\max}(M_1)/\varepsilon_1^{\max}(M_Z)$ due to the RG evolution in the MSSM with a SUSY-breaking scale of $M_{\rm SUSY} = 1$ TeV, a leptogenesis scale of $M_1 = 10^{10}$ GeV, and a normal mass hierarchy. The plots are virtually unchanged for an inverted hierarchy. We used vanishing phases, $\theta_{13} = 0$ and best-fit values for the remaining oscillation parameters.

5.3 RG Evolution of Bounds on the Absolute Neutrino Mass Scale

5.3.1 Neutrinoless Double Beta Decay

The significant running of the neutrino mass eigenvalues is also important for studying the predictions of high-energy models for the absolute neutrino mass scale and their compatibility with restrictions from searches for $0\nu\beta\beta$ decay and from cosmology, for example. The amplitude of $0\nu\beta\beta$ decay is proportional to the effective neutrino mass $\langle m_\nu \rangle$ of eq. (2.18), which is a rather complicated combination of parameters, so that the calculation of the energy dependence from the formulae in sec. 4.1.2 is lengthy. However, this effort can be avoided if one remembers that $\langle m_\nu \rangle$ is nothing but the 11-element of the neutrino mass matrix, which allows us to use eq. (4.2) and easily find

$$16\pi^2 \frac{\mathrm{d}}{\mathrm{d}t} \langle m_\nu \rangle = \left(2C\, y_e^2 + \alpha\right) \langle m_\nu \rangle \,. \tag{5.6}$$

As the first term is negligible, the RG change of the effective neutrino mass is basically caused by the universal rescaling of the mass eigenvalues alone. It is completely independent of the other neutrino mass parameters, since neither the running of y_e nor that of the terms in α is sensitive to them. Besides, the value of $\tan\beta$ is not very important here, because y_e^2 is always tiny and because α contains only the up-type quark Yukawa couplings in the MSSM. However, there is a dependence on the Higgs mass in the SM.

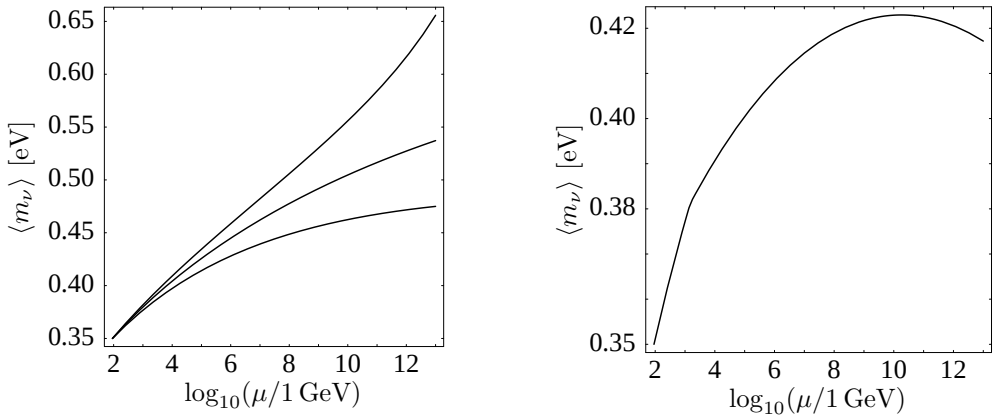

(a) SM

(b) MSSM ($\tan\beta = 50$, $M_{\mathrm{SUSY}} = 1.5$ TeV)

Figure 5.4: Extrapolation of the experimental upper limit on the effective neutrino mass for $0\nu\beta\beta$ decay, $\langle m_\nu \rangle < 0.35$ eV, to higher energies. The SM curves correspond to Higgs masses of 114 GeV, 165 GeV and 190 GeV (from bottom to top). In the MSSM, a light Higgs mass of 120 GeV is used.

Fig. 5.4 shows the running of the experimental upper limit $\langle m_\nu \rangle < 0.35$ eV [8, 9] in the SM and the MSSM. As it is rather close to the best-fit value of the recently claimed evidence for $0\nu\beta\beta$ decay, $\langle m_\nu \rangle = 0.44$ eV [30], the evolution of the latter is nearly identical. The SM plot contains three curves corresponding to different Higgs masses in the current experimentally allowed region. In the MSSM, the light Higgs mass is chosen to be about 120 GeV. The running is more significant in the SM than in the MSSM because of the contribution of the Higgs self-coupling.

5.3.2 WMAP Bound

As explained in sec. 2.3.2, cosmological observations allow to place an upper bound of about 0.7 eV onto the sum of the light neutrino masses [10], i.e. $m_i \lesssim 0.23$ eV for each mass eigenvalue. Analogous to the limit from $0\nu\beta\beta$ decay, this bound is modified substantially by the RG evolution. This is shown in fig. 5.5 for the eigenvalue m_3. As discussed in sec. 4.1.2, the running of the mass eigenvalues is not sensitive to the mixing parameters in the SM, but it depends on the Higgs mass. In the MSSM, the variation of the phases causes a slight modification of the running, but its order of magnitude is only a few percent even for the large $\tan\beta$ used in the plot. The influence of θ_{13} is negligible. Interestingly, the evolution of the sum of the mass eigenvalues is virtually independent of the mixing parameters for nearly degenerate neutrinos both in the SM and in the MSSM. This can be explained by considering the sum of the RGEs (4.25). For $m_1 \sim m_2 \sim m_3$, the terms proportional to y_τ^2 add up to 1, with small corrections of the order of $\frac{\Delta m_a^2}{m^2}$ and θ_{13}.

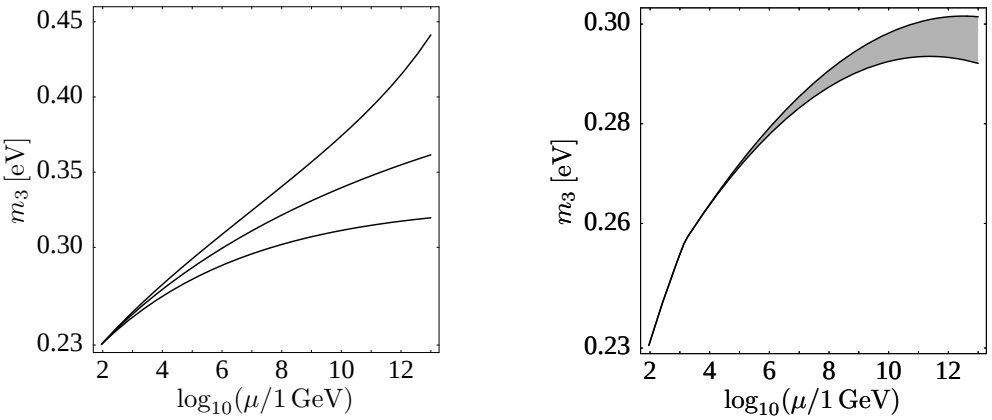

(a) SM (b) MSSM ($\tan\beta = 50$, $M_{\mathrm{SUSY}} = 1.5$ TeV)

Figure 5.5: Extrapolation of the upper limit on the neutrino mass from cosmology, $m_i \lesssim 0.23$ eV, to higher energies, represented by the running of the mass eigenvalue m_3. The SM curves correspond to Higgs masses of 114 GeV, 165 GeV and 190 GeV (from bottom to top). In the MSSM, a light Higgs mass of 120 GeV is used, and the CP phases are varied between 0 and 2π, which results in the gray-shaded region.

5.4 From Bimaximal Mixing to the LMA Solution

One application for the RG evolution in the type I see-saw scenario is to open up new possibilities for model building. Among the neutrino mixing parameters, the solar angle θ_{12} is especially interesting in this context, since it is not easy to find a flavour symmetry that can explain its sizable deviation from maximal mixing while keeping θ_{23} close to maximal and θ_{13} small at the same time. Of course, the large but non-maximal solar angle could simply be a random number, as favored by the anarchy hypothesis [132–134]. The alternative that we will discuss in this section is that it is instead explained by a more symmetric theory with bimaximal mixing, i.e. $\theta_{12} = \theta_{23} = \pi/4$ and $\theta_{13} = 0$, at high energies whose predictions are changed by quantum corrections [20, 135, 136]. As the running below the see-saw scale is too small in the SM and as the solar angle always increases when running downwards in the MSSM (cf. sec. 4.1.2), this is only possible if the dominant RG effects occur above this scale, i.e. if they are caused by the neutrino Yukawa couplings.

We will restrict ourselves to the CP-conserving case of real mass matrices and Yukawa couplings. Except for one example, we also assume positive neutrino mass eigenvalues, i.e. vanishing Majorana phases. Besides, we have to specify the neutrino Yukawa couplings in order to determine the initial conditions for all neutrino mass parameters uniquely. We choose

$$Y_\nu = X \ \mathrm{diag}(1, \varepsilon, \varepsilon^2) \tag{5.7}$$

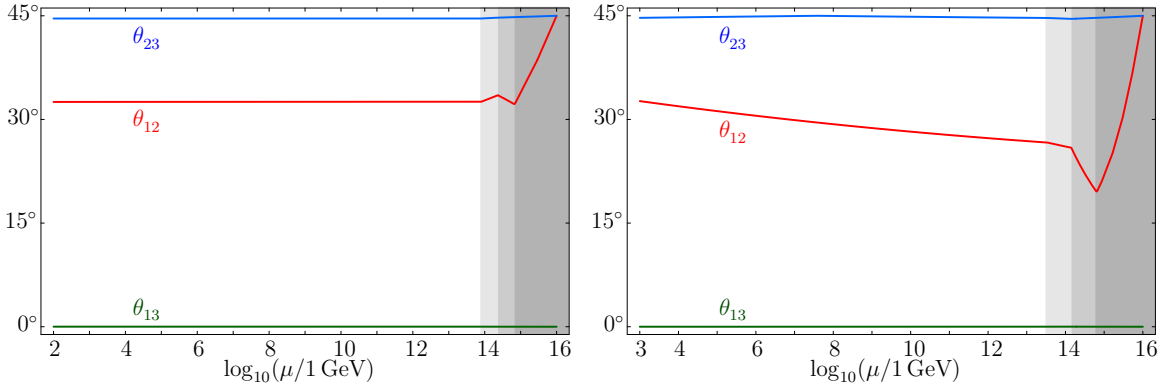

(a) SM, $\varepsilon = 0.65$, $m_1 = 0.024$ eV

(b) MSSM, $\tan\beta = 5$, $\varepsilon = 0.525$, $m_1 = 0.025$ eV

Figure 5.6: Running of the leptonic mixing angles from bimaximal mixing at the GUT scale to (a) the electroweak scale in the SM and (b) the SUSY-breaking scale (taken to be about 1 TeV) in the MSSM. In both cases we used the type I see-saw scenario, and the gray-shaded regions mark the effective theories obtained from integrating out the singlets, as described in sec. 4.2.2. We chose a normal mass hierarchy, i.e. m_1 is the mass of the lightest neutrino (the given numbers are valid at low energy), and vanishing CP phases. The initial condition for the neutrino Yukawa couplings was $Y_\nu(M_{\mathrm{GUT}}) = \mathrm{diag}(1, \varepsilon, \varepsilon^2)$.

at the GUT scale. The singlet mass matrix M_{R} is then determined from the effective light neutrino mass matrix m_ν with bimaximal mixing and Y_ν via eq. (4.37).

5.4.1 Examples for the Running of the Mixing Angles

Fig. 5.6 shows typical examples for the running of the mixing angles from the GUT scale to the electroweak or SUSY-breaking scale, respectively. They demonstrate an important effect that appears for most choices of the initial parameters: the solar angle θ_{12} changes drastically, while the changes in θ_{13} and θ_{23} are comparatively small. This makes it possible to reconcile bimaximal mixing at high energies with observations, since the evolution of the solar mixing can produce a large deviation from $\pi/4$, as required by the LMA solution. At the same time, the changes of the other angles are small enough to avoid spoiling their agreement with experimental data.

If one of the Majorana phases equals π, i.e. one of the states with masses m_1 and m_2 has a negative CP parity, it is much harder to obtain the desired RG effects, since the running of θ_{12} is strongly damped. Nevertheless, the evolution to the LMA solution is still possible in the SM due to the non-degeneracy of the see-saw scales. An example with $\varphi_2 = \pi$ is shown in fig. 5.7. There we have chosen a different form of Y_ν at the GUT scale, $Y_\nu = 0.5\,\mathrm{diag}(\varepsilon^2, \varepsilon, 1)$. We will not study this possibility in detail and return to the case of zero Majorana phases in the following.

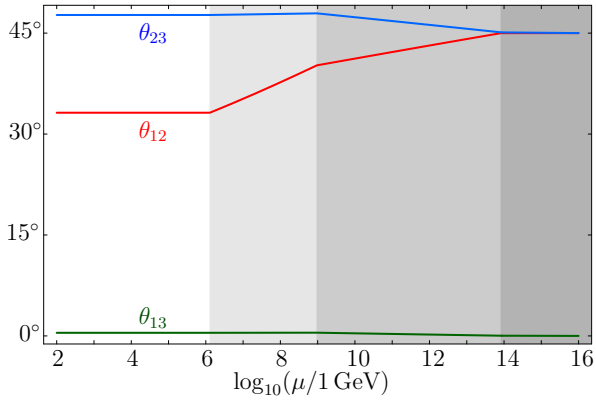

Figure 5.7: RG evolution in the SM with a negative CP parity for the neutrino with mass m_2 (corresponding to $\varphi_2 = \pi$), $Y_\nu(M_{\mathrm{GUT}}) = 0.5\ \mathrm{diag}(\varepsilon^2, \varepsilon, 1)$, $\varepsilon = 0.0035$ and a strong normal mass hierarchy with a mass of 0.004 eV for the lightest neutrino. The running from bimaximal mixing to the LMA solution takes place exclusively between the see-saw scales.

5.4.2 Analytic Approximations

In order to systematically understand the effect found in the previous section, let us study the RG evolution of the mixing angles at the GUT scale analytically. Analogously to the derivation of the RGEs for the mixing parameters below the see-saw scale in sec. 4.1.2, we differentiate the relation between m_ν, its eigenvalues and the neutrino mixing matrix, eq. (4.5), and insert the relevant RGE, in this case (4.38). Afterwards, we plug in the initial values of the mixing parameters at the GUT scale, $\theta_{12} = \theta_{23} = \pi/4$, $\theta_{13} = 0$ and $\delta = \varphi_1 = \varphi_2 = 0$. We assume that the RG evolution is dominated by the effect of the neutrino Yukawa couplings. This is not necessarily true in the MSSM for a large $\tan\beta$, where the contribution from the tau Yukawa coupling is also sizable, but the approximation is nevertheless accurate enough to obtain a qualitative understanding of the situation.

For the neutrino Yukawa couplings, we use the parameterization

$$Y_\nu = \mathrm{diag}(y_1, y_2, y_3) \cdot V^T(\phi_{12}, \phi_{13}, \phi_{32}) \ , \tag{5.8}$$

where $V(\phi_{12}, \phi_{13}, \phi_{32})$ denotes an orthogonal matrix parameterized as in eq. (2.15b), with the angles θ_{ij} exchanged by ϕ_{ij} and the phase set to zero. To obtain the most general real Yukawa matrix, an additional orthogonal matrix multiplying the above Y_ν from the left is needed. However, in our case we can change to a basis where this additional matrix does not appear by transforming $Y_\nu \to V^T Y_\nu$, $M_{\mathrm{R}} \to V^T M_{\mathrm{R}}\, V$, and $\nu_{\mathrm{R}} \to V^T \nu_{\mathrm{R}}$, since this leaves m_ν invariant.

Both in the SM and in the MSSM, this procedure yields for the ratios of the deriva-

tives of the mixing angles at the GUT scale [20]

$$\left.\frac{\dot\theta_{12}}{\dot\theta_{13}}\right|_{M_{\rm GUT}} = \frac{2\sqrt{2}\;(m_1+m_2)\;(m_3-m_1)\;(m_3-m_2)\;F_1}{(m_2-m_1)\;\left[8\;(m_3^2-m_1\,m_2)\;F_2+4\sqrt{2}\;(m_2-m_1)\;m_3\,F_3\right]}$$

$$\approx \begin{cases} \pm\dfrac{1}{2\sqrt{2}}\,\dfrac{m_2+m_1}{m_2-m_1}\,\dfrac{F_1}{F_2} & \text{for hierarchical neutrino masses}^1 \\ \dfrac{1}{2\sqrt{2}}\,\dfrac{\Delta m^2_{\rm a}}{\Delta m^2_\odot}\,\dfrac{F_1}{F_2} & \text{for degenerate neutrino masses} \end{cases} \tag{5.9a}$$

$$\left.\frac{\dot\theta_{12}}{\dot\theta_{23}}\right|_{M_{\rm GUT}} = \frac{2\sqrt{2}\;(m_1+m_2)\;(m_3-m_1)\;(m_3-m_2)\;F_1}{(m_2-m_1)\;\left[8\;(m_2-m_1)\;m_3\,F_2+4\sqrt{2}\;(m_3^2-m_1\,m_2)\,F_3\right]}$$

$$\approx \begin{cases} \pm\dfrac{1}{2}\,\dfrac{m_2+m_1}{m_2-m_1}\,\dfrac{F_1}{F_3} & \text{for hierarchical neutrino masses}^1 \\ \dfrac{1}{2}\,\dfrac{\Delta m^2_{\rm a}}{\Delta m^2_\odot}\,\dfrac{F_1}{F_3} & \text{for degenerate neutrino masses} \end{cases} \tag{5.9b}$$

with

$$\begin{aligned} F_1 = {} & \left(y_1^2-y_2^2\right)\left\{\cos 2\phi_{12}\left[(\cos 2\phi_{13}-3)\sin 2\phi_{23}-6\cos^2\phi_{13}\right]-\right. \\ & \left.-\,4\cos 2\phi_{23}\;\sin 2\phi_{12}\;\sin\phi_{13}\right\}+ \\ & +\left(y_1^2+y_2^2-2y_3^2\right)\left[\cos 2\phi_{13}\,(\sin 2\phi_{23}-3)+(1+\sin 2\phi_{23})\right], \end{aligned} \tag{5.10a}$$

$$\begin{aligned} F_2 = {} & 2\left(y_1^2-y_2^2\right)\cos\phi_{13}\;\sin 2\phi_{12}\,(\sin\phi_{23}-\cos\phi_{23})- \\ & -\left(y_1^2+y_2^2-2y_3^2+(y_1^2-y_2^2)\;\cos 2\phi_{12}\right)\sin 2\phi_{13}\,(\cos\phi_{23}+\sin\phi_{23}), \end{aligned} \tag{5.10b}$$

$$\begin{aligned} F_3 = {} & \left(y_1^2-y_2^2\right)\left[\cos 2\phi_{12}\,(\cos 2\phi_{13}-3)\cos 2\phi_{23}+4\sin 2\phi_{12}\;\sin\phi_{13}\;\sin 2\phi_{23}\right]+ \\ & +2\left(y_1^2+y_2^2-2y_3^2\right)\;\cos^2\phi_{13}\;\cos 2\phi_{23}\;. \end{aligned} \tag{5.10c}$$

These results can also be obtained from the formulae derived in [93] in principle. Note that F_2 is zero for diagonal Y_ν, so that the approximation in the second line of eq. (5.9a) cannot be used. However, this does not affect our main conclusion. The constants F_1, F_2 and F_3 depend on the choice of Yukawa couplings, of course, but we expect their ratios to be of the order of one if they are not fine-tuned. Consequently, the RG change of θ_{12} is larger than that of the other angles if the mass-dependent factors in eqs. (5.9) are large. This is always the case for degenerate neutrino masses, since $\Delta m^2_{\rm a} \gg \Delta m^2_\odot$. As $m_1 - m_2$ is related to the small solar mass squared difference, it is also true for non-degenerate mass schemes, unless m_1 is very small, in which case the ratio approaches 1. Finally, it can be shown that the running of θ_{12} is always enhanced compared to that of θ_{13} and θ_{23} for inverted schemes. Hence, we conclude that as in the region below the see-saw scale, this is a generic effect.

[1] This approximation is also valid for a relatively weak hierarchy, where m_3 is a few times larger or smaller than m_1 and m_2.

5.4.3 Parameter Space Regions Compatible with the LMA Solution

These analytical results show that the examples of sec. 5.4.1 are not just special cases obtained by fine-tuning. Hence, it is reasonable to ask how large the parameter space region is which yields low-energy masses and mixings within the experimentally allowed region at the 3σ CL. This question can be answered by scanning over the parameters at the GUT scale, computing the running for each sample and comparing the resulting quantities at low energies with the experimental data.

The requirement of bimaximal mixing and zero CP phases fixes 6 of the 9 parameters in the light neutrino mass matrix at the GUT scale. The remaining ones are linear combinations of the three mass eigenvalues, which we call a, b and c. In the basis where the charged lepton Yukawa matrix is diagonal, we have from eq. (2.12a) together with (2.14) and (2.15)

$$m_\nu^{\text{bimax}} = V_{\text{bimax}} \cdot \text{diag}(m_1, m_2, m_3) \cdot V_{\text{bimax}}^T = \begin{pmatrix} a-b & c & -c \\ c & a & b \\ -c & b & a \end{pmatrix} , \tag{5.11}$$

and

$$a = \frac{1}{4}\left(m_1 + m_2 + 2\,m_3\right) \ , \tag{5.12a}$$

$$b = \frac{1}{4}\left(-m_1 - m_2 + 2\,m_3\right) \ , \tag{5.12b}$$

$$c = \frac{m_2 - m_1}{2\sqrt{2}} \ , \tag{5.12c}$$

where V_{bimax} is the orthogonal matrix obtained from inserting the bimaximal mixing angles into the parameterization (2.15b). It can be seen that a is related to the absolute neutrino mass scale, while b and c determine the mass differences. Therefore, we fix them by requiring $\Delta m^2_\odot$ and Δm^2_{a} at the electroweak scale to be compatible with observations, which leaves a as the only free parameter in m_ν^{bimax}.

As the mass matrix M_{R} is given by the see-saw formula, the remaining parameters are the 9 real entries of the neutrino Yukawa couplings. A scan over the complete 10-dimensional parameter space is clearly not feasible, so that we have to apply an additional restriction. We choose the diagonal form given in eq. (5.7) for Y_ν, which contains only 2 parameters, X and ε. The latter controls the hierarchy of the entries in Y_ν and thus the degeneracy of the see-saw scales.

Varying a and ε for a fixed value of $X = 1$, we find that the low-energy oscillation parameters lie within the experimentally allowed range at 3σ, if a and ε are taken from the shaded regions in the plots in fig. 5.8. We show the results for the SM and the MSSM with a normal mass hierarchy. The comparison with experimental data is performed at the electroweak scale or at 1 TeV for the SM and the MSSM, respectively. Both a and

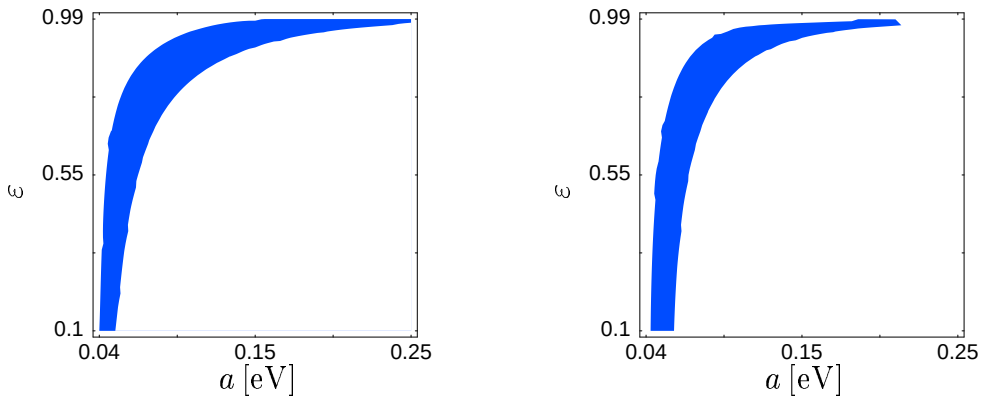

(a) SM (b) MSSM

Figure 5.8: Parameter space regions for which bimaximal neutrino mixing at the GUT scale $M_{\mathrm{GUT}} = 10^{16}$ GeV is compatible with experimental results at the 3σ CL. The quantities a and ε are defined in the text. We have chosen a normal mass hierarchy and $X = 1$ for the scale factor of the neutrino Yukawa couplings.

ε may vary within rather broad ranges. This means that hierarchical and degenerate masses are possible for both the light and the heavy neutrinos. However, there is a correlation: if the former masses are degenerate, the latter have to be degenerate as well, and vice versa. This is due to the fact that for degenerate light masses, the solar angle tends to run too much unless the region where the neutrino Yukawa couplings contribute is minimized by making the heavy masses degenerate as well.

For smaller values of X, the contribution from Y_ν to the evolution of the mixing angles above the largest see-saw scale is suppressed by a factor of X^2. Nevertheless, satisfactory low-energy values can still be reached. A SM example is displayed in fig. 5.9. Here the large change of θ_{12} takes place between the see-saw scales. Due to this effect, fig. 5.8(a) does not change much. This again demonstrates that one cannot avoid integrating out the singlet neutrinos one by one and using the complete series of effective theories as discussed in sec. 4.2.2. In the MSSM the behavior is different. For X around 0.1, the allowed region moves to the lower right quarter in the a-ε plane, i.e. one needs the lightest neutrino mass to exceed a minimal value in order to generate enough running.

For an inverted neutrino mass ordering, there are allowed parameter space regions, too. They are rather small for $X = 1$, since the change of θ_{12} tends to be too large, but they increase for smaller values of X.

Of course, different choices for the Yukawa couplings at the GUT scale are possible, which lead to different shapes of the allowed parameter space regions. A restriction stems from the requirement by the LMA solution that the solar mixing lie on the "light side", which means that $\Delta m^2_\odot > 0$ and $\theta_{12} < \pi/4$. With bimaximal mixing at the GUT

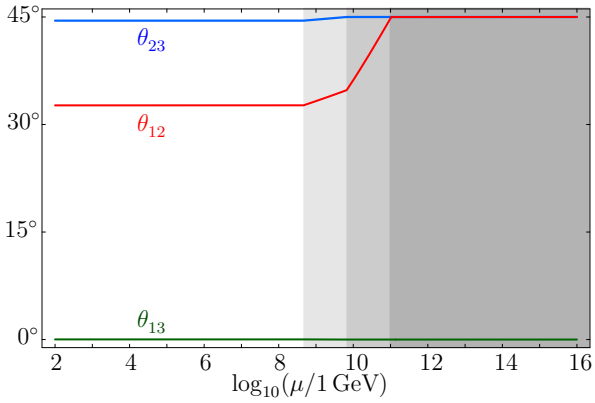

Figure 5.9: Running of the lepton mixing angles in the SM for very small neutrino Yukawa couplings with a scale factor $X = 0.01$, $\varepsilon = 0.3$, $a = 0.0535$ eV and a normal mass hierarchy. The mass of the lightest neutrino at the electroweak scale is 0.017 eV.

scale, the sign of $\Delta m^2_\odot$ is not defined. However, using the analytic approximation of sec. 5.4.2, the sign just below the GUT scale can be calculated, which yields a hint towards the sign at low energies. We find $\Delta m^2_\odot > 0$ if and only if $F_1 < 0$. This excludes some forms of Y_ν, for example $Y_\nu = \mathrm{diag}(\varepsilon^2, \varepsilon, 1)$.

In the next section, we will study the running in see-saw scenarios from a different point of view. Rather than considering the mixing angles, we will discuss the evolution of the elements of the neutrino mass matrix in connection with texture zeros.

5.5 Stability of Texture Zeros under Radiative Corrections

A widely used approach towards explaining the masses and mixing parameters of neutrinos is to assume certain elements of the neutrino mass matrix to be zero, cf. sec. 2.5.1. A number of studies have investigated which textures with one or more zeros are compatible with experimental data, for instance [61, 62, 137–142]. If such texture zeros are more than just a numerical coincidence, they have to be connected to some flavour symmetry, see e.g. [63]. Typically, this symmetry will be broken at a very high energy such as the GUT scale. Therefore, its predictions are subject to corrections due to the RG running. In this section, we will investigate how these corrections affect the known statements about texture zeros. In particular, we will show that some of the patterns that are considered excluded [61, 62] can become compatible with experimental data, if the running leads to sufficiently large entries in the positions of the former zeros.

We work in the basis where the Yukawa matrix of the charged leptons is diagonal, i.e. we use the same classification of textures as in [61, 62]. Then, eq. (4.2) shows that the radiative corrections to each element of the neutrino mass matrix (or, equivalently, κ) are proportional to this element itself, so that a zero entry remains zero. However,

this changes in the type I see-saw scenario in the energy region above the see-saw scale, where the neutrino Yukawa couplings contribute to the β-functions. In general, they are non-diagonal and hence cause a mixing of the mass matrix elements, so that the elements which are zero at the high-energy scale obtain a finite value at low energies and thus texture zeros are destroyed. We will determine under which conditions this modifies the compatibility of textures with experimental data in the following. We will apply a bottom-up approach, i.e. we will study if the RG running from low to high energies can lead to a zero element. Therefore, we will refer to this possibility as radiative generation rather than destruction of texture zeros.

The relevant quantity in the full theory with singlet neutrinos present is the effective light neutrino mass matrix of eq. (4.37), whose energy dependence was given in eq. (4.38). Between the mass thresholds, the RG equations are modified because the singlets are successively integrated out so that their Yukawa couplings do not contribute any longer, as discussed in sec. 4.2.2.

5.5.1 Conditions for Stability

Mass Matrix Elements

In the bottom-up approach, one can understand under which circumstances the radiative generation of texture zeros is possible. If an element of the neutrino mass matrix, say $m_{\nu_{ij}}$, is to be zero at the GUT scale M_{GUT}, the sum of its value at the see-saw scale M_1 and its change due to the running between this scale and M_{GUT} has to be zero. To a first approximation, this means that

$$m_{\nu_{ij}}\big|_{M_1} \approx -\dot{m}_{\nu_{ij}}\big|_{M_1} \cdot \ln \frac{M_{\mathrm{GUT}}}{M_1} \,. \tag{5.13}$$

If $m_{\nu_{ij}}$ is complex, this relation must be satisfied for both its real and its complex part. Hence, we can assume m_ν to be real in the following derivation if we keep in mind that each equation actually stands for two. For the moment, we neglect the mass differences of the singlet neutrinos, so that all their Yukawa couplings begin to influence the running at the mass of the lightest singlet, M_1. To obtain a conservative bound, we assume this mass to be larger than about 10^9 GeV. Of course, smaller values are possible in principle, but then the neutrino Yukawa couplings have to be rather small as well, so that the RG evolution is actually suppressed. In the numerical examples presented later on, the see-saw scale lies comfortably above this lower bound. With $M_1 \gtrsim 10^9$ GeV and $M_{\mathrm{GUT}} \sim 10^{16}$ GeV, eq. (5.13) becomes

$$-\frac{16\pi^2\,\dot{m}_{\nu_{ij}}}{m_{\nu_{ij}}} \gtrsim 10 \,. \tag{5.14}$$

Here and in the following, we implicitly assume the values of energy-dependent quantities like m_ν to be taken at M_1. Keeping only the top and tau Yukawa couplings and

introducing the abbreviation $H := Y_\nu^\dagger Y_\nu$, the RG equation (4.38) can be rewritten for an individual matrix element,

$$16\pi^2\,\dot{m}_{\nu_{ij}} = (m_\nu H)_{ij} + (m_\nu H)_{ji} + \sigma\, m_{\nu_{ij}} \tag{5.15}$$

with

$$\sigma := 2\,\mathrm{Tr}\,H + (\delta_{i3}+\delta_{j3})\,y_\tau^2 + 6y_t^2 - \frac{6}{5}g_1^2 - 6g_2^2 \approx 2\,\mathrm{Tr}\,H + (\delta_{i3}+\delta_{j3})\,y_\tau^2 + 1 \tag{5.16}$$

in the MSSM. The number 1 in the last expression is the approximate value of $6y_t^2 - \frac{6}{5}g_1^2 - 6g_2^2$ at 10^{13} GeV. For different energies it changes by less than a factor of 2, which is not a problem for our considerations. For later use, note that σ is always positive. Plugging (5.15) into (5.14) yields

$$-\frac{(m_\nu H)_{ij} + (m_\nu H)_{ji}}{m_{\nu_{ij}}} \gtrsim 10 + \sigma \tag{5.17}$$

or, collecting all terms independent of m_ν on the right hand side,

$$-\frac{\sum_{k\neq j} m_{\nu_{ik}} H_{kj} + \sum_{k\neq i} m_{\nu_{jk}} H_{ki}}{m_{\nu_{ij}}} \gtrsim 10 + \sigma + H_{ii} + H_{jj}\ . \tag{5.18}$$

Careful inspection of this relation shows that the radiative generation of texture zeros requires at least one element of m_ν to be roughly an order of magnitude larger than the value of the zero candidate at the see-saw scale. In the complex case, both the real and the imaginary parts of the matrix elements have to satisfy this requirement.

To see this, consider the easiest case first: let us assume that the left hand side of ineq. (5.18) is dominated by a single term, say $m_{\nu_{ik}} H_{kj}$ $(i \neq j)$, and that $H_{kj} \sim 1$. Then $H_{jj} \sim 1$, H_{ii} is small, and $\mathrm{Tr}\,H \sim 2$. Hence, we obtain

$$-\frac{m_{\nu_{ik}}}{m_{\nu_{ij}}} \gtrsim 16\ . \tag{5.19}$$

In principle, H_{kj} could be as large as 3 as long as all $|Y_{\nu_{ij}}| \lesssim 1$. This would reduce the required hierarchy somewhat, but the difference is not dramatic as the terms containing H on the right hand side become larger as well.

The smallest hierarchy is expected if all elements of H are large. For $H_{ij} \sim 1$, we find

$$-\frac{\sum_{k\neq j} m_{\nu_{ik}} + \sum_{k\neq i} m_{\nu_{jk}}}{m_{\nu_{ij}}} \gtrsim 19\ , \tag{5.20}$$

so that

$$-\frac{m_{\nu_{ik}}}{m_{\nu_{ij}}} \gtrsim 5 \tag{5.21}$$

if all elements of the neutrino mass matrix except $m_{\nu_{ij}}$ are approximately equal. Thus, the required hierarchy can be a bit smaller than an order of magnitude. However, it is difficult to find a Yukawa matrix in this case which is perturbative and still reproduces the correct neutrino mass parameters via the see-saw formula. Hence, we conclude that the above statement about the required hierarchy in m_ν is reasonably conservative.

In the SM, the first two terms on the right hand side of eq. (5.15) are multiplied by an additional factor of $\frac{1}{2}$, and σ is replaced by

$$\sigma = 2\,\mathrm{Tr}\,H + 6y_t^2 - \frac{9}{10}g_1^2 - \frac{9}{2}g_2^2 \overset{M_1\approx 10^{13}\ \mathrm{GeV}}{\approx} 2\,\mathrm{Tr}\,H + 0.4\ , \tag{5.22}$$

where we have neglected the tau Yukawa coupling, too, since it is always small in the SM. Because of the change in eq. (5.15), the right hand side of ineq. (5.17) has to be multiplied by 2. Thus, a hierarchy is necessary in the SM as well, and it has to be even larger than in the MSSM, so that the generation of texture zeros becomes harder. On the other hand, the effects of the running between the mass scales of the heavy singlets can be especially significant in the SM, as we have seen in sec. 4.2.2, and might provide a loophole attenuating the restrictions found in this section.

Mass Eigenvalues

Let us now see what the hierarchy requirement for the elements of the neutrino mass matrix means for the mass eigenvalues. For this purpose, we express the matrix elements in terms of the eigenvalues m_1, m_2, m_3 and the mixing parameters. We use the approximations $\theta_{13} \approx 0$ and $\Delta m^2_\odot \ll \Delta m^2_{\mathrm{a}}$. For a normal mass hierarchy, we have $m_1 := m$, $m_2 = \sqrt{m^2 + \Delta m^2_\odot}$ and $m_3 \approx \sqrt{m^2 + \Delta m^2_{\mathrm{a}}}$. Using eq. (2.12a) and the standard parameterization (2.15) in the limit $\theta_{13} = 0$, we obtain (assuming without loss of generality that all unphysical phases in the MNS matrix are zero)

$$m_{\nu_{11}} \approx \sqrt{m^2 + \Delta m^2_\odot}\, s_{12}^2\, e^{i\varphi_2} + m\, c_{12}^2\, e^{i\varphi_1}\ , \tag{5.23a}$$

$$m_{\nu_{22}} \approx \sqrt{m^2 + \Delta m^2_{\mathrm{a}}}\, s_{23}^2 + \sqrt{m^2 + \Delta m^2_\odot}\, c_{12}^2 c_{23}^2\, e^{i\varphi_2} + m\, s_{12}^2 c_{23}^2\, e^{i\varphi_1}\ , \tag{5.23b}$$

$$m_{\nu_{33}} \approx \sqrt{m^2 + \Delta m^2_{\mathrm{a}}}\, c_{23}^2 + \sqrt{m^2 + \Delta m^2_\odot}\, c_{12}^2 s_{23}^2\, e^{i\varphi_2} + m\, s_{12}^2 s_{23}^2\, e^{i\varphi_1}\ , \tag{5.23c}$$

$$m_{\nu_{12}} \approx \left(\sqrt{m^2 + \Delta m^2_\odot}\, e^{i\varphi_2} - m\, e^{i\varphi_1}\right) c_{12} s_{12} c_{23}\ , \tag{5.23d}$$

$$m_{\nu_{13}} \approx -\left(\sqrt{m^2 + \Delta m^2_\odot}\, e^{i\varphi_2} - m\, e^{i\varphi_1}\right) c_{12} s_{12} s_{23}\ , \tag{5.23e}$$

$$m_{\nu_{23}} \approx \left(\sqrt{m^2 + \Delta m^2_{\mathrm{a}}} - \sqrt{m^2 + \Delta m^2_\odot}\, c_{12}^2\, e^{i\varphi_2} - m\, s_{12}^2\, e^{i\varphi_1}\right) c_{23} s_{23}\ . \tag{5.23f}$$

If the mass spectrum is hierarchical, i.e. $m \approx 0$, the elements of the first row and column of m_ν are of the order of $\sqrt{\Delta m^2_\odot}$, while the others are of the order of $\sqrt{\Delta m^2_{\mathrm{a}}}$. Hence, the maximal hierarchy between two elements of m_ν is roughly $\sqrt{\Delta m^2_\odot / \Delta m^2_{\mathrm{a}}} \sim 1/6$, which is not enough for the generation of a texture zero. This statement holds independent

of the Majorana phases φ_1 and φ_2, since each matrix element is dominated by just a single term. Note that the running of the mixing angles between the electroweak and the see-saw scale does not change this conclusion, since it is not significant for a strong normal hierarchy, as shown in ch. 4.

For quasi-degenerate neutrinos, i.e. $m^2 \gg \Delta m^2_{\mathrm{a}}$, the above formulae simplify to

$$m_{\nu_{11}} \approx m \left(s_{12}^2\, e^{i\varphi_2} + c_{12}^2\, e^{i\varphi_1}\right), \tag{5.24a}$$
$$m_{\nu_{22}} \approx m \left(s_{23}^2 + c_{12}^2 c_{23}^2\, e^{i\varphi_2} + s_{12}^2 c_{23}^2\, e^{i\varphi_1}\right), \tag{5.24b}$$
$$m_{\nu_{33}} \approx m \left(c_{23}^2 + c_{12}^2 s_{23}^2\, e^{i\varphi_2} + s_{12}^2 s_{23}^2\, e^{i\varphi_1}\right), \tag{5.24c}$$
$$m_{\nu_{12}} \approx m \left(e^{i\varphi_2} - e^{i\varphi_1}\right) c_{12} s_{12} c_{23}\ , \tag{5.24d}$$
$$m_{\nu_{13}} \approx -m \left(e^{i\varphi_2} - e^{i\varphi_1}\right) c_{12} s_{12} s_{23}\ , \tag{5.24e}$$
$$m_{\nu_{23}} \approx m \left(1 - c_{12}^2\, e^{i\varphi_2} - s_{12}^2\, e^{i\varphi_1}\right) c_{23} s_{23}\ . \tag{5.24f}$$

As the situation now depends on the values of the Majorana phases, we consider the real cases first. For $\varphi_1 = \varphi_2 = 0$ the diagonal elements of the mass matrix approach m, while the off-diagonal entries go to zero. One can show that $m_{\nu_{ij}}/m_{\nu_{ii}}$ $(i \neq j)$ are monotonous functions of m. Hence, for a sufficiently large neutrino mass scale the required hierarchy in the matrix elements arises and the radiative generation of zeros in the off-diagonal elements becomes possible. In contrast, it is not possible to generate zeros in the diagonal entries.

If one Majorana phase is π and the other one zero, i.e. one of the mass eigenstates has a negative CP parity, all $|m_{\nu_{ij}}|$ become large for $m \to \infty$. The smallest entry is $|m_{\nu_{11}}| \approx m \cos 2\theta_{12}$, but it cannot be much smaller than the other matrix elements due to the experimental bound $\cos 2\theta_{12} > 0.22$ at the 3σ level, cf. tab. 2.1. Quantum corrections between the electroweak and the see-saw scale are not likely to change this situation, since they are not significant in the SM, and since they only cause a decrease of θ_{12} in the MSSM unless θ_{13} is close to its experimental upper limit, as we have found before. Consequently, the generation of a texture zero is unlikely.

The last real case, $\varphi_1 = \varphi_2 = \pi$, leads to the same conclusions for the first row and column as $\varphi_1 = \varphi_2 = 0$, because only the phase difference is relevant here. The situation changes for the diagonal elements $m_{\nu_{22}}$ and $m_{\nu_{33}}$, which go to $\pm m \cos 2\theta_{23}$ now, so that zeros can be generated in these elements if θ_{23} is close to 45°. The remaining off-diagonal entry $m_{\nu_{23}}$ stays large for large atmospheric mixing and thus cannot be driven to zero by the RG in this case.

For a complex mass matrix, i.e. arbitrary phases, the hierarchy requirement must be satisfied by both the real and the imaginary parts of the respective matrix elements, as mentioned in the beginning of this section. As an example, consider $m_{\nu_{23}}$ and $m_{\nu_{33}}$ in the limit of degenerate masses and negligible θ_{13}:

$$\mathrm{Re}\, m_{\nu_{23}} \approx m \left(1 - c_{12}^2 \cos\varphi_2 - s_{12}^2 \cos\varphi_1\right) c_{23} s_{23}\ , \tag{5.25a}$$
$$\mathrm{Re}\, m_{\nu_{33}} \approx m \left(c_{23}^2 + c_{12}^2 s_{23}^2 \cos\varphi_2 + s_{12}^2 s_{23}^2 \cos\varphi_1\right), \tag{5.25b}$$

$$\mathrm{Im}\, m_{\nu_{23}} \approx -m \left(c_{12}^2 \sin\varphi_2 + s_{12}^2 \sin\varphi_1\right) c_{23} s_{23} \,, \tag{5.25c}$$

$$\mathrm{Im}\, m_{\nu_{33}} \approx m \left(c_{12}^2 s_{23}^2 \sin\varphi_2 + s_{12}^2 s_{23}^2 \sin\varphi_1\right) . \tag{5.25d}$$

While the real parts can still be hierarchical as long as the phases are close to 0 or π, this is not possible for the imaginary parts. The reason is that the hierarchy in the real cases is due to a cancellation between the three terms contributing to $m_{\nu_{23}}$, In the real part, non-zero phases only cause a misalignment of these terms, which can be small. However, only two of them contribute to the imaginary part, so that the cancellation cannot work here. The same reasoning holds for $m_{\nu_{33}}$ and $m_{\nu_{22}}$ in the case $\varphi_1 = \varphi_2 = \pi$. Consequently, one expects at first sight that texture zeros can only be generated radiatively in the CP-conserving cases. However, this is too pessimistic, since adding a small imaginary part to the neutrino mass matrix does not change the mixing angles and mass squared differences significantly, except for special cases such as degenerate mass eigenvalues. This allows us to make the imaginary part vanish by slightly adjusting the initial mass matrix, if the values of the Majorana phases are not too far away from 0 or π. For the elements of the first row and column, only the difference of the phases is relevant. Hence, there the radiative generation of a texture zero is possible for arbitrary Majorana phases, provided that their difference is small.

If θ_{13} is non-zero, a finite Dirac phase δ could be an obstacle for the generation of texture zeros as well. However, as θ_{13} is experimentally restricted to be relatively small and does not grow too much under the RG, the same argument holds as for small Majorana phases, so that the value of δ is not very important.

In the case of an inverted mass hierarchy, we have $m_3 := m$, $m_2 = \sqrt{m^2 + |\Delta m_\mathrm{a}^2|}$ and $m_1 = \sqrt{m^2 + |\Delta m_\mathrm{a}^2| - \Delta m_\odot^2} \approx m_2$. Then the elements of the neutrino mass matrix can be expressed as

$$m_{\nu_{11}} \approx \sqrt{m^2 + |\Delta m_\mathrm{a}^2|} \left(s_{12}^2\, e^{i\varphi_2} + c_{12}^2\, e^{i\varphi_1}\right) , \tag{5.26a}$$

$$m_{\nu_{22}} \approx \sqrt{m^2 + |\Delta m_\mathrm{a}^2|}\, c_{23}^2 \left(c_{12}^2\, e^{i\varphi_2} + s_{12}^2\, e^{i\varphi_1}\right) + m\, s_{23}^2 \,, \tag{5.26b}$$

$$m_{\nu_{33}} \approx \sqrt{m^2 + |\Delta m_\mathrm{a}^2|}\, s_{23}^2 \left(c_{12}^2\, e^{i\varphi_2} + s_{12}^2\, e^{i\varphi_1}\right) + m\, c_{23}^2 \,, \tag{5.26c}$$

$$m_{\nu_{12}} \approx \left(\sqrt{m^2 + |\Delta m_\mathrm{a}^2|}\, e^{i\varphi_2} - \sqrt{m^2 + |\Delta m_\mathrm{a}^2| - \Delta m_\odot^2}\, e^{i\varphi_1}\right) c_{12} s_{12} c_{23} \,, \tag{5.26d}$$

$$m_{\nu_{13}} \approx -\left(\sqrt{m^2 + |\Delta m_\mathrm{a}^2|}\, e^{i\varphi_2} - \sqrt{m^2 + |\Delta m_\mathrm{a}^2| - \Delta m_\odot^2}\, e^{i\varphi_1}\right) c_{12} s_{12} s_{23} \,, \tag{5.26e}$$

$$m_{\nu_{23}} \approx \left(-\sqrt{m^2 + |\Delta m_\mathrm{a}^2|} \left(c_{12}^2\, e^{i\varphi_2} + s_{12}^2\, e^{i\varphi_1}\right) + m\right) c_{23} s_{23} \tag{5.26f}$$

for $\theta_{13} \approx 0$. We have not used the approximation $m_1 \approx m_2$ for $m_{\nu_{12}}$ and $m_{\nu_{13}}$ to avoid underestimating the size of these entries for small m and equal Majorana phases. For the other matrix elements, this approximation is sufficiently accurate, since the mass eigenvalues are multiplied by s_{12}^2 and c_{12}^2, respectively. Experimentally, these numbers are known to be unequal, so that there is no complete cancellation if $\Delta m_\odot^2$ is neglected.

A strong mass hierarchy causes most elements of m_ν to be of the order of $\sqrt{\Delta m_\mathrm{a}^2}$, so that the radiative generation of texture zeros in these positions is not possible. The

Neutrino masses	Majorana phases	
Normal hierarchy, $m_1 \approx 0$	arbitrary	$\begin{pmatrix} \cdot & \cdot & \cdot \\ \cdot & \cdot & \cdot \\ \cdot & \cdot & \cdot \end{pmatrix}$
Inverted hierarchy, $m_3 \approx 0$	$\varphi_1 \approx \varphi_2$	$\begin{pmatrix} \cdot & \circ & \circ \\ \circ & \cdot & \cdot \\ \circ & \cdot & \cdot \end{pmatrix}$
	$\varphi_1 \not\approx \varphi_2$	$\begin{pmatrix} \cdot & \cdot & \cdot \\ \cdot & \cdot & \cdot \\ \cdot & \cdot & \cdot \end{pmatrix}$
Quasi-degenerate	$\varphi_1 \approx \varphi_2 \approx 0$	$\begin{pmatrix} \cdot & \circ & \circ \\ \circ & \cdot & \circ \\ \circ & \circ & \cdot \end{pmatrix}$
	$\varphi_{1,2} \approx 0,\ \varphi_{2,1} \approx \pi$	$\begin{pmatrix} \cdot & \cdot & \cdot \\ \cdot & \cdot & \cdot \\ \cdot & \cdot & \cdot \end{pmatrix}$
	$\varphi_1 \approx \varphi_2 \approx \pi$	$\begin{pmatrix} \cdot & \circ & \circ \\ \circ & \circ & \cdot \\ \circ & \cdot & \circ \end{pmatrix}$
	$\varphi_1 \approx \varphi_2 \not\approx 0, \pi$	$\begin{pmatrix} \cdot & \circ & \circ \\ \circ & \cdot & \cdot \\ \circ & \cdot & \cdot \end{pmatrix}$
	$\varphi_1 \not\approx \varphi_2$	$\begin{pmatrix} \cdot & \cdot & \cdot \\ \cdot & \cdot & \cdot \\ \cdot & \cdot & \cdot \end{pmatrix}$

Table 5.1: Possible positions of radiatively generated texture zeros in the neutrino mass matrix, marked by a "$\circ$". For $\varphi_1 \approx \varphi_2 \approx \pi$, at most 3 of the 4 zeros can be produced at the same time.

exceptions are $m_{\nu_{12}}$ and $m_{\nu_{13}}$, which are smaller than the other elements by a factor of about $\Delta m^2_\odot / \Delta m^2_{\rm a}$ for equal Majorana phases. Hence, these entries can become zero at the GUT scale even for relatively small values of m.

For quasi-degenerate masses, the conclusions are the same as for a normal mass ordering. This is not surprising as the only difference is the sign of the atmospheric mass squared difference, which is not important for $|\Delta m^2_{\rm a}| \ll m^2$.

An overview of the results of this section is given in tab. 5.1. The positions in the neutrino mass matrix where a texture zero can be generated radiatively are marked by a "$\circ$". Comparing these results with the classification of two-zero textures in the literature, we find that three of the six forbidden textures in [62] can be reconciled with data by the RG evolution. These are the patterns of class F,

$$\begin{pmatrix} \times & 0 & 0 \\ 0 & \times & \times \\ 0 & \times & \times \end{pmatrix}, \begin{pmatrix} \times & 0 & \times \\ 0 & \times & 0 \\ \times & 0 & \times \end{pmatrix}, \begin{pmatrix} \times & \times & 0 \\ \times & \times & 0 \\ 0 & 0 & \times \end{pmatrix},$$

where the crosses "$\times$" stand for the non-zero entries. On the other hand, class E, i.e. the matrices of the form

$$\begin{pmatrix} 0 & \times & \times \\ \times & 0 & \times \\ \times & \times & \times \end{pmatrix}, \begin{pmatrix} 0 & \times & \times \\ \times & \times & \times \\ \times & \times & 0 \end{pmatrix}, \begin{pmatrix} 0 & \times & \times \\ \times & \times & 0 \\ \times & 0 & \times \end{pmatrix},$$

remain forbidden. The reason for this is the zero in the 11-element, which cannot be generated radiatively due to the large deviation of the solar mixing angle from $\pi/4$. One

could hope to circumvent this problem by assuming that this texture zero exists already at low energies and that only the second one is created by the running. However, this is not possible, since $m_{\nu_{11}} = 0$ requires either a strong hierarchy or a difference of π between the Majorana phases, both of which prevent the generation of another texture zero.

Thus, the number of two-zero textures which are at least marginally compatible with experimental data can be raised from 9 to 12 if one includes RG effects. Furthermore, tab. 5.1 shows that a number of textures with three zeros, none of which is allowed at low energies [61], should be possible as well.

5.5.2 Examples for Radiatively Created Texture Zeros

Heuristics: Running There and Back Again

In this section we give numerical examples for the radiative generation of texture zeros. In order to find suitable cases, we proceed in three steps:

1. The neutrino mass matrix at the see-saw scale is calculated from the RGE (4.2) as well as the LMA best-fit values and some choice of initial values for the unknown neutrino mass parameters at the electroweak scale. The running of all other parameters up to the GUT scale is calculated, neglecting the contributions from neutrino Yukawa couplings above the see-saw scale.

2. For each desired texture zero, we apply an equation of the form (5.13) in order to determine the matrix H at the see-saw scale, which in turn allows to find the neutrino Yukawa couplings. Clearly, the number of unknowns is larger than the number of equations, hence we pick arbitrary values smaller than 1 for the unknowns until the remaining ones can be determined. From the result, we estimate Y_ν and the effective neutrino mass matrix at the GUT scale by using their RGEs with constant right hand sides. If necessary, small imaginary parts in the position of the texture zeros are removed manually.

3. The set of parameters determined in the previous steps is evolved numerically from the GUT scale to low energy. This time, we solve the complete set of coupled differential equations and take into account the threshold corrections arising when the singlet neutrinos are successively integrated out at different energies. The resulting parameters are compared with their experimental values. If they do not agree, some non-zero entries of Y_ν and m_ν at the GUT scale are changed slightly, and the last step is repeated.

The examples are intended as a proof of principle, and therefore we only show one particular set of parameters for each case rather than trying to determine the complete allowed region in parameter space. For the same reason, we do not consider higher-order corrections from MSSM thresholds [113] or two-loop effects [143], for instance,

which could change the low-energy value of the solar angle and may make it necessary to adjust some of the initial values, but do not spoil the general viability of the scenario.

Zeros in the 12- and 13-Entries

The texture with $m_{\nu_{12}} = m_{\nu_{13}} = 0$ (pattern F_2 in the classification of [62]) implies either $m_1 = m_2 = m_3$ or $\theta_{12} = 0$ and is therefore not compatible with data unless these predictions are changed by quantum corrections. Both cases have been studied in the literature [117, 144, 145], and it has been found that both can be compatible with the LMA solution at low energy. Therefore, we do not give an example here.

Zero 23-Entry

As a first concrete example, we consider the one-zero texture with $m_{\nu_{23}} = 0$ in the case of small Majorana phases. From the discussion in the previous section, it follows that it is possible to remove this zero by RG running between the GUT and the see-saw scale. We start with the neutrino mass matrix and Yukawa couplings

$$m_\nu(M_{\rm GUT}) = \begin{pmatrix} 0.3026 & 9\cdot 10^{-5} & -9\cdot 10^{-5} \\ 9\cdot 10^{-5} & 0.3108 & 0 \\ -9\cdot 10^{-5} & 0 & 0.3165 \end{pmatrix} \text{eV} \,, \tag{5.27a}$$

$$Y_\nu(M_{\rm GUT}) = \begin{pmatrix} -0.057 & 0 & 0 \\ 0 & 0.285 & -0.006 \\ 0 & -0.445 & 0.81 \end{pmatrix} \tag{5.27b}$$

at $M_{\rm GUT} = 10^{16}$ GeV in the SM. The mass of the lightest neutrino at low energy is about 0.2 eV, and the masses of the heavy singlets are $M_1 \approx 3\cdot 10^{11}$ GeV, $M_2 \approx 6\cdot 10^{12}$ GeV, and $M_3 \approx 8\cdot 10^{13}$ GeV. The running of the mixing angles and masses is shown in fig. 5.10. It can be seen that low-energy parameters compatible with the experimental constraints are obtained. Explicitly, we find $\theta_{12} \approx 36^\circ$, $\theta_{13} \approx 0.1^\circ$, $\theta_{23} \approx 40^\circ$, $\delta = 0$, $\Delta m^2_\odot \approx 7.3\cdot 10^{-5}$ eV^2, and $\Delta m^2_{\rm a} \approx 2.2\cdot 10^{-3}$ eV^2. In order to verify that small Majorana phases do not spoil the result, we repeated the calculation with small imaginary parts in $m_\nu(M_{\rm GUT})$. The 12- and 21-entries were multiplied by $e^{-0.1\,i}$, and the 22-entry by $e^{0.5\,i}$. The resulting oscillation parameters remained in the allowed range, with the largest change taking place for θ_{12}, which became about 31°. The values of the CP phases at M_Z were $\delta \approx 181^\circ$ and $\varphi_1 \approx \varphi_2 \approx 1^\circ$.

One can see from the precision of the numbers in eqs. (5.27) that some tuning is necessary to obtain acceptable results. However, this is not that surprising considering that one needs an $\mathcal{O}(10^{-5}\,\text{eV}^2)$ mass squared difference between mass eigenvalues whose squares are of the order of 10^{-2} eV^2. Furthermore, there is a lot of freedom to rearrange the values of the Yukawa couplings.

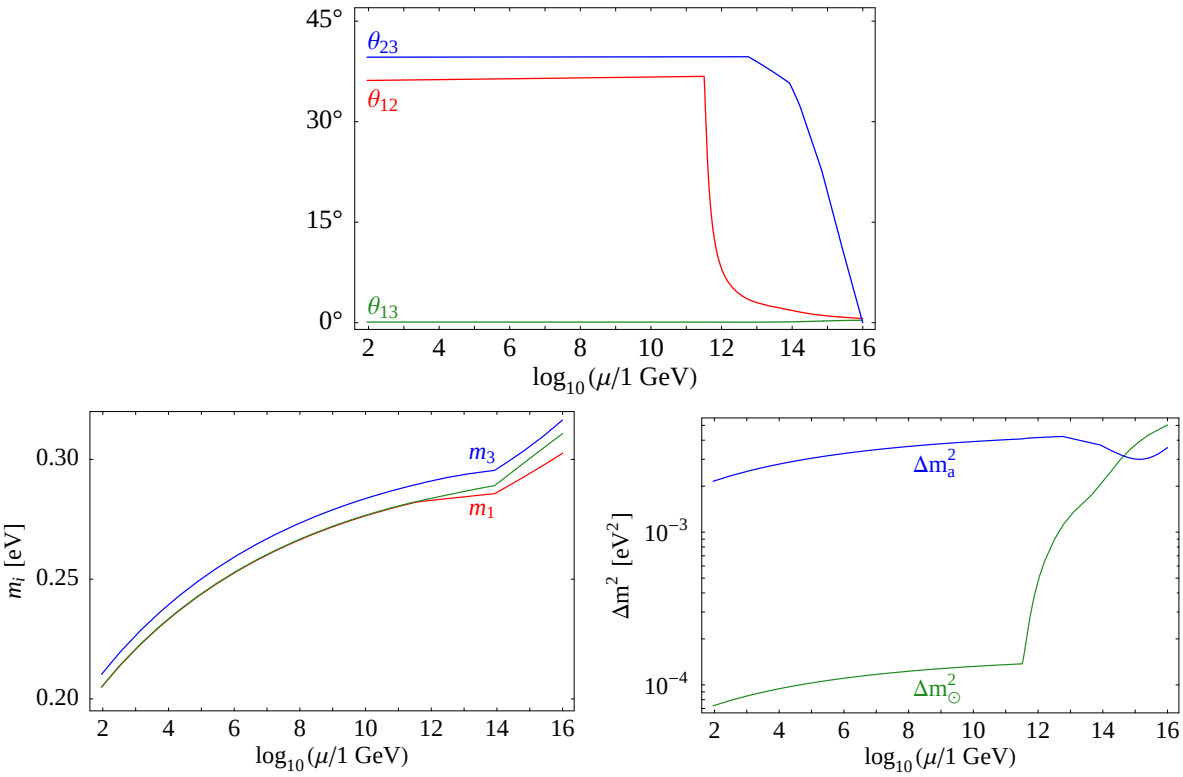

Figure 5.10: Running from a neutrino mass matrix with a texture zero in the 23 position at the GUT scale $M_{\mathrm{GUT}} = 10^{16}$ GeV to the LMA solution at low energy in the SM. The kinks in the plots stem from integrating out the heavy singlets at their mass thresholds.

Vanishing Neutrino Mixings at High Energy

In fig. 5.10, the mixing angles at high energy are very small. This prompts one to ask whether exactly vanishing mixings might be possible as well. As shown in fig. 5.11, this is indeed the case. In this example, we choose a diagonal neutrino mass matrix at $M_{\mathrm{GUT}} = 10^{16}$ GeV and use the MSSM with $\tan\beta = 50$ and a SUSY breaking scale of $M_{\mathrm{SUSY}} = 1$ TeV, below which the Standard Model is assumed to be valid as an effective theory. The mass of the lightest neutrino at low energy is about 0.2 eV. The Majorana phases are set to zero without loss of generality, since they can be absorbed by a redefinition of the neutrino fields for a diagonal mass matrix. The numerical values of the light neutrino masses and Yukawa couplings at the GUT scale are

$$m_\nu(M_{\mathrm{GUT}}) = \begin{pmatrix} 0.2902 & 0 & 0 \\ 0 & 0.3056 & 0 \\ 0 & 0 & 0.3434 \end{pmatrix} \mathrm{eV}\ , \tag{5.28a}$$

$$Y_\nu(M_{\mathrm{GUT}}) = \begin{pmatrix} -0.04 & 0 & 0 \\ -0.01 & 0.71 & -0.02 \\ 0.004 & -0.37 & 0.93 \end{pmatrix}\ . \tag{5.28b}$$

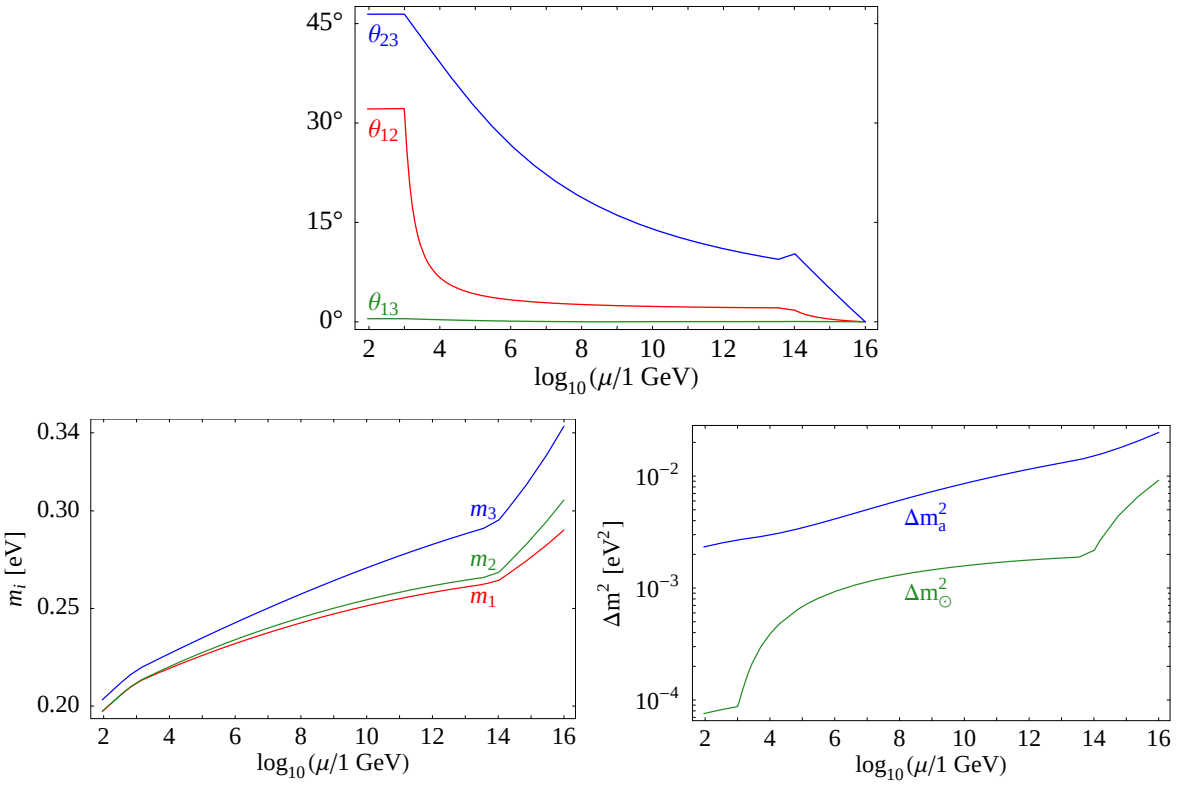

Figure 5.11: Running from vanishing neutrino mixing at the GUT scale to the LMA solution at low energy. We used the MSSM with $\tan\beta = 50$ and a SUSY breaking scale $M_{\mathrm{SUSY}} = 1$ TeV.

The masses of the singlet neutrinos are $M_1 \approx 2 \cdot 10^{11}$ GeV, $M_2 \approx 3 \cdot 10^{13}$ GeV, and $M_3 \approx 10^{14}$ GeV. At M_Z, we obtain $\theta_{12} \approx 32°$, $\theta_{13} \approx 0.5°$, $\theta_{23} \approx 46°$, $\delta = 0$, $\Delta m^2_\odot \approx 7.6 \cdot 10^{-5}$ eV^2, and $\Delta m^2_{\mathrm{a}} \approx 2.3 \cdot 10^{-3}$ eV^2, all well within the experimentally allowed 2σ ranges. For the neutrino mass matrix at the lowest see-saw scale, we find

$$m_\nu(M_1) = \begin{pmatrix} 0.2558 & 1.2 \cdot 10^{-4} & -4.0 \cdot 10^{-5} \\ 1.2 \cdot 10^{-4} & 0.2600 & 0.0041 \\ -4.0 \cdot 10^{-5} & 0.0041 & 0.2774 \end{pmatrix} \text{eV} \,. \tag{5.29}$$

It clearly satisfies the requirement of a strong hierarchy between those elements that vanish at the GUT scale and the other entries, which we derived in sec. 5.5.1. Especially the large θ_{23} at low energies is easier to obtain in the MSSM than in the SM, since in the former the contribution of the running below the see-saw scale is also significant, if $\tan\beta$ is not too small, and drives the angle in the desired direction. Nevertheless, working examples can be found in the SM, too.

Obviously, this result implies that the two-zero textures with $m_{\nu_{12}} = m_{\nu_{23}} = 0$ and $m_{\nu_{13}} = m_{\nu_{23}} = 0$ are possible as well.

Zeros in the 33-, 12- and 13-Entries

Finally, we consider an example where both Majorana phases equal π. As we derived in sec. 5.5.1, it should be possible to create zeros in the entries $m_{\nu_{22}}$, $m_{\nu_{33}}$, $m_{\nu_{12}}$, or $m_{\nu_{13}}$ in this case. The two-zero textures involving these elements (cases B and C in the classification of [61, 62]) are compatible with data anyway. Therefore, we pursue the more ambitious goal of creating a three-zero texture with $m_{\nu_{33}} = m_{\nu_{12}} = m_{\nu_{13}} = 0$. Again, we use the MSSM with $\tan\beta = 50$ and $M_{\text{SUSY}} = 1$ TeV. The mass of the lightest neutrino at low energy is about 0.21 eV. The light neutrino mass matrix and the Yukawa couplings at the GUT scale are

$$m_\nu(M_{\text{GUT}}) = \begin{pmatrix} -0.30554 & 0 & 0 \\ 0 & -0.0006 & 0.3328 \\ 0 & 0.3328 & 0 \end{pmatrix} \text{eV} \,, \tag{5.30a}$$

$$Y_\nu(M_{\text{GUT}}) = \begin{pmatrix} -0.04 & 0 & -0.05 \\ 0.01 & 0.27 & 0 \\ 0.01 & -0.35 & 0.61 \end{pmatrix} . \tag{5.30b}$$

The singlet neutrinos have the masses $M_1 \approx 10^{11}$ GeV, $M_2 \approx 5 \cdot 10^{12}$ GeV, and $M_3 \approx 4 \cdot 10^{13}$ GeV. For the oscillation parameters at low energy, we find $\theta_{12} \approx 35°$, $\theta_{13} \approx 0.01°$, $\theta_{23} \approx 45°$, $\delta = 0$, $\Delta m^2_\odot \approx 7.6 \cdot 10^{-5}$ eV^2, and $\Delta m^2_{\text{a}} \approx 2.0 \cdot 10^{-3}$ eV^2. Their running is displayed in fig. 5.12. In this example, the value of θ_{23} remains approximately 45° at all energies, since its RG evolution is strongly damped by the Majorana phases. At high energies, the mass ordering is inverted, but it changes to a normal hierarchy because the running of $\Delta m^2_\odot$ is very different from that of Δm^2_{a}. Of course, it is also possible to create a zero $m_{\nu_{22}}$ instead of $m_{\nu_{33}}$. However, both diagonal elements can vanish at the same time only if $m_{\nu_{12}}$ or $m_{\nu_{13}}$ remains finite.

5.5.3 Discussion

One should note that the light neutrino mass matrix at high energy is a secondary quantity derived from the neutrino Yukawa couplings and the Majorana mass matrix of the singlet neutrinos. Hence, a more complete theory of flavour with texture zeros would probably have to be based on zeros in these matrices. As there are many more possible patterns, see for example [146, 147], the analysis of this case is beyond the scope of this work and remains to be done in future studies. However, it is clear that a statement which was found to be stable under radiative corrections in the present context will not change, as the stability does not depend on the origin of the zeros in the neutrino mass matrix. A change is more likely the other way round: as the requirement of zeros in the Yukawa couplings and the Majorana mass matrix removes some free parameters, the radiative generation of texture zeros becomes harder. It does not necessarily become impossible, however, since zeros in these matrices can be generated radiatively as well. It is also possible that a flavour symmetry guarantees the

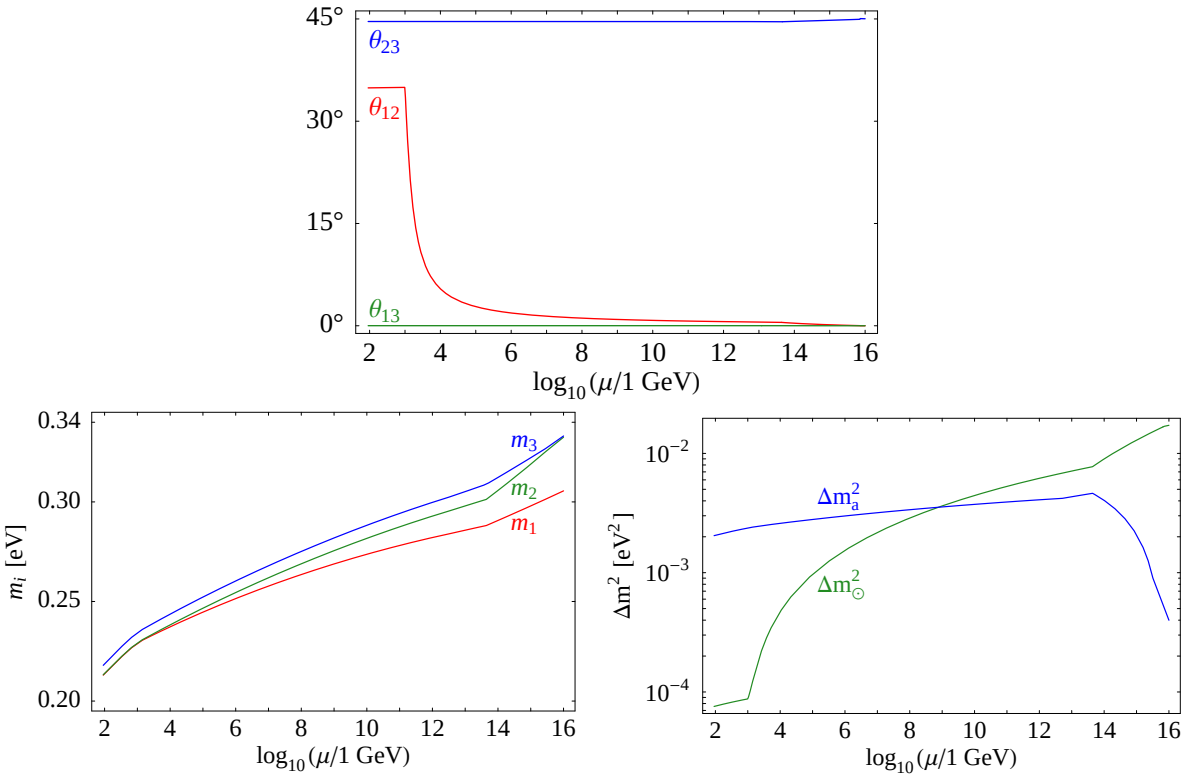

Figure 5.12: Running from a three-zero texture with $m_{\nu_{33}} = m_{\nu_{12}} = m_{\nu_{13}} = 0$ at the GUT scale to the LMA solution at low energy in the MSSM with $\tan\beta = 50$.

changes in the positions of the zeros below the GUT scale to be small. This obviously depends on the details of the breaking of this symmetry, which makes general statements very hard.

Another complication we have not taken into account are restrictions from flavour-violating decays of charged leptons such as $\mu \to e\gamma$, whose branching ratios can exceed the experimental limits in supersymmetric models for large $\tan\beta$ and large neutrino Yukawa couplings. It should be possible to suppress these processes sufficiently by adjusting the Yukawa couplings in such a way that the relevant elements of $Y_\nu^\dagger Y_\nu$ are very small.

Finally, one could also ask if an originally allowed texture can become forbidden at low energy. In particular examples, this is certainly possible, but it can always be avoided by choosing smaller Yukawa couplings, a smaller mass of the lightest neutrino or different values of the Majorana phases, all of which are not very strongly restricted by experiment. Hence, a complete exclusion of an allowed texture is not possible. In other words, the RG evolution can make a forbidden texture allowed, but not vice versa.

Chapter 6

Conclusions

In this work we have discussed the energy-dependence of the lepton flavour structure caused by radiative corrections. This effect is vital for the comparison of theoretical models for the flavour structure with experimental data, since the former typically operate at very high energy scales while the latter are obtained at relatively low energies. After introducing the theoretical and experimental framework, we have described the idea of renormalization and renormalization group equations (RGEs), which determine the energy dependence or running of all parameters of a quantum field theory.

Applying these methods to the mass parameters in the lepton sector, we have derived differential equations for the running of the neutrino masses as well as the leptonic mixing angles and CP phases in the Standard Model and MSSM below the see-saw scale. As the results are expressed directly in terms of these quantities, and as they are well approximated by simple formulae for a small CHOOZ angle θ_{13}, they allow an analytical understanding of the RG effects. With very little effort, one can determine both their generic size and the influence of the various parameters, in particular the CP phases. Thus, the formulae make it possible to easily estimate whether quantum corrections cause significant changes to the predictions of a particular model or not and therefore are a helpful tool for model builders. The most important statements can be summarized as follows: on the one hand, the RG evolution can be significant in the MSSM, if $\tan\beta$ is large and if the masses are either quasi-degenerate or hierarchical with an inverted mass ordering. On the other hand, the running of the mixing parameters is not very important in the MSSM with a small $\tan\beta$ or a strong normal mass hierarchy, and in the Standard Model in all cases. However, the mass eigenvalues always undergo a significant change.

As regards the dependence of the evolution on the mixing parameters, we have shown that the CP phases play an important role. In most cases, non-zero phases have a damping effect. We have reproduced some findings previously described in the literature and derived new results, too, for example concerning the running of the CP phases, which we have found to be significant in general. Consequently, vanishing phases at low energy appear unnatural unless exact CP conservation is a boundary condition at high energy, which seems unlikely, since the CP phase in the quark sector is sizable. As a particularly interesting example, we have discussed the radiative generation of a

non-zero Dirac phase from the Majorana phases.

Moreover, we have considered the simplest extension of the Standard Model and MSSM particle content accommodating neutrino masses, the see-saw scenario, where three gauge singlet neutrinos with large Majorana masses are added. Both in the Standard Model and in the MSSM, large RG effects can occur in the energy region above the masses of the singlets, since the neutrino Yukawa couplings can be large and contribute to the β-functions. The singlet masses are not degenerate in general, so that the heavy particles have to be integrated out one by one at the respective mass thresholds. This leads to several intermediate effective theories, each with a different RG evolution, usually causing pronounced kinks in the plots for the lepton mixing angles and phases. In a simplified numerical analysis for two flavours and two singlets, we have found that the correct RG evolution of the mixing angle can in general not be reproduced by integrating out all heavy neutrinos at a common energy scale.

Turning to model-independent consequences of RG effects, we have determined the size of the deviations of θ_{13} and θ_{23} from 0 and $\pi/4$, respectively, that result from the running, assuming that these special values are realized at a high scale. We have found that in the MSSM the deviations lie within the reach of planned long-baseline oscillation experiments in a large part of the parameter space. Thus, radiative corrections lead us to expect a good discovery potential for these precision measurements. However, the non-observation of a non-zero CHOOZ angle or deviations from maximal atmospheric mixing would be as interesting as a positive signal, if not even more interesting, since it would severely restrict the parameters relevant for the running and favor a symmetry explanation for this flavour structure over a mere numerical coincidence.

As we have seen, the change of the neutrino masses under the RG flow is always large and has to be taken into account in any analysis involving different energy scales. One example is leptogenesis, where the masses are needed as input parameters. We have estimated the corrections due to their running and have found that the upper bound on neutrino masses from thermal leptogenesis is likely to become stronger when they are taken into account. Furthermore, we have investigated the extrapolation of the upper bounds on the neutrino mass scale from neutrinoless double beta decay experiments and cosmology to higher energy scales, where they become restrictions for model building.

As an application for quantum corrections in the see-saw scenario, we have shown that the observed neutrino mass parameters, in particular the large deviation of the solar angle from $\pi/4$, can be compatible with bimaximal mixing at the GUT scale. This becomes possible because also for energies above the see-saw scale, θ_{12} generically runs faster than θ_{13} and θ_{23}. In the Standard Model and MSSM, we have found that allowed regions in parameter space, where the LMA solution of the solar neutrino problem is obtained at low energies, exist for a normal and an inverted mass hierarchy as well as for large and small values of the neutrino Yukawa couplings.

Finally, we have discussed the stability of statements about texture zeros and their compatibility with experimental data under quantum corrections in the see-saw scenario. We have assumed texture zeros in the effective mass matrix of the light neutri-

nos, defined at the GUT scale and in the basis where the mass matrix of the charged leptons is diagonal. The contributions of the off-diagonal elements of the neutrino Yukawa couplings to the running of the neutrino mass matrix can then produce non-vanishing entries in the positions of the texture zeros, thus reconciling an originally forbidden texture with observations. Looking at this from a bottom-up perspective, we have called the mechanism radiative generation of texture zeros. We have shown that it requires quasi-degenerate neutrino masses and a sufficiently small imaginary part of the mass matrix. The positions where zeros can be generated depend on the CP parity of the mass eigenstates. In the 12- and 13-entries of the mass matrix, zeros can also be created for large Majorana phases as long as they are approximately equal. Consequently, some patterns of the neutrino mass matrix that have been classified as incompatible with experimental data in the literature are not strictly excluded. They include three of the six forbidden two-zero textures as well as a number of three-zero textures. However, we have also shown that for hierarchical neutrino masses or Majorana phases far away from 0 and π, the radiative generation of texture zeros is not possible. Hence, the usual classification of forbidden and allowed textures remains valid in these cases. We have presented numerical examples to demonstrate the validity of these statements, including a case where acceptable low-energy mixings are generated starting from a diagonal effective neutrino mass matrix at the GUT scale.

Thus, the effects of renormalization can induce significant differences between the lepton flavour structures at low and high energies. This not only causes corrections to the predictions of theoretical models of fermion mass but also opens up new possibilities for model building. In order to find out whether parameter values implying large radiative corrections are realized in nature, further theoretical and experimental work is required. An important quantity in this context is the absolute neutrino mass scale, which might be determined by cosmological measurements or by the observation of neutrinoless double beta decay in the future. Further questions concerning neutrino masses and mixings that will be addressed by experiments in the coming years are if neutrinos are Majorana particles, if their mass ordering is normal or inverted, the size of the reactor angle θ_{13}, and if there is CP violation in the lepton sector. Moreover, the existence of light sterile neutrinos will be probed very soon. A test of the see-saw mechanism might be possible via the observation of lepton flavour violation, which is indirectly caused by the neutrino Yukawa couplings in supersymmetric models. Finally, several other fundamental properties of neutrinos are unknown, for instance the size of their magnetic moments or if they have non-standard interactions. If the progress in neutrino physics keeps up the pace of the recent years, we can hope to find answers to a lot of these questions in the not too distant future, and history teaches us that further surprises are to be expected.

Appendix A

Charge Conjugation

An operator needed in connection with Majorana mass terms is the charge conjugation operator $\boldsymbol{\mathcal{C}}$. On fermions and Higgs doublets it acts according to

$$\boldsymbol{\mathcal{C}}: \quad \psi \;\rightarrow\; \psi^{\mathcal{C}} = \mathcal{C}\,\overline{\psi}^{T}\,, \tag{A.1a}$$

$$\boldsymbol{\mathcal{C}}: \quad \phi \;\rightarrow\; \widetilde{\phi} = i\tau^{2}\phi^{*}\,. \tag{A.1b}$$

τ^{i} ($i \in \{1,2,3\}$) are the Pauli matrices, and $\mathcal{C}$ is the charge conjugation matrix, which satisfies

$$\mathcal{C}^{\dagger} = \mathcal{C}^{-1}\,, \tag{A.2a}$$

$$\mathcal{C}^{T} = -\mathcal{C}\,, \tag{A.2b}$$

$$\mathcal{C}\gamma_{\mu}^{T}\mathcal{C}^{-1} = -\gamma_{\mu}\,. \tag{A.2c}$$

In the standard representation, $\mathcal{C}$ is equal to $i\gamma_{2}\gamma_{0}$. From eq. (A.2c), it follows that

$$\mathcal{C}\gamma_{5}\mathcal{C}^{-1} = \gamma_{5} \quad \Leftrightarrow \quad \mathcal{C}\gamma_{5} = \gamma_{5}\mathcal{C}\,. \tag{A.2d}$$

It can also be used together with eq. (A.2a) to show that

$$\overline{\psi^{\mathcal{C}}} = -\psi^{T}\mathcal{C}^{-1}\,. \tag{A.3}$$

In connection with chiral fermion fields, it is important to note that

$$(\psi_{\mathrm{L}})^{\mathcal{C}} = \mathcal{C}\overline{\psi_{\mathrm{L}}}^{T} = \mathcal{C}(\overline{\psi}P_{\mathrm{R}})^{T} = \mathcal{C}P_{\mathrm{R}}\overline{\psi}^{T} = P_{\mathrm{R}}\mathcal{C}\overline{\psi}^{T} = P_{\mathrm{R}}\psi^{\mathcal{C}}\,,$$

i.e. the charge conjugate of a left-handed spinor is right-handed and vice versa,

$$(\psi_{\mathrm{L}})^{\mathcal{C}} = (\psi^{\mathcal{C}})_{\mathrm{R}} \quad \text{and} \quad (\psi_{\mathrm{R}})^{\mathcal{C}} = (\psi^{\mathcal{C}})_{\mathrm{L}}\,. \tag{A.4}$$

In order to streamline notation, we use the abbreviations $\psi_{\mathrm{L}}^{\mathcal{C}} := (\psi_{\mathrm{L}})^{\mathcal{C}}$ and $\psi_{\mathrm{R}}^{\mathcal{C}} := (\psi_{\mathrm{R}})^{\mathcal{C}}$.

Finally, a field that satisfies

$$\psi^{\mathcal{C}} = \psi \tag{A.5}$$

(neglecting a possible phase factor), is called a Majorana field. Together with eq. (A.4), this implies that the left- and right-handed components of such a field are related by

$$\psi_{\mathrm{L}} = \psi_{\mathrm{R}}^{\mathcal{C}} \quad \Leftrightarrow \quad \psi_{\mathrm{R}} = \psi_{\mathrm{L}}^{\mathcal{C}}\,. \tag{A.6}$$

Appendix B

Summary of Renormalization Group Equations

Effective Neutrino Mass Operators

In the SM and MSSM extended by heavy singlet neutrinos, a series of effective theories is obtained from integrating out the singlets, as explained in sec. 4.2.2. In each of them, a dimension 5 neutrino mass operator appears. In the energy region between the $(n-1)$th and the nth threshold, its coupling constant is denoted by $\overset{(n)}{\kappa}$. In this region, the neutrino Yukawa matrix is denoted by $\overset{(n)}{Y_\nu}$, and the Majorana mass matrix of the remaining singlet neutrinos by $\overset{(n)}{M_{\mathrm{R}}}$. Below the lowest see-saw scale, the coupling of the effective mass operator is $\overset{(1)}{\kappa} \equiv \kappa$, and Y_ν as well as M_{R} are absent ($\overset{(1)}{Y_\nu} = \overset{(1)}{M_{\mathrm{R}}} \equiv 0$). The RGE for the coupling of the neutrino mass operator in the SM is [19, 86, 89]

$$\begin{aligned} 16\pi^2 \frac{\mathrm{d}}{\mathrm{d}t} \overset{(n)}{\kappa} = &- \frac{3}{2}(Y_e^\dagger Y_e)^T \overset{(n)}{\kappa} - \frac{3}{2} \overset{(n)}{\kappa} (Y_e^\dagger Y_e) + \frac{1}{2}\big(\overset{(n)}{Y_\nu^\dagger} \overset{(n)}{Y_\nu}\big)^T \overset{(n)}{\kappa} + \frac{1}{2} \overset{(n)}{\kappa} \big(\overset{(n)}{Y_\nu^\dagger} \overset{(n)}{Y_\nu}\big) - \\ &- 3g_2^2 \overset{(n)}{\kappa} + 2\,\mathrm{Tr}\big(Y_e^\dagger Y_e + \overset{(n)}{Y_\nu^\dagger} \overset{(n)}{Y_\nu}\big) \overset{(n)}{\kappa} + 6\,\mathrm{Tr}\big(Y_u^\dagger Y_u + Y_d^\dagger Y_d\big) \overset{(n)}{\kappa} + \lambda \overset{(n)}{\kappa}\,. \end{aligned} \tag{B.1}$$

As before, t is defined as $t = \ln(\mu/\mu_0)$, where μ is the renormalization scale. The MSSM equivalent of eq. (4.41) reads

$$\begin{aligned} 16\pi^2 \frac{\mathrm{d}}{\mathrm{d}t} \overset{(n)}{\kappa} = &(Y_e^\dagger Y_e)^T \overset{(n)}{\kappa} + \overset{(n)}{\kappa} (Y_e^\dagger Y_e) + \big(\overset{(n)}{Y_\nu^\dagger} \overset{(n)}{Y_\nu}\big)^T \overset{(n)}{\kappa} + \overset{(n)}{\kappa} \big(\overset{(n)}{Y_\nu^\dagger} \overset{(n)}{Y_\nu}\big) - \\ &- \frac{6}{5} g_1^2 \overset{(n)}{\kappa} - 6g_2^2 \overset{(n)}{\kappa} + 2\,\mathrm{Tr}\big(\overset{(n)}{Y_\nu^\dagger} \overset{(n)}{Y_\nu}\big) \overset{(n)}{\kappa} + 6\,\mathrm{Tr}\big(Y_u^\dagger Y_u\big) \overset{(n)}{\kappa}\,. \end{aligned} \tag{B.2}$$

For $\mathrm{U}(1)_{\mathrm{Y}}$ and its coupling constant g_1, we use GUT charge normalization.

Further RGEs in the Type I See-Saw Scenario

Standard Model

At energies above the highest see-saw scale in the type I see-saw scenario, the SM RGEs for the gauge and Yukawa couplings, the singlet mass matrix, and the Higgs self-coupling are given by [85, 86, 89, 97, 114, 148]

$$16\pi^2 \frac{\mathrm{d}g_1}{\mathrm{d}t} = \frac{41}{10} g_1^3 \,, \tag{B.3a}$$

$$16\pi^2 \frac{\mathrm{d}g_2}{\mathrm{d}t} = -\frac{19}{6} g_2^3 \,, \tag{B.3b}$$

$$16\pi^2 \frac{\mathrm{d}g_3}{\mathrm{d}t} = -7 g_3^3 \,, \tag{B.3c}$$

$$16\pi^2 \frac{\mathrm{d}Y_u}{\mathrm{d}t} = Y_u \left\{ \frac{3}{2} Y_u^\dagger Y_u - \frac{3}{2} Y_d^\dagger Y_d + T - \frac{17}{20} g_1^2 - \frac{9}{4} g_2^2 - 8 g_3^2 \right\} , \tag{B.3d}$$

$$16\pi^2 \frac{\mathrm{d}Y_d}{\mathrm{d}t} = Y_d \left\{ \frac{3}{2} Y_d^\dagger Y_d - \frac{3}{2} Y_u^\dagger Y_u + T - \frac{1}{4} g_1^2 - \frac{9}{4} g_2^2 - 8 g_3^2 \right\} , \tag{B.3e}$$

$$16\pi^2 \frac{\mathrm{d}Y_e}{\mathrm{d}t} = Y_e \left\{ \frac{3}{2} Y_e^\dagger Y_e - \frac{3}{2} Y_\nu^\dagger Y_\nu + T - \frac{9}{4} g_1^2 - \frac{9}{4} g_2^2 \right\} , \tag{B.3f}$$

$$16\pi^2 \frac{\mathrm{d}Y_\nu}{\mathrm{d}t} = Y_\nu \left\{ \frac{3}{2} Y_\nu^\dagger Y_\nu - \frac{3}{2} Y_e^\dagger Y_e + T - \frac{9}{20} g_1^2 - \frac{9}{4} g_2^2 \right\} , \tag{B.3g}$$

$$16\pi^2 \frac{\mathrm{d}M_\mathrm{R}}{\mathrm{d}t} = \left(Y_\nu Y_\nu^\dagger\right) M_\mathrm{R} + M_\mathrm{R} \left(Y_\nu Y_\nu^\dagger\right)^T \,, \tag{B.3h}$$

$$\begin{aligned} 16\pi^2 \frac{\mathrm{d}\lambda}{\mathrm{d}t} = {} & 6\lambda^2 - 3\lambda \left(\frac{3}{5} g_1^2 + 3 g_2^2 \right) + 3 g_2^4 + \frac{3}{2} \left(\frac{3}{5} g_1^2 + g_2^2 \right)^2 + 4\lambda\, T - \\ & - 8\,\mathrm{Tr}\big(Y_e^\dagger Y_e\, Y_e^\dagger Y_e + Y_\nu^\dagger Y_\nu\, Y_\nu^\dagger Y_\nu + 3 Y_u^\dagger Y_u\, Y_u^\dagger Y_u + 3 Y_d^\dagger Y_d\, Y_d^\dagger Y_d \big) \,, \end{aligned} \tag{B.3i}$$

where

$$T := \mathrm{Tr}\big(Y_\nu^\dagger Y_\nu + Y_e^\dagger Y_e + 3 Y_u^\dagger Y_u + 3 Y_d^\dagger Y_d \big) \,. \tag{B.4}$$

The RGEs in the effective theories valid at energies below the mass of the heaviest singlet neutrino are the same as above, if one substitutes $Y_\nu \to \overset{(n)}{Y}_\nu$ and $M_\mathrm{R} \to \overset{(n)}{M}_\mathrm{R}$ [19]. In particular, the RGEs for the SM are recovered by setting Y_ν to zero.

Note that in our notation for the Higgs self-coupling, the corresponding term in the Lagrangian is $-\frac{1}{4}\lambda(\phi^\dagger\phi)^2$, which differs from the notation used in several other studies by a factor of 2. Our convention for the Yukawa matrices is that the Lagrangian contains the terms $-\overline{e_\mathrm{R}} Y_e \ell_\mathrm{L} \phi^\dagger$ etc.

MSSM

In the MSSM with additional singlet superfields, the RGEs relevant for this work are [86, 89, 98, 115]

$$16\pi^2 \frac{\mathrm{d}g_1}{\mathrm{d}t} = \frac{33}{5} g_1^3 \,, \tag{B.5a}$$

$$16\pi^2 \frac{\mathrm{d}g_2}{\mathrm{d}t} = g_2^3 \,, \tag{B.5b}$$

$$16\pi^2 \frac{\mathrm{d}g_3}{\mathrm{d}t} = -3 g_3^3 \,, \tag{B.5c}$$

$$16\pi^2 \frac{\mathrm{d}Y_u}{\mathrm{d}t} = Y_u \left\{ 3Y_u^\dagger Y_u + Y_d^\dagger Y_d + T_u - \frac{13}{15} g_1^2 - 3g_2^2 - \frac{16}{3} g_3^2 \right\}, \tag{B.5d}$$

$$16\pi^2 \frac{\mathrm{d}Y_d}{\mathrm{d}t} = Y_d \left\{ 3Y_d^\dagger Y_d + Y_u^\dagger Y_u + T_d - \frac{7}{15} g_1^2 - 3g_2^2 - \frac{16}{3} g_3^2 \right\}, \tag{B.5e}$$

$$16\pi^2 \frac{\mathrm{d}Y_e}{\mathrm{d}t} = Y_e \left\{ 3Y_e^\dagger Y_e + Y_\nu^\dagger Y_\nu + T_d - \frac{9}{5} g_1^2 - 3g_2^2 \right\}, \tag{B.5f}$$

$$16\pi^2 \frac{\mathrm{d}Y_\nu}{\mathrm{d}t} = Y_\nu \left\{ 3Y_\nu^\dagger Y_\nu + Y_e^\dagger Y_e + T_u - \frac{3}{5} g_1^2 - 3g_2^2 \right\}, \tag{B.5g}$$

$$16\pi^2 \frac{\mathrm{d}M_\mathrm{R}}{\mathrm{d}t} = 2\big(Y_\nu Y_\nu^\dagger\big) M_\mathrm{R} + 2 M_\mathrm{R} \big(Y_\nu Y_\nu^\dagger\big)^T \,, \tag{B.5h}$$

where

$$T_u := \mathrm{Tr}\big(Y_\nu^\dagger Y_\nu + 3 Y_u^\dagger Y_u\big) \,, \tag{B.6a}$$

$$T_d := \mathrm{Tr}\big(Y_e^\dagger Y_e + 3 Y_d^\dagger Y_d\big) \,. \tag{B.6b}$$

The RGEs for the effective theories are obtained in the same way as in the SM case.

Acknowledgements

I would like to thank everybody who helped to make this work possible. In particular, thanks are due to

- my supervisor Prof. Manfred Lindner for accompanying this work, for always having time for questions and discussions, and for providing an excellent working environment in general;
- Claudia Hagedorn, Patrick Huber, Michael Schmidt, Thomas Schwetz, Walter Winter, and especially Stefan Antusch and Michael Ratz for great teamwork;
- Markus "MMM" Müller for being a perfect office mate and helpful root, and for proofreading the manuscript;
- the whole crowd of T30d for being great colleagues and for interesting discussions, not only about physics;
- our secretary Karin Ramm for friendly smiles in the morning, ample supply with paper and pencils as well as help with coping with the bureaucracy;
- the "Sonderforschungsbereich 375 für Astro-Teilchenphysik der Deutschen Forschungsgemeinschaft" for financial support and secretary Alexandra Füldner for help with the accompanying paperwork;
- Prof. Andrzej Buras, Prof. Manuel Drees and Prof. Jisuke Kubo for interesting discussions and answers to many questions;
- Felix Schwab for translation and intelligence work;
- our system administrators for keeping the computers running;
- the Dr.-Ing. Leonhard-Lorenz-Stiftung for a travel grant;
- the folks from E18 for my office chair;
- Lin Soft for stimulating support in the afternoon.

Last but not least, very special thanks to my parents for all their support during the many years up to the completion of this thesis.

Nomenclature

a, b, c, d	SU(2) indices, page 20
CL	Confidence level
CMB	Cosmic microwave background
EFT	Effective field theory
GUT	Grand Unified Theory
h.c.	Hermitian conjugate
α	Flavour-diagonal term in the RGE of the effective neutrino mass operator, page 37
α'	Flavour-diagonal term in the RGE of the effective mass matrix of the light neutrinos above the highest see-saw scale, page 55
MSSM	Minimal Supersymmetric Standard Model
RGE	Renormalization group equation
SM	Standard Model
VEV	Vacuum expectation value
c_{12}, s_{12}	$\cos\theta_{12}, \sin\theta_{12}$
d	Number of spacetime dimensions in dimensional regularization, page 28
δ	Dirac CP phase in the MNS matrix, page 14
$\delta_e, \delta_\mu, \delta_\tau$	Unphysical phases in the MNS matrix, page 14
$\Delta m^2_{\text{a}} := m_3^2 - m_2^2$	Atmospheric mass squared difference, page 15
$\Delta m^2_{\odot} := m_2^2 - m_1^2$	Solar mass squared difference , page 15
$\epsilon := 4 - d$	Parameter in dimensional regularization, page 28

ε	Totally antisymmetric tensor, page 20
f, g	Generation indices, page 20
ϕ	SM Higgs, page 20
$\phi^{(2)}$	MSSM up-type Higgs
g_1	Gauge coupling of $\mathrm{U}(1)_\mathrm{Y}$ in GUT charge normalization, page 37
g_2	Gauge coupling of $\mathrm{SU}(2)_\mathrm{L}$
κ	Coupling constant of the effective neutrino mass operator, page 20
ℓ_L	Left-handed lepton doublet, page 20
λ	Quartic Higgs self-coupling
m_1, m_2, m_3	Mass eigenvalues of the light neutrinos
m_ν	Mass matrix of the light neutrinos
$m_\mathrm{R}, M_\mathrm{R}$	Majorana mass matrix of the heavy singlets in the see-saw scenario, page 54
M_SUSY	Supersymmetry-breaking scale
μ	Renormalization scale in dimensional regularization, page 28
ν_R	Right-handed, gauge singlet neutrino field
P_L	Left-handed chirality projector, page 36
φ_1, φ_2	Majorana phases in the MNS matrix, page 14
$\widetilde{\phi}$	Charge conjugate of the Higgs field, page 93
$\psi^\mathcal{C}$	Charge conjugate of the fermion field ψ, page 93
t	$\ln(\mu/\mu_0)$, where μ is the renormalization scale, page 36
$\tan\beta$	Ratio of the VEVs of the two MSSM Higgs fields
$\theta_{12}, \theta_{13}, \theta_{23}$	Lepton mixing angles in the MNS matrix, page 14
v	Vacuum expectation value of the Higgs field coupling to the up-type quarks; $v \approx 246$ GeV in the SM and $v \approx \sin\beta \cdot 246$ GeV in the MSSM, page 20
$V_\mathrm{MNS} := U_\mathrm{L}^{e\dagger} U^\nu$	MNS matrix, page 14
Y_e	Charged lepton Yukawa couplings
Y_ν	Neutrino Yukawa couplings, page 54

Bibliography

[1] Super-Kamiokande Collaboration, Y. Fukuda et al., *Evidence for oscillation of atmospheric neutrinos*, Phys. Rev. Lett. **81** (1998), 1562–1567, hep-ex/9807003.

[2] SNO Collaboration, Q. R. Ahmad et al., *Measurement of charged current interactions produced by 8B solar neutrinos at the Sudbury Neutrino Observatory*, Phys. Rev. Lett. **87** (2001), 071301, nucl-ex/0106015.

[3] SNO Collaboration, Q. R. Ahmad et al., *Direct evidence for neutrino flavor transformation from neutral-current interactions in the Sudbury Neutrino Observatory*, Phys. Rev. Lett. **89** (2002), 011301, nucl-ex/0204008.

[4] KamLAND Collaboration, K. Eguchi et al., *First results from KamLAND: Evidence for reactor anti- neutrino disappearance*, Phys. Rev. Lett. **90** (2003), 021802, hep-ex/0212021.

[5] Super-Kamiokande Collaboration, Y. Ashie et al., *Evidence for an oscillatory signature in atmospheric neutrino oscillation*, (2004), hep-ex/0404034.

[6] T. Nakaya, *New K2K results*, Talk given at the XXIst International Conference on Neutrino Physics and Astrophysics (Neutrino 2004), Paris, France, 2004, http://neutrino2004.in2p3.fr/program.htm.

[7] C. Weinheimer, *Direct neutrino mass experiments – present and future*, Nucl. Phys. Proc. Suppl. **118** (2003), 279–286.

[8] H. V. Klapdor-Kleingrothaus et al., *Latest results from the Heidelberg-Moscow double-beta-decay experiment*, Eur. Phys. J. **A12** (2001), 147–154, hep-ph/0103062.

[9] 16EX Collaboration, C. E. Aalseth et al., *The IGEX Ge-76 neutrinoless double-beta decay experiment: Prospects for next generation experiments*, Phys. Rev. **D65** (2002), 092007, hep-ex/0202026.

[10] D. N. Spergel et al., *First year Wilkinson Microwave Anisotropy Probe (WMAP) observations: Determination of cosmological parameters*, (2003), astro-ph/0302209.

[11] C. Athanassopoulos et al., *Candidate events in a search for anti-muon-neutrino → anti-electron-neutrino oscillations*, Phys. Rev. Lett. **75** (1995), 2650–2653, nucl-ex/9504002.

[12] LSND Collaboration, A. Aguilar et al., *Evidence for neutrino oscillations from the observation of anti-nu/e appearance in a anti-nu/mu beam*, Phys. Rev. **D64** (2001), 112007, hep-ex/0104049.

[13] T. Yanagida, in *Proceedings of the Workshop on the Unified Theory and the Baryon Number in the Universe* (O. Sawada and A. Sugamoto, eds.), KEK, Tsukuba, Japan, 1979, p. 95.

[14] S. L. Glashow, *The future of elementary particle physics*, in *Proceedings of the 1979 Cargèse Summer Institute on Quarks and Leptons* (M. Lévy, J.-L. Basdevant, D. Speiser, J. Weyers, R. Gastmans, and M. Jacob, eds.), Plenum Press, New York, 1980, pp. 687–713.

[15] M. Gell-Mann, P. Ramond, and R. Slansky, *Complex spinors and unified theories*, in *Supergravity* (P. van Nieuwenhuizen and D. Z. Freedman, eds.), North Holland, Amsterdam, 1979, p. 315.

[16] R. N. Mohapatra and G. Senjanović, *Neutrino mass and spontaneous parity violation*, Phys. Rev. Lett. **44** (1980), 912.

[17] S. Antusch, M. Drees, J. Kersten, M. Lindner, and M. Ratz, *Neutrino mass operator renormalization revisited*, Phys. Lett. **B519** (2001), 238–242, hep-ph/0108005.

[18] S. Antusch, M. Drees, J. Kersten, M. Lindner, and M. Ratz, *Neutrino mass operator renormalization in two Higgs doublet models and the MSSM*, Phys. Lett. **B525** (2002), 130–134, hep-ph/0110366.

[19] S. Antusch, J. Kersten, M. Lindner, and M. Ratz, *Neutrino mass matrix running for non-degenerate see-saw scales*, Phys. Lett. **B538** (2002), 87–95, hep-ph/0203233.

[20] S. Antusch, J. Kersten, M. Lindner, and M. Ratz, *The LMA solution from bimaximal lepton mixing at the GUT scale by renormalization group running*, Phys. Lett. **B544** (2002), 1–10, hep-ph/0206078.

[21] S. Antusch, J. Kersten, M. Lindner, and M. Ratz, *Running neutrino masses, mixings and CP phases: Analytical results and phenomenological consequences*, Nucl. Phys. **B674** (2003), 401–433, hep-ph/0305273.

[22] S. Antusch, P. Huber, J. Kersten, T. Schwetz, and W. Winter, *Is there maximal mixing in the lepton sector?*, (2004), hep-ph/0404268.

[23] C. Hagedorn, J. Kersten, and M. Lindner, *Stability of texture zeros under radiative corrections in see-saw models*, (2004), hep-ph/0406103.

[24] CHOOZ, M. Apollonio et al., *Limits on neutrino oscillations from the CHOOZ experiment*, Phys. Lett. **B466** (1999), 415–430, hep-ex/9907037.

[25] H. Murayama and T. Yanagida, *LSND, SN1987A, and CPT violation*, Phys. Lett. **B520** (2001), 263–268, hep-ph/0010178.

[26] M. Maltoni, T. Schwetz, M. A. Tortola, and J. W. F. Valle, *Ruling out four-neutrino oscillation interpretations of the LSND anomaly?*, Nucl. Phys. **B643** (2002), 321–338, hep-ph/0207157.

[27] M. Sorel, J. M. Conrad, and M. Shaevitz, *A combined analysis of short-baseline neutrino experiments in the (3+1) and (3+2) sterile neutrino oscillation hypotheses*, (2003), hep-ph/0305255.

[28] KARMEN, B. Armbruster et al., *Upper limits for neutrino oscillations anti-nu/mu –> anti-nu/e from muon decay at rest*, Phys. Rev. **D65** (2002), 112001, hep-ex/0203021.

[29] MiniBooNE, I. Stancu, *Status of the MiniBooNE experiment*, Prepared for International Workshop on Astroparticle and High-Energy Physics (AHEP-2003), Valencia, Spain, 14-18 Oct 2003.

[30] H. V. Klapdor-Kleingrothaus, I. V. Krivosheina, A. Dietz, and O. Chkvorets, *Search for neutrinoless double beta decay with enriched Ge-76 in Gran Sasso 1990-2003*, Phys. Lett. **B586** (2004), 198–212, hep-ph/0404088.

[31] S. Hannestad, *Neutrino masses and the number of neutrino species from WMAP and 2dFGRS*, JCAP **0305** (2003), 004, astro-ph/0303076.

[32] M. Maltoni, T. Schwetz, M. A. Tortola, and J. W. F. Valle, *Status of global fits to neutrino oscillations*, (2004), hep-ph/0405172.

[33] M. Maltoni, T. Schwetz, M. A. Tortola, and J. W. F. Valle, *Status of three-neutrino oscillations after the SNO-salt data*, Phys. Rev. **D68** (2003), 113010, hep-ph/0309130.

[34] A. B. Balantekin and H. Yuksel, *Constraints on neutrino parameters from neutral-current solar neutrino measurements*, Phys. Rev. **D68** (2003), 113002, hep-ph/0309079.

[35] P. Aliani, V. Antonelli, M. Picariello, and E. Torrente-Lujan, *The neutrino mass matrix after Kamland and SNO salt enhanced results*, (2003), hep-ph/0309156.

[36] A. Bandyopadhyay, S. Choubey, S. Goswami, S. T. Petcov, and D. P. Roy, *Constraints on neutrino oscillation parameters from the SNO salt phase data*, Phys. Lett. **B583** (2004), 134–148, hep-ph/0309174.

[37] P. C. de Holanda and A. Y. Smirnov, *Solar neutrinos: The SNO salt phase results and physics of conversion*, (2003), hep-ph/0309299.

[38] P. Huber, M. Lindner, and W. Winter, *Superbeams versus neutrino factories*, Nucl. Phys. **B645** (2002), 3–48, hep-ph/0204352.

[39] P. Huber and W. Winter, *Neutrino factories and the "magic" baseline*, Phys. Rev. **D68** (2003), 037301, hep-ph/0301257.

[40] P. Huber, M. Lindner, M. Rolinec, T. Schwetz, and W. Winter, *Prospects of accelerator and reactor neutrino oscillation experiments for the coming ten years*, (2004), hep-ph/0403068.

[41] S. R. Elliott and J. Engel, *Double beta decay*, (2004), hep-ph/0405078.

[42] K. S. Babu and C. N. Leung, *Classification of effective neutrino mass operators*, Nucl. Phys. **B619** (2001), 667–689, hep-ph/0106054.

[43] J. A. Casas, J. R. Espinosa, and I. Navarro, *New supersymmetric source of neutrino masses and mixings*, Phys. Rev. Lett. **89** (2002), 161801, hep-ph/0206276.

[44] Particle Data Group, D. E. Groom et al., *Review of particle physics*, Eur. Phys. J. **C15** (2000), 1, http://pdg.lbl.gov.

[45] G. B. Gelmini and M. Roncadelli, *Lefthanded neutrino mass scale and spontaneously broken lepton number*, Phys. Lett. **B99** (1981), 411.

[46] G. Lazarides, Q. Shafi, and C. Wetterich, *Proton lifetime and fermion masses in an SO(10) model*, Nucl. Phys. **B181** (1981), 287.

[47] R. N. Mohapatra and G. Senjanović, *Neutrino masses and mixings in gauge models with spontaneous parity violation*, Phys. Rev. **D23** (1981), 165.

[48] C. Wetterich, *Neutrino masses and the scale of $B-L$ violation*, Nucl. Phys. **B187** (1981), 343.

[49] E. Ma and U. Sarkar, *Neutrino masses and leptogenesis with heavy Higgs triplets*, Phys. Rev. Lett. **80** (1998), 5716–5719, hep-ph/9802445.

[50] A. Zee, *A theory of lepton number violation, neutrino Majorana mass, and oscillation*, Phys. Lett. **B93** (1980), 389.

[51] K. S. Babu, *Model of 'calculable' Majorana neutrino masses*, Phys. Lett. **B203** (1988), 132.

[52] N. Arkani-Hamed, L. J. Hall, H. Murayama, D. R. Smith, and N. Weiner, *Small neutrino masses from supersymmetry breaking*, Phys. Rev. **D64** (2001), 115011, hep-ph/0006312.

[53] F. Borzumati and Y. Nomura, *Low-scale see-saw mechanisms for light neutrinos*, Phys. Rev. **D64** (2001), 053005, hep-ph/0007018.

[54] E. Ma, *Unified supersymmetric model of naturally small Dirac neutrino masses and the axionic solution of the strong CP problem*, Nucl. Phys. **B623** (2002), 126–132, hep-ph/0108209.

[55] E. Ma, *New U(1) gauge extension of the supersymmetric standard model*, Phys. Rev. Lett. **89** (2002), 041801, hep-ph/0201083.

[56] R. Kitano, *Small Dirac neutrino masses in supersymmetric grand unified theories*, Phys. Lett. **B539** (2002), 102–106, hep-ph/0204164.

[57] R. Arnowitt, B. Dutta, and B. Hu, *Yukawa textures, neutrino masses and Horava-Witten M-theory*, Nucl. Phys. **B682** (2004), 347–366, hep-th/0309033.

[58] H. Fritzsch, *Weak interaction mixing in the six-quark theory*, Phys. Lett. **B73** (1978), 317–322.

[59] H. Georgi and C. Jarlskog, *A new lepton-quark mass relation in a unified theory*, Phys. Lett. **B86** (1979), 297–300.

[60] J. A. Harvey, P. Ramond, and D. B. Reiss, *CP violation and mass relations in SO(10)*, Phys. Lett. **B92** (1980), 309.

[61] P. H. Frampton, S. L. Glashow, and D. Marfatia, *Zeroes of the neutrino mass matrix*, Phys. Lett. **B536** (2002), 79–82, hep-ph/0201008.

[62] W.-l. Guo and Z.-z. Xing, *Implications of the KamLAND measurement on the lepton flavor mixing matrix and the neutrino mass matrix*, Phys. Rev. **D67** (2003), 053002, hep-ph/0212142.

[63] W. Grimus, A. S. Joshipura, L. Lavoura, and M. Tanimoto, *Symmetry realization of texture zeros*, (2004), hep-ph/0405016.

[64] S. F. King, *Atmospheric and solar neutrinos from single right-handed neutrino dominance and U(1) family symmetry*, Nucl. Phys. **B562** (1999), 57–77, hep-ph/9904210.

[65] S. F. King, *Large mixing angle MSW and atmospheric neutrinos from single right-handed neutrino dominance and U(1) family symmetry*, Nucl. Phys. **B576** (2000), 85–105, hep-ph/9912492.

[66] S. Antusch and S. F. King, *Neutrino mixing from the charged lepton sector with sequential right-handed lepton dominance*, Phys. Lett. **B591** (2004), 104–112, hep-ph/0403053.

[67] K. S. Babu and S. M. Barr, *Large neutrino mixing angles in unified theories*, Phys. Lett. **B381** (1996), 202–208, hep-ph/9511446.

[68] S. M. Barr, *Predictive models of large neutrino mixing angles*, Phys. Rev. **D55** (1997), 1659–1664, hep-ph/9607419.

[69] B. Bajc, G. Senjanovic, and F. Vissani, *b - tau unification and large atmospheric mixing: A case for non-canonical see-saw*, Phys. Rev. Lett. **90** (2003), 051802, hep-ph/0210207.

[70] H. S. Goh, R. N. Mohapatra, and S.-P. Ng, *Minimal SUSY SO(10), b tau unification and large neutrino mixings*, Phys. Lett. **B570** (2003), 215–221, hep-ph/0303055.

[71] B. Dutta, Y. Mimura, and R. N. Mohapatra, *CKM CP violation in a minimal SO(10) model for neutrinos and its implications*, (2004), hep-ph/0402113.

[72] S. T. Petcov, *On pseudodirac neutrinos, neutrino oscillations and neutrinoless double beta decay*, Phys. Lett. **B110** (1982), 245–249.

[73] C. N. Leung and S. T. Petcov, *A comment on the coexistence of Dirac and Majorana massive neutrinos*, Phys. Lett. **B125** (1983), 461.

[74] C. D. Froggatt and H. B. Nielsen, *Hierarchy of quark masses, Cabibbo angles and CP violation*, Nucl. Phys. **B147** (1979), 277.

[75] N. Arkani-Hamed, S. Dimopoulos, and G. R. Dvali, *The hierarchy problem and new dimensions at a millimeter*, Phys. Lett. **B429** (1998), 263–272, hep-ph/9803315.

[76] S. Weinberg, *Implications of dynamical symmetry breaking: An addendum*, Phys. Rev. **D19** (1979), 1277–1280.

[77] L. Susskind, *Dynamics of spontaneous symmetry breaking in the Weinberg-Salam theory*, Phys. Rev. **D20** (1979), 2619–2625.

[78] W. A. Bardeen, C. T. Hill, and M. Lindner, *Minimal dynamical symmetry breaking of the standard model*, Phys. Rev. **D41** (1990), 1647.

[79] S. Antusch, J. Kersten, M. Lindner, and M. Ratz, *Dynamical electroweak symmetry breaking by a neutrino condensate*, Nucl. Phys. **B658** (2003), 203–216, hep-ph/0211385.

[80] J. C. Collins, *Renormalization*, Cambridge University Press, Cambridge, UK, 1984.

[81] G. 't Hooft, *Renormalization of massless Yang-Mills fields*, Nucl. Phys. **B33** (1971), 173–199.

[82] G. 't Hooft, *Renormalizable Lagrangians for massive Yang-Mills fields*, Nucl. Phys. **B35** (1971), 167–188.

[83] G. 't Hooft and M. J. G. Veltman, *Regularization and renormalization of gauge fields*, Nucl. Phys. **B44** (1972), 189–213.

[84] W. A. Bardeen, A. J. Buras, D. W. Duke, and T. Muta, *Deep inelastic scattering beyond the leading order in asymptotically free gauge theories*, Phys. Rev. **D18** (1978), 3998.

[85] J. Kersten, *Renormalization group evolution of neutrino masses*, Diploma thesis, TU München, 2001.

[86] M. Ratz, *Running neutrino masses*, Ph.D. thesis, TU München, 2002.

[87] T. Appelquist and J. Carazzone, *Infrared singularities and massive fields*, Phys. Rev. **D11** (1975), 2856.

[88] A. Pich, *Effective field theory*, hep-ph/9806303 (1998).

[89] S. Antusch, *The running of neutrino masses, lepton mixings and CP phases*, Ph.D. thesis, TU München, 2003.

[90] P. H. Chankowski and Z. Pluciennik, *Renormalization group equations for seesaw neutrino masses*, Phys. Lett. **B316** (1993), 312–317, hep-ph/9306333.

[91] K. S. Babu, C. N. Leung, and J. Pantaleone, *Renormalization of the neutrino mass operator*, Phys. Lett. **B319** (1993), 191–198, hep-ph/9309223.

[92] P. H. Chankowski, W. Krolikowski, and S. Pokorski, *Fixed points in the evolution of neutrino mixings*, Phys. Lett. **B473** (2000), 109, hep-ph/9910231.

[93] J. A. Casas, J. R. Espinosa, A. Ibarra, and I. Navarro, *General RG equations for physical neutrino parameters and their phenomenological implications*, Nucl. Phys. **B573** (2000), 652, hep-ph/9910420.

[94] K. S. Babu, *Renormalization-Group analysis of the Kobayashi-Maskawa matrix*, Z. Phys. **C35** (1987), 69.

[95] P. Kielanowski and S. R. Juarez W., *Precise bounds on the Higgs boson mass*, (2003), hep-ph/0310122.

[96] J. R. Ellis and S. Lola, *Can neutrinos be degenerate in mass?*, Phys. Lett. **B458** (1999), 310–321, hep-ph/9904279.

[97] J. A. Casas, J. R. Espinosa, A. Ibarra, and I. Navarro, *Naturalness of nearly degenerate neutrinos*, Nucl. Phys. **B556** (1999), 3–22, hep-ph/9904395.

[98] J. A. Casas, J. R. Espinosa, A. Ibarra, and I. Navarro, *Nearly degenerate neutrinos, supersymmetry and radiative corrections*, Nucl. Phys. **B569** (2000), 82–106, hep-ph/9905381.

[99] A. S. Joshipura, S. D. Rindani, and N. N. Singh, *Predictive framework with a pair of degenerate neutrinos at a high scale*, Nucl. Phys. **B660** (2003), 362–372, hep-ph/0211378.

[100] A. S. Joshipura and S. D. Rindani, *Radiatively generated ν_e oscillations: General analysis, textures and models*, Phys. Rev. **D67** (2003), 073009, hep-ph/0211404.

[101] K. R. S. Balaji, A. S. Dighe, R. N. Mohapatra, and M. K. Parida, *Generation of large flavor mixing from radiative corrections*, Phys. Rev. Lett. **84** (2000), 5034–5037, hep-ph/0001310.

[102] N. Haba, Y. Matsui, and N. Okamura, *The effects of Majorana phases in three-generation neutrinos*, Eur. Phys. J. **C17** (2000), 513–520, hep-ph/0005075.

[103] P. H. Chankowski and S. Pokorski, *Quantum corrections to neutrino masses and mixing angles*, Int. J. Mod. Phys. **A17** (2002), 575–614, hep-ph/0110249.

[104] T. Miura, T. Shindou, and E. Takasugi, *Exploring the neutrino mass matrix at M(R) scale*, Phys. Rev. **D66** (2002), 093002, hep-ph/0206207.

[105] G. Bhattacharyya, A. Raychaudhuri, and A. Sil, *Can radiative magnification of mixing angles occur for two-zero neutrino mass matrix textures?*, (2002), hep-ph/0211074.

[106] G. C. Branco, T. Morozumi, B. M. Nobre, and M. N. Rebelo, *A bridge between CP violation at low energies and leptogenesis*, Nucl. Phys. **B617** (2001), 475–492, hep-ph/0107164.

[107] P. H. Frampton, S. L. Glashow, and T. Yanagida, *Cosmological sign of neutrino CP violation*, Phys. Lett. **B548** (2002), 119–121, hep-ph/0208157.

[108] T. Endoh, S. Kaneko, S. K. Kang, T. Morozumi, and M. Tanimoto, *CP violation in neutrino oscillation and leptogenesis*, Phys. Rev. Lett. **89** (2002), 231601, hep-ph/0209020.

[109] S. F. King, *Leptogenesis - MNS link in unified models with natural neutrino mass hierarchy*, Phys. Rev. **D67** (2003), 113010, hep-ph/0211228.

[110] S. Pascoli, S. T. Petcov, and W. Rodejohann, *On the connection of leptogenesis with low energy CP violation and LFV charged lepton decays*, (2003), hep-ph/0302054.

[111] G. C. Branco, P. A. Parada, and M. N. Rebelo, *A common origin for all CP violations*, (2003), hep-ph/0307119.

[112] D0 Collaboration, V. M. Abazov et al., *A precision measurement of the mass of the top quark*, Nature **429** (2004), 638–642, hep-ex/0406031.

[113] E. J. Chun and S. Pokorski, *Slepton flavour mixing and neutrino masses*, Phys. Rev. **D62** (2000), 053001, hep-ph/9912210.

[114] B. Grzadkowski and M. Lindner, *Nonlinear evolution of Yukawa couplings*, Phys. Lett. **B193** (1987), 71.

[115] B. Grzadkowski, M. Lindner, and S. Theisen, *Nonlinear evolution of Yukawa couplings in the double Higgs and supersymmetric extensions of the standard model*, Phys. Lett. **B198** (1987), 64.

[116] S. F. King and N. N. Singh, *Renormalisation group analysis of single right-handed neutrino dominance*, Nucl. Phys. **B591** (2000), 3–25, hep-ph/0006229.

[117] S. Antusch and M. Ratz, *Radiative generation of the LMA solution from small solar neutrino mixing at the GUT scale*, JHEP **11** (2002), 010, hep-ph/0208136.

[118] J.-w. Mei and Z.-z. Xing, *Radiative generation of θ_{13} with the seesaw threshold effect*, (2004), hep-ph/0404081.

[119] F. Vissani, M. Narayan, and V. Berezinsky, *U(e3) from physics above the GUT scale*, Phys. Lett. **B571** (2003), 209–216, hep-ph/0305233.

[120] M. Fukugita and T. Yanagida, *Baryogenesis without grand unification*, Phys. Lett. **174B** (1986), 45.

[121] F. R. Klinkhamer and N. S. Manton, *A saddle point solution in the Weinberg-Salam theory*, Phys. Rev. **D30** (1984), 2212.

[122] V. A. Kuzmin, V. A. Rubakov, and M. E. Shaposhnikov, *On the anomalous electroweak baryon number nonconservation in the early universe*, Phys. Lett. **B155** (1985), 36.

[123] K. Hamaguchi, H. Murayama, and T. Yanagida, *Leptogenesis from sneutrino-dominated early universe*, Phys. Rev. **D65** (2002), 043512, hep-ph/0109030.

[124] S. Davidson and A. Ibarra, *A lower bound on the right-handed neutrino mass from leptogenesis*, Phys. Lett. **B535** (2002), 25–32, hep-ph/0202239.

[125] W. Buchmüller, P. Di Bari, and M. Plümacher, *Leptogenesis for pedestrians*, (2004), hep-ph/0401240.

[126] W. Buchmüller, P. Di Bari, and M. Plümacher, *The neutrino mass window for baryogenesis*, Nucl. Phys. **B665** (2003), 445–468, hep-ph/0302092.

[127] W. Buchmüller, P. Di Bari, and M. Plümacher, *A bound on neutrino masses from baryogenesis*, Phys. Lett. **B547** (2002), 128–132, hep-ph/0209301.

[128] R. Barbieri, P. Creminelli, A. Strumia, and N. Tetradis, *Baryogenesis through leptogenesis*, (2002), hep-ph/9911315 v3.

[129] G. F. Giudice, A. Notari, M. Raidal, A. Riotto, and A. Strumia, *Towards a complete theory of thermal leptogenesis in the SM and MSSM*, Nucl. Phys. **B685** (2004), 89–149, hep-ph/0310123.

[130] K. Kumekawa, T. Moroi, and T. Yanagida, *Flat potential for inflaton with a discrete R invariance in supergravity*, Prog. Theor. Phys. **92** (1994), 437–448, hep-ph/9405337.

[131] M. Fujii, K. Hamaguchi, and T. Yanagida, *Leptogenesis with almost degenerate Majorana neutrinos*, Phys. Rev. **D65** (2002), 115012, hep-ph/0202210.

[132] L. J. Hall, H. Murayama, and N. Weiner, *Neutrino mass anarchy*, Phys. Rev. Lett. **84** (2000), 2572–2575, hep-ph/9911341.

[133] N. Haba and H. Murayama, *Anarchy and hierarchy*, Phys. Rev. **D63** (2001), 053010, hep-ph/0009174.

[134] A. de Gouvea and H. Murayama, *Statistical test of anarchy*, Phys. Lett. **B573** (2003), 94–100, hep-ph/0301050.

[135] T. Miura, T. Shindou, and E. Takasugi, *The renormalization group effect to the bi-maximal mixing*, Phys. Rev. **D68** (2003), 093009, hep-ph/0308109.

[136] T. Shindou and E. Takasugi, *The role of Majorana CP phases in the bi-maximal mixing scheme: Hierarchical Dirac mass case*, (2004), hep-ph/0402106.

[137] M. Randhawa, G. Ahuja, and M. Gupta, *Implications of texture 4 zero lepton mass matrices for U(e3)*, Phys. Rev. **D65** (2002), 093016, hep-ph/0203109.

[138] B. R. Desai, D. P. Roy, and A. R. Vaucher, *Three-neutrino mass matrices with two texture zeros*, Mod. Phys. Lett. **A18** (2003), 1355–1366, hep-ph/0209035.

[139] Y. Koide, H. Nishiura, K. Matsuda, T. Kikuchi, and T. Fukuyama, *Universal texture of quark and lepton mass matrices and a discrete symmetry Z(3)*, Phys. Rev. **D66** (2002), 093006, hep-ph/0209333.

[140] M. Honda, S. Kaneko, and M. Tanimoto, *Prediction of U_{e3} and its stability in neutrino mass matrix with two zeros*, JHEP **09** (2003), 028, hep-ph/0303227.

[141] Z.-z. Xing, *The Majorana neutrino mass matrix with one texture zero and one vanishing eigenvalue*, Phys. Rev. **D69** (2004), 013006, hep-ph/0307007.

[142] M. Bando, S. Kaneko, M. Obara, and M. Tanimoto, *Can symmetric texture reproduce neutrino bi-large mixing?*, Phys. Lett. **B580** (2004), 229–235, hep-ph/0309310.

[143] S. Antusch and M. Ratz, *Supergraph techniques and two-loop beta-functions for renormalizable and non-renormalizable operators*, JHEP **07** (2002), 059, hep-ph/0203027.

[144] P. H. Chankowski, A. Ioannisian, S. Pokorski, and J. W. F. Valle, *Neutrino unification*, Phys. Rev. Lett. **86** (2001), 3488–3491, hep-ph/0011150.

[145] E. Ma, *A(4) origin of the neutrino mass matrix*, (2004), hep-ph/0404199.

[146] A. Kageyama, S. Kaneko, N. Shimoyama, and M. Tanimoto, *See-saw realization of the texture zeros in the neutrino mass matrix*, Phys. Lett. **B538** (2002), 96–106, hep-ph/0204291.

[147] S. Zhou and Z.-z. Xing, *A systematic study of neutrino mixing and CP violation from lepton mass matrices with six texture zeros*, (2004), hep-ph/0404188.

[148] Y. F. Pirogov and O. V. Zenin, *Two-loop renormalization group restrictions on the standard model and the fourth chiral family*, Eur. Phys. J. **C10** (1999), 629–638, hep-ph/9808396.